Construction of a Numerical Ship Navigation System for Optimum Ship Routing

Chen, Chen

(Degree)
博士（工学）

(Date of Degree)
2016-03-25

(Date of Publication)
2017-03-01

(Resource Type)
doctoral thesis

(Report Number)
甲第6668号

(URL)
https://hdl.handle.net/20.500.14094/D1006668

Doctoral Dissertation

Construction of a Numerical Ship Navigation System for Optimum Ship Routing

（最適航法のための船舶数値ナビゲーションシステムの構築）

January, 2016

Graduate School of Maritime Sciences, Kobe University

Chen Chen

(陳　辰)

ABSTRACT

Marine transportation capacity is much superior (occupies about 95%) to other transportation methods, thus making researches on a safe, economical and environment-friendly marine transportation is very important in global economic activations and the comfort of people throughout the world. In the past, ships have been operated with experience and intuition of ship crews. However, six-degree ship motions of ocean-going vessels are strongly influenced by weather conditions such as heavy ocean winds, strong ocean current as well as rough ocean waves in the ocean. It is difficult for seafarers to operate ships without scientific techniques about those points. To avoid such heavy ocean winds, rough ocean states and make use of beneficial ocean current, an exact ship position considering about the weather and ocean information is of great importance. However, reproducing such maritime transport ocean environment is difficult and complex.

As one of the well-known methods among improvement of hull-form, propeller design, engine performance, and assistant thrust, optimum ship routing for ocean-going ships has been studied for several decades, which is of great importance for the economic and safety of both ships and cargoes (James, 1957; Motte, et al, 1975; Chen, 1978; Miller, 1983; Hagiwara, 1985).

Because of the low computation abilities of earlier computers, most of those former studies mainly focused on the influences of ocean winds and ocean waves on transoceanic ocean-going vessels, for which the long distance and transit time have a larger flexibility to make their optimum routing algorithms help ships save considerable navigational cost of both time and fuel even by using the relative coarse-resolution atmospheric and oceanic modeling methods.

According to SAETRA (SAETRA et al, 2004), the benefits of any ship routing system, however good the model is, will always depend on the quality of the forecasted weather parameters that are used to force the system. Therefore, the best code is useless if the upcoming weather condition is not known sufficiently.

Nowadays, compared with the situations several decades ago that computer techniques limitations reduced the ability to effectively advise ships to take advantage of favorable

weather, the advent of larger range forecasting and the development of selective climatology, along with more powerful computer modeling techniques, have led to the emergency of modernized regional atmospheric and oceanic models such as the Weather Research and Forecasting Model (Skamarock, 2005), Simulating WAves Nearshore (Booij, Ris, Holthuijsen, 1999) and Princeton Ocean Model (Mellor, 1998), which can conduct wind, wave and ocean current calculations, providing high-resolution weather and ocean data for specific scales and ocean areas, respectively. These model-generated data can then be applied to help vessels select the optimum route, reducing both the shipping cost and dangerous risk.

Therefore, compared with such long-distance cross-ocean navigation using ocean winds and waves, it have become possible for us to do study on the effects of weather and ocean for ship navigation in coastal areas owning to the high ship density and powerful tropical storms as the first step to build a numerical ship navigation system, for which the Osaka Bay of Japan was chosen (Chen et al., 2013). Numerical estimations and simulations of meteorological and marine phenomena have been conducted as the first step. Then the results were utilized to make the numerical simulations of ship navigation by using the widely-used ship maneuvering model named Mathematical Model for Manoeuvring Ship Motion (Kose, et al., 1981;Ogawa, 1981; Yoshimura, 1986), and wave resistances to ship in ocean were calculated by using the Enhanced United Theory built in Research Initiative on Oceangoing Ships system (Kashiwagi, Mizokami, and Tasukawa, 1999). Finally, the risk results from weather and ocean will be obtained by ship crew to avoid possible marine accidents. High-resolution numerical calculations of meteorological and marine phenomena have been successfully generated, and then ship drifting due to such effects has also been well calculated and helps reduce possible ship accidents. Results also show that ship navigation can be significantly affected own to the complex topography and high ship density.

Then we mainly focus on high-resolution current routing by using the strong western-boundary ocean currents like the Kuroshio Current in the East China Sea Area, which can also affect the sailing time and fuel cost even for a shorter distance along the main path of the Kuroshio Current (Chen et al., 2015). Results show that the Kuroshio Current can have a significant effects on navigation time and fuel cost. If it is possible to numerically estimate meteorological and marine phenomena that ships are likely to encounter, economic transport routes can be formulated to reduce fuel consumption by optimally using currents to select the minimum time or fuel ship routes.

Additionally, as the increases of average temperature currently, extreme weather conditions have become more probable. Toffolia et al (Toffolia et al, 2005) studied about the relation between ship accidents and typhoons and he found that in the East China Sea, where approximately 15% of the accidents took place, has a close relationship with the strong ocean winds. Because of the huge amount of warm ocean waters the Kuroshio Current carries, it can provide huge and continuous energy; therefore, the warm sea surface water can lead to a high possibility of tropical typhoons in the East China Sea Area, which also have large effects on ship safety directly by strong ocean wind as well as indirectly through rough wind-induced ocean waves (Chen et al., 2015).

Beside to those regional atmospheric and oceanic models, the Multi-Scale Simulator for the Geo-environment model (MSSG) (Takahashi, et al. 2003; Baba, et al. 2010) and WAVEWATCH-III model (Tolman, 1997, 1999a, 2009) are also studied and used in building our numerical ship navigation system to make a global scale calculation of weather and ocean. Calculation results of these two models show that a global scale numerical ship navigation system is possible to be achieved based on the present method.

Totally, the Numerical Navigation System constructed here shows its feasibility to study about influences of weather and ocean on ship navigation. Variable resolutions could be selected to calculate different cases by using numerical weather and ocean models. Fine enough information of meteorological and marine phenomena could be provided to make the numerical simulation of ship navigation.

Finally, to complete the global-scale optimum ship routing system combined with the above-built numerical ship navigation system, an optimum routing algorithm is also needed. Among those existed mostly used optimization algorithms available for optimum ship routing such as Dijkstra algorithm (Dijkstra, 1959; Padhy, 2008), Dynamic Programming (Chen, 1978; Avgouleas, 2008), Genetic Evolutionary Algorithm (Szlapczynska, et al, 2007) and Monte Carlo (Hoffschildt et al. 1999; Saetra 2004; Böttner 2007), the modified isochrone method, which computes an isochrones repeatedly, i.e. the certain time front that describes the outer boundary achievable from the departure point after a certain time to decide the optimum route, (HAGIWARA et al. 1999) has been chosen because of its higher acceptance by the navigational staff and

its good accuracy compared with others.

Several groups of numerical experiments of ship navigation between the Malacca strait and the Osaka Bay, where the Kuroshio Current flows and powerful typhoons also happen frequently, have been conducted based on necessary ship performance parameters of an actual container ship to study about the global-scale optimum ship routing system. Analysis of experiment results show that considerable navigational cost of both fuel and time could be saved. A safer, more economical as well as environment-friendly shipping navigation is possible to be achieved by utilizing the present optimum ship routing system. Recommendations for future development preferences of the present system have also been given for improvements.

CONTENTS

CHAPTER 1 *1*

INTRODUCTION *1*

1.1 Introduction to Optimum Ship Routing (OSR) 1

1.2 Introduction to Numerical Ship Navigation System 3

1.2.1 Definition of the Numerical Ship Navigation System 3

1.2.2 Motivation of the Numerical Ship Navigation System 4

1.2.3 Study Progress of The Numerical Ship Navigation System 5

1.2.4 Future Development of the Numerical Ship Navigation System 6

1.3 Objective and Outline of This Thesis 7

1.3.1 Objective 7

1.3.2 Limitations....7

1.3.3 Outlines 7

References *9*

CHAPTER 2 *12*

NUMERICAL CALCULATIONS OF WEATHER AND OCEAN *12*

2.1 Description of Atmospheric and Oceanic Models 12

2.1.1 Weather Research & Forecasting Model....12

2.1.2 Simulating Waves Nearshore....15

2.1.3 Princeton Ocean Model 16

2.2 Coastal Sea Areas 19

2.2.1 Osaka Bay Area....19

2.2.2 The East China Sea Area (ECSA) 28

2.3 Global Scale....46

2.3.1 Multi-Scale Simulator for the Geoenvironment (MSSG-A & MSSG-O) 46

2.3.2 WAVEWATCH III (WW3) 47

2.3.3 Numerical Calculations of Weather and Ocean by MSSG and WW3 52

2.4. Summary.....61

References 63

CHAPTER 3 ***67***

CONSTRUCTION OF THE NUMERICAL SHIP NAVIGATION SYSTEM ***67***

3.1 Description of ship model (SR108), wave resistance model (RIOS) and ship maneuvering model (MMG).....67

3.1.1 Ship Model SR108.....67

3.1.2 Ship response to ocean waves.....68

3.1.3 Ship maneuvering model.....69

3.2 Numerical simulations of ship navigation 72

3.2.1 Osaka Bay Area.....72

3.2.2 East China Sea Area 80

3.3 Summary 97

References ***99***

CHAPTER 4 ***100***

OPTIMUM SHIP ROUTING BASED ON NUMERICAL SHIP NAVIGATION SYSTEM ***100***

4.1 Introduction to optimization algorithms for optimum ship routing 100

4.2 Optimum ship routing by the combination of optimization algorithm and numerical ship navigation system 101

4.3 Summary 105

References ***107***

CHAPTER 5 ***108***

REVIEWS, CONCLUSIONS AND RECOMMENDATIONS FOR FUTURE

DEVELOPMENT PREFERENCES *108*
PUBLICATIONS *110*
ACKNOWLEDGEMENTS *113*
FIGURE LIST *117*
TABLE LIST *120*

CHAPTER 1

INTRODUCTION

Maritime transport is essential to the world's economy as over 90% of the world's trade is carried by sea and it is, by far, the most cost-effective way to move masse goods and raw materials around the world, making researches on a safe, economical and environment-friendly marine transportation very important in global economic activation and the comfort of people throughout the world.

As the art and science of finding the best route for a ship by utilizing the forecasting weather information, ship characteristics, ocean currents and cargo requirements, optimum ship routing has been studied for a long time. It has been known for decades that the weather and ocean states such as ocean winds, ocean waves and ocean current is of great importance for optimal ship routing. Medium range forecast of such variables for about one week is an essential factor for optimal ship routing crossing the ocean, besides, for heavy weather avoidance, such as the typhoon period, exact analysis and short term forecast of these variables are necessary.

Recently, with the development of important issues such as global warming, higher fuel prices and higher requirements of ocean environmental protection, higher-efficiency ship navigation has attracted people's attention recently.

Delitala et al (Delitala, et al. 2010) performed a route simulator by using a 2-year climatology simulation for two different routes, and they showed their approach could help either improve ship performance or support ship captain. In the North Indian Ocean, Padhy et al (Padhy et al, 2008) achieved a reliable optimum route in a given random sea-state by applying the wave height information from GEOSAT altimeter records as well as Dijkstra's path optimization scheme. As Padhy mentioned, to obtain an optimal ship routing, several important parts including the weather and ocean modeling, ship motions, and a suitable path optimization algorithm are necessary.

1.1 Introduction to Optimum Ship Routing (OSR)

According to George L. Hanssen and Richard W. James (George L. and Richard W., 1960), an average reduction in travel time of 14 hours have been achieved by using over 1000 optimum ship routes for over a period of two years, optimum track routing can best be defined as the selection of an optimum track for a transoceanic crossing by the application of long-range predictions of wind, waves and currents to the knowledge of how the routed vessel reacts to these variables. Although 'optimum' is usually interpreted as least time, these techniques can be utilized with equal success to prepare tracks of maximum safety, passenger comfort, minimum fuel consumption or any desired combination of these factors.

Compared with George L. Hanssen and Richard W. James, Chen (Chen, 2011.) treated the optimum ship routing as a problem of a dynamic program or a multi-stage decision process by solving the stochastic minimum cost ship routing problem. He made a comparison of various solution methods for ship routing problems by others and came to a conclusion that all those models are deterministic which may be unrealistic in view of the uncertainties in wind and wave conditions along the route. Then he argued that ship routing is concerned with the choice of the most suitable strategic trajectory or route and the corresponding control options from the voyage origin to destination so that a desired objective function or performance index is optimized. And as possible objective functions to be optimized, he gave a list of criteria as follows (including both the commercial ship operation and logistics of interests to military interests):

Ship safety
Prevention of damage to hull, cargo, and deck equipment, etc.
Economy in navigation, e.g. Minimum costs, Minimum transit time, etc.
Crew/passenger comfort
Maintenance of fleet schedule
Minimum probability of detection
Minimum time of intercept
Maximum combat effectiveness
Optimum search and rescue effectiveness

Other researchers or shipping industries staffs also have their views on optimum ship routing. Bowditch, et al (Bowditch, 2002) consider ship weather routing as the development of an optimum route and speed for ocean voyages based on predicted

weather, ocean states, and those individual characteristics of a ship for a certain transit. Notteboom, et al (Notteboom and Carriou, 2009) think that both the fuel consumption and expected time of arrival are not only related with the optimum route but are also directly connected with speed and power profiles. Therefore most ocean-crossing ships are equipped with a weather routing system for achieving the least fuel consuming route while arriving on time. Other documents about the benefits of using these routing systems for avoiding dangerous ship situations in adverse weather and ocean states can be found in e.g. (Chen et al., 1998; IMO 2007).

To conclude, for most transits this will mean the best route in terms of categories like: ETA for schedule keeping (estimated time of arrival), fuel consumption, safety (of ship, crew, passengers, cargo and ocean environment), and comfort of passengers and crew. To increase the cost-efficiency of shipping transportation, avoid cargo and life dangers from various accidents and reduce possible pollution to the weather and ocean environments, a numerical ship navigation system has been built as the first step for a global scale optimum ship routing system.

1.2 Introduction to Numerical Ship Navigation System

1.2.1 Definition of the Numerical Ship Navigation System

As the basic study to complete a weather routing system, a Numerical Navigation System has been partly constructed in the past several years (Shiotani, et al., 2006; Shiotani, et al., 2008; Shiotani, et al., 2010; Chen et al., 2013; Chen et al., 2015). The Numerical Navigation System can be briefly defined as follows. It is a numerical simulation of ship navigation, aiming at making safer and more economical ship navigation by figuring out the ship motions, speed loss and ship drifting under effects of certain sea states. In details, it consists of both numerical calculation of weather & ocean by utilizing modernized atmospheric and oceanic models and then the influence of weather & ocean on ship navigation by utilizing a ship maneuvering model, shown as Fig.1.1. In the next step, the present-constructed Numerical Navigation System will be included in an advanced weather routing system, aiming at making safer, more economical ship navigation.

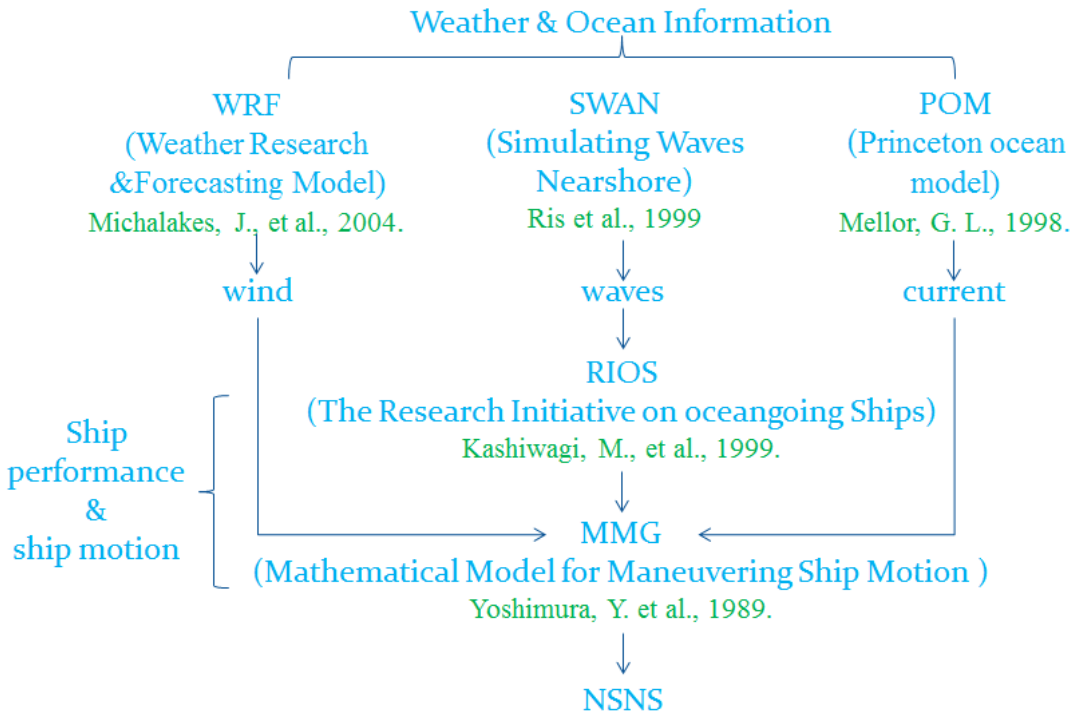

Fig.1.1. Compositions of the Numerical Ship Navigation System

1.2.2 Motivation of the Numerical Ship Navigation System

Maritime transport accounts for the largest percentage of all means of transport and offers the greatest transport capacity; as a result, maritime transport research is indispensable for achieving market advances in the global economy and supporting the prosperous lifestyles of mankind. However, according to the casual statistics of IMO (IMO, 2000) for ocean-going ships of 100GT and above, 533 registered serious and very serious casualties happened at sea, while 64 of them occurred in heavy weather. All these comprise 145 total losses, 38 happened in heavy weather. And in 2003, the number of severe casualties amount to 150, among which 109 total losses of ships larger than 100GT were registered, while 40 of them came from heavy weather. General cargo ships are the most affected ships, suffering over 40% of the total losses with only accounting for about 20% of the world merchant fleet. However, total loss is only one aspect in the consequences of heavy weather besides others such as structural damages, the loss of cargo, crew damage and pollution to ocean environments (Hinnenthal, et al., 2010). Additionally, according to Table.1.1 (http://docs.imo.org/Shared/Download.aspx?did=68898), number of ships lost 2006-2010 can be found.

Table.1.1. Number of ships lost 2006-2010

Number of ships lost 2006-2010 2006	2006	2007	2008	2009	2010
Ships of 500 GT and above	88	91	80	98	119
Ships between 100 and 499 GT	32	44	55	44	53
Ships of 100GT and above	120	135	135	142	172
Loss rate (all ships)*	1.3	1.4	1.4	1.4	1.7

In the past, ships have been operated with the experience and intuition of ship crews. However, ships are strongly influenced by weather conditions such as waves, winds, currents in the ocean. It is difficult for seafarers to operate ships without scientific techniques about those points. However, reproducing such maritime transport ocean environment is difficult and complex. As a result, numerical estimation and simulations of meteorological and marine phenomena is conducted as the first step. Then the results are utilized to make the numerical simulation of ship navigation by using a ship maneuvering model. Finally, the risk results from weather and ocean will be obtained by ship crew in advance to avoid possible marine accidents.

1.2.3 Study Progress of The Numerical Ship Navigation System

In 2006, Shiotani (Shiotani, et al., ISOPE 2006) started the concept of construction of a numerical ship navigation system to improve the level of ship safety, navigational economics, and oceanic environment protection. After that, a calculation and verification of influences of tidal current and ocean winds on ship navigation in a bay area has been done to make the first-step trail in 2008 (Shiotani, et al., ASME 2008). As the next-step, calculation and verification of influences of ocean waves in a bay area was conducted (Shiotani, et al., ISOPE 2010), and significant effects of ocean waves on ship navigation has been verified by his method.

In the past several years of my study, owning to the high ship density and powerful tropical storms, bay and regional areas such as the Osaka Bay of Japan and East China Sea have been studied to complete the construction of the numerical ship navigation system. High-resolution numerical calculations of meteorological and marine

phenomena have been successfully generated, and then ship drifting due to such effects has also been well calculated and helps reduce possible ship accidents. Finally, variable resolutions could be selected to calculate different cases by using numerical weather and ocean models. Fine enough information of meteorological and marine phenomena could be provided to conduct the numerical simulation of ship navigation.

1.2.4 Future Development of the Numerical Ship Navigation System

To further develop the present numerical ship navigation system, global scale weather and ocean information as well as a proper optimization algorithm are needed to extend it into an optimum ship routing system. The flow chart of the completed optimum ship routing system should be as Fig.1.2.

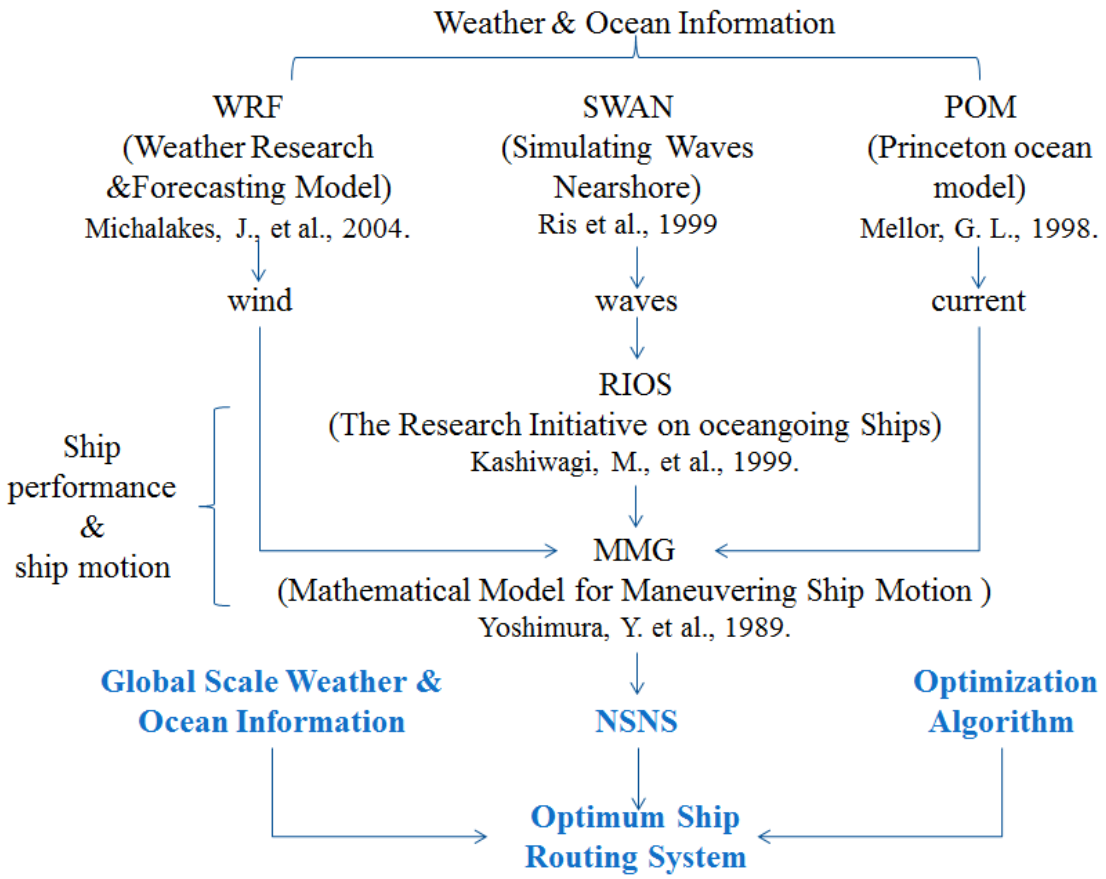

Fig.1.2.Flow chart of the supposed optimum ship routing system

1.3 Objective and Outline of This Thesis

1.3.1 Objective

The main objective of this study is the development of an optimum ship routing system with respect to time cost, fuel consumption, and ship safety. The optimum ship routing system should have the capability of considering both numerical calculation of weather and ocean as well as ship motions regardless of ocean states based on ship's operational performance.

The whole study may be divided into two main aspects to accomplish the main objective:

1. The construction of a numerical ship navigation system
2. The development of an optimum ship routing system by the combination of both the numerical ship navigation system and the optimization algorithm.

1.3.2 Limitations

The objective of an optimum ship routing system should also include real ship experiments to make the verification of the accuracy of the system. However, due to the limitation of detailed ship data of engine performance and lack of conditions to do real-case experiments, a ship model has been used to conduct the optimum ship routing experiments.

Second, past weather and ocean data instead of forecasted information has been utilized to construct the numerical ship navigation system and the optimum ship routing system, although real-case ship routing problem needs forecasted ocean states, with the time period depended on the sailing distance from the voyage plan, to construct the optimum ship routing system, I have to make verifications of our calculation results of weather and ocean, for which past observation data is necessary.

1.3.3 Outlines

This thesis is divided into five chapters:

Chapter 1 gives a brief introduction to the optimum ship routing by talking about the definition and the previous studies of the optimum ship routing. Then the concept, motivation and the future development direction of numerical ship navigation system has also been described.

Chapter 2 includes the numerical simulations of weather and ocean environments in both coastal sea area and global scale area. Necessary weather and ocean information were generated by utilizing atmospheric and oceanic models in both regional and global scale, and then simulation results are analyzed and discussed.

Chapter 3 describes how the numerical simulations of ship navigation are conducted and how the numerical ship navigation systems are constructed in coastal sea area and global sea area, respectively.

Chapter 4 has added the optimization algorithm into the above-created numerical ship navigation system to complete the optimum ship routing system based on numerical ship navigation system. Results of calculation results and efficiency of the completed optimum ship routing system are also discussed.

Reviews, conclusions and recommendations for future development preferences are found in Chapter 5.

References

Avgouleas, Kyriakos. Optimal ship routing. Diss. Massachusetts Institute of Technology, 2008.

Booij, N.; Ris, R. C.; Holthuijsen, Leo H., 1999. A Third‐Generation Wave Model For Coastal Regions: 1. Model Description And Validation. Journal Of Geophysical Research: Oceans (1978–2012), 104.C4: 7649-7666.

Böttner CU (2007) Weather routing for ships in degraded conditions. International Symposium on Safety, Security and Environmental Protection. National Technical University of Athens, Athens

Bowditch, N (2002). "The American Practical Naviga-tor; originally by Nathaniel Bowditch." National Im-agery and Mapping Agency, Bethesda, Maryland, USA.

Chen, H., 1978. A dynamic problem for minimum cost ship routing under uncertainty. Ph.D. thesis, MIT, Cambridge, MA.

Chen, H. Voyage optimization supersedes weather routing. Technical report, 2011.

Chen, Chen, Shigeaki Shiotani, and Kenji Sasa. "Numerical ship navigation based on weather and ocean simulation." Ocean Engineering 69 (2013): 44-53.

Chen, Chen, Shigeaki Shiotani, and Kenji Sasa. "Effect of ocean currents on ship navigation in the east China sea." Ocean Engineering 104 (2015): 283-293.

Chen, Chen, Shiotani Shigeaki, and Sasa Kenji. "Study on a Numerical Navigation System in the East China Sea." Applied Ocean Research 53 (2015): 257-266.

Delitala, Alessandro Mario Sergio, et al. 2010. "Weather routing in long-distance Mediterranean routes." Theoretical and applied climatology, 102.1-2, 125-137.

Dijkstra, Edsger W. "A note on two problems in connexion with graphs." Numerische mathematik 1.1 (1959): 269-271.

George L. Hanssen and Richard W. James (1960). Optimum Ship Routing. Journal of Navigation, 13, pp 253-272. doi:10.1017/S0373463300033580.

H. Chen, V. Cardone, and P. Lacey. Use of operation support information technology to increase ship safety and efficiency. SNAME transactions, 106:105-127, 1998.

Hagiwara, H., 1985. A study on the minimum fuel consumption route-II: Simulation in the North Pacific Ocean. Journal of Japan Institute of Navigation, 72, 87–96.

Hinnenthal, Jörn, and Günther Clauss. "Robust Pareto-optimum routing of ships utilising deterministic and ensemble weather forecasts." Ships and Offshore Structures 5.2 (2010): 105-114.

Hoffschildt M, Bidlot JR, Hansen B, Janssen PAEM (1999) Potential benefit of

ensemble forecasts for shiprouting. ECMWF Technical Memorandum no. 287.
IMO. Msc.1/circ.1228 - revised guidance to the master for avoiding dangerous situations in adverse weather and sea conditions. Technical report, IMO – International Maritme Organization, 2007.
IMO (2000 and 2003), Casualty Statistics and Investigations, International Maritime Organization, Ref. T1/2.02, FSI3/Circ.3 and 6, UK
James, R. W., 1957. Application of wave forecasts to marine navigation. U.S. Oceanographic Office, SP-1, July, 1957.
Lo, Hong Kam, Mark R. McCord, and Cori K. Wall. "Value of ocean current information for strategic routing." European journal of operational research 55.2 (1991): 124-135.
Lo, Hong K., and Mark R. McCord. "Adaptive ship routing through stochastic ocean currents: General formulations and empirical results." Transportation Research Part A: Policy and Practice 32.7 (1998): 547-561.
Miller, J. N., 1983. Does ocean routing reduce casualties? An analysis of the incidence of serious weather-related casualties in North Atlantic and North pacific crossings from 9-1-78 through 12-31-82. Technical Paper, Oceanroutes, Inc., Sunnyvale, CA.
Mellor, George L. Users guide for a three dimensional, primitive equation, numerical ocean model. Princeton, NJ 08544-0710: Program in Atmospheric and Oceanic Sciences, Princeton University, 1998.
Motte, Roger. "Weather Routing of Ships." Safety at Sea International 74 (1975).
Notteboom, Theo, and Pierre Cariou. "Fuel surcharge practices of container shipping lines: Is it about cost recovery or revenue-making." Proceedings of the 2009 International Association of Maritime Economists (IAME) Conference. IAME, 2009.
Padhy CP, Sen D, Bhaskaran PK. Application of wave model for weather routing of ships in the North Indian Ocean. Natural Hazards 2008, 44 : 373–85 .
SAETRA, Ø. (2004), Ensemble Shiprouting, ECMWF Technical Memorandum 435, Reading/UK
Szlapczynska, Joanna, and Roman Smierzchalski. Adopted isochrone method improving ship safety in weather routing with evolutionary approach. International Journal of Reliability, Quality and Safety Engineering 14.06 (2007): 635-645.
Shiotani Shigeaki, Haibo Xia. "A Basic Study on the Numerical Estimation of Ship Positioning for Weather Routing in Coastal Water." The Sixteenth International Offshore and Polar Engineering Conference. International Society of Offshore and Polar Engineers, 2006.
Shiotani Shigeaki. "Numerical Simulation of Tidal Current or Wind Over the Sea and

Applications to Navigational Simulation of a Sailing Ship." ASME 2008 27th International Conference on Offshore Mechanics and Arctic Engineering. American Society of Mechanical Engineers, 2008.
Shiotani Shigeaki, et al. "Numerical Navigation for a Ship in Simulation of Waves." The Twentieth International Offshore and Polar Engineering Conference. International Society of Offshore and Polar Engineers, 2010.
Tolman, H. L., 1997: User manual and system documentation of WAVEWATCH-III version 1.15. NOAA / NWS / NCEP / OMB Technical Note 151, 97 pp.
Tolman, H. L., 1999a: User manual and system documentation of WAVEWATCH-III version 1.18. NOAA / NWS / NCEP / OMB Technical Note 166, 110 pp.
Tolman, H. L., 2009: User manual and system documentation of WAVEWATCH III version 3.14. NOAA / NWS / NCEP / MMAB Technical Note 276, 194 pp.
Keiko Takahashi, Development of coupled ocean-atmosphere-sea ice model with optimized computational performance on the Earth Simulator. Annual Report of the Earth Simulator Center (April 2002-March 2003), 73-77, 2003.
Yuya Baba, Keiko Takahashi, Takeshi Sugimura, Koji Goto, “Dynamical core of an atmospheric general circulation model on a Yin-Yang grid”, Monthly Weather Review, Vol.138 (2010), pp.3988-4005.
Skamarock, William C., et al. A description of the advanced research WRF version 2. National Center For Atmospheric Research Boulder Co Mesoscale and Microscale Meteorology Div, 2005.
Yu-Chia Chang, Ruo-Shan Tseng, Guan-Yu Chen, Peter C Chu and Yung-Ting Shen (2013). Ship Routing Utilizing Strong Ocean Currents. Journal of Navigation, 66, pp 825-835.

CHAPTER 2

NUMERICAL CALCULATIONS OF WEATHER AND OCEAN

2.1 Description of Atmospheric and Oceanic Models

Several modernized regional atmospheric and oceanic models are utilized here to generate the necessary high-resolution weather and ocean information to be used as the ocean states for numerical simulation of ship navigation in the next step.

2.1.1 Weather Research & Forecasting Model

As known to all, the large gradients in wind velocity and the rapidly varying wind directions of the typhoon vortex can generate very complex ocean wave fields. In this study, the simulation of wind was carried out by Weather Research & Forecasting Model (WRF) (Skamarock et al., 2005), which has been widely used for operational forecasts as well as for realistic and idealized research experiments. It can predict three-dimensional wind momentum components, surface pressure, dew point, precipitation, surface-sensible and latent heat fluxes, relative humidity, and air temperature on a sigma-pressure vertical coordinate grid. The equation set for WRF-ARW is fully compressible, Eulerian, and non-hydrostatic, with a run-time hydrostatic option. The time integration scheme in the model uses the third-order Runge-Kutta scheme, and the spatial discretization employs 2nd to 6th order schemes.

The ARW applied in the WRF model are formulated using a terrain-following hydrostatic-pressure vertical coordinate denoted by η and defined as:

$$\eta = (p_h - p_{ht})/\mu \tag{2.1}$$

Where $\mu = p_h - p_{ht}$. p_h is the hydrostatic component of the pressure, and p_{ht} are values along the surface and top boundaries, respectively.

The coordinate definition (2.1), proposed by Laprise (Laprise, 1992), is the traditional σ coordinate used in many hydrostatic atmospheric models. η varies from a value of 1 at the surface to 0 at the upper boundary of the model domain (Fig.2.1). This vertical

coordinate is also called a mass vertical coordinate.

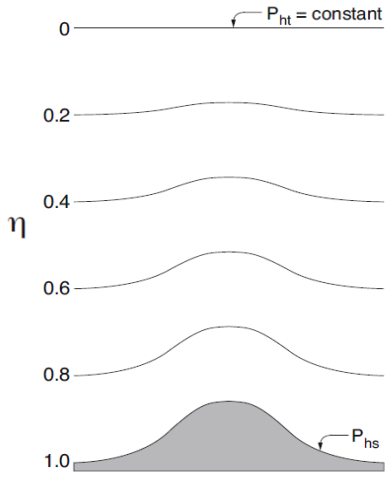

Fig.2.1. WRF-ARW η coordinate

Since μ(x, y) represents the mass per unit area within the column in the model domain at (x, y), the appropriate flux form variables are:

$$V = \mu v = (U, V, W); \quad \Omega = \mu\eta; \quad \Theta = \mu\theta \tag{2.2}$$

Where $V = \mu v = (U, V, W)$ are the covariant velocities in the two horizontal and vertical directions, respectively, while ω = ˙η is the contravariant 'vertical' velocity. θ is the potential temperature. Also appearing in the governing equations of the ARW are the non-conserved variables φ = gz (the geopotential), p (pressure), and α = 1/ρ (the inverse density).

Using the variables defined above, the flux-form Euler equations can be written as:

$$\alpha_t U + (\nabla * V_u) - \alpha_x(p\emptyset_\eta) + \alpha_\eta(p\emptyset_x) = F_U \tag{2.3}$$
$$\alpha_t V + (\nabla * V_v) - \alpha_y(p\emptyset_\eta) + \alpha_\eta(p\emptyset_y) = F_V \tag{2.4}$$
$$\alpha_t W + (\nabla * V_w) - g(\alpha_\eta - \mu) = F_W \tag{2.5}$$
$$\alpha_t \Theta + (\nabla * V_\theta) = F_\Theta \tag{2.6}$$
$$\alpha_t \mu + (\nabla * V) = 0 \tag{2.7}$$
$$\alpha_t \emptyset + \mu^{-1}[(V * \nabla) - gW = 0 \tag{2.8}$$

Along with the diagnostic relation for the inverse density:

$$\alpha_\eta \emptyset = -\alpha\mu \tag{2.9}$$

And the equation of state:

$$p = p_0(R_d/p_0\alpha)^\gamma \tag{2.10}$$

In (2.3) – (2.10), the subscripts x, y and η denote differentiation,

$$\nabla * V_\alpha = \alpha_x(U_\alpha) + \alpha_y(V_\alpha) + \alpha_\eta(\Omega_\alpha) \tag{2.11}$$

And

$$V * \nabla_\alpha = U\alpha_x a + V\alpha_y a + \Omega\alpha_\eta a \tag{2.12}$$

Where a represents a generic variable, $\gamma = {}^{c_p}/_{c_v} = 1.4$ is the ratio of the heat capacities for dry air, R_d is the gas constant for dry air, and p_0 is a reference pressure (typically 105 Pascals). The right-hand-side (RHS) terms F_U, F_V , F_W, and F_Θ represent forcing terms arising from model physics, turbulent mixing, spherical projections, and the earth's rotation.

The prognostic equations (2.3) – (2.8) are cast in conservative form except for (2.8) which is the material derivative of the definition of the geopotential. (2.8) could be cast in flux form but there is no advantage in doing so since $\mu_\emptyset$ is not a conserved quantity. A prognostic pressure equation could also be used in place of (2.8) (see Laprise, 1992), but the pressure is not a conserved variable and a pressure equation could not be used together with the conservation equation for Θ (2.6) because they are linearly dependent. Additionally, prognostic pressure equations have the disadvantage of possessing a mass divergence term multiplied by a large coefficient (proportional to the sound speed) which makes spatial and temporal discretization problematic. It should be noted that the relation for the hydrostatic balance (2.9) does not represent a constraint on the solution, rather it is a diagnostic relation that formally is part of the coordinate definition. In the hydrostatic counterpart to the non-hydrostatic equations, (2.9) replaces the vertical momentum equation (2.5) and it becomes a constraint on the solution.

As boundary data, GFS-FNL data were used. The GFS (Global Forecast System) is operationally run four times a day in near-real time at NCEP. GFS-FNL (Final) Operational Global Analysis data are on 1.0x1.0-degree grids every six hours.

2.1.2 Simulating Waves Nearshore

As a numerical model for simulating waves, Simulating WAves in the Nearshore (SWAN; Booij et al., 1999), a third-generation wave simulation model developed at Delft University of Technology was applied here to simulate waves affected by the low pressures. Implemented with the wave spectrum method, it is a third-generation wave model that can compute random, short-crested, wind-generated waves in coastal regions as well as inland waters. The SWAN model is used to solve the spectral action balance equation without any prior restriction on the spectrum for the effects of spatial propagation, refraction, reflection, shoaling, generation, dissipation, and nonlinear wave-wave interactions.

A typhoon with intense and fast-varying winds forms a complex ocean wave field which can propagate thousands of kilometers away from the storm center, resulting in dramatic variation of the wave field in space and time. Waves under typhoon wind were simulated successfully by SWAN wave model (Ou et al. 2002). As a very important way, ocean wave modeling is a very useful and convenient way to obtain the spatial and temporal distribution of directional spectra without the limitations associated with measurements.

After being satisfactorily verified with field measurements (Holthuijsen, Booij et al., 1999), it is considered to be an ideal candidate as a reliable simulating model of typhoon waves in coastal waters once a typhoon's cyclonic wind fields have been determined.

Consequently, the SWAN model is suitable for estimating waves in bay areas with shallow water and ambient currents. Information about the sea surface is contained in the wave variance spectrum of energy density $E(\sigma, \theta)$. Wave energy is distributed over frequencies (θ) and propagation directions (σ). σ is observed in a frame of reference moving with the current velocity, and θ is the direction normal to the wave crest of each spectral component. The expressions for these propagation speeds are taken from linear wave theory (Whitham, 1974; Dingemans, 1997), while diffraction is not considered in the model. The action balance equation of the SWAN model in Cartesian coordinates is as follows:

$$\frac{\partial}{\partial x}c_x N + \frac{\partial}{\partial y}c_y N + \frac{\partial}{\partial \sigma}c_\sigma N + \frac{\partial}{\partial \theta}c_\theta N = \frac{S}{\sigma} \quad (2.13)$$

where the right-hand side contains S, which is the source/sink term that represents all physical processes that generate, dissipate, or redistribute wave energy. The equation of S is as follows:

$$S = S_{in} + S_{ds,w} + S_{ds,b} + S_{ds,br} + S_{nl4} + S_{nl3} \quad (2.14)$$

where S_{in} is the term for transferring of wind energy to the waves (Komen et al., 1984), $S_{ds,w}$ is the term for the energy of whitecapping (Komen et al., 1984), $S_{ds,b}$ is the term for the energy of bottom friction (Hasselmann et al., 1973), and $S_{ds,br}$ is the term for the energy of depth-induced breaking.

2.1.3 Princeton Ocean Model

The Princeton Ocean Model was used to simulate the tidal current affected by these two typhoons. As a three-dimensional primitive equation ocean model, it includes thermodynamics and the level-2.5 Mellor-Yamada turbulence closure and uses a sigma coordinate in the vertical to resolve the variation of bottom topography (Blumberg and Mellor 1987).

The principal attributes of the POM model are as follows (Blumberg and Mellor 1987):

1. It contains an imbedded second moment turbulence closure sub-model to provide vertical mixing coefficients.
2. It is a sigma coordinate model in that the vertical coordinate is scaled on the water column depth.
3. The horizontal grid uses curvilinear orthogonal coordinates and an "Arakawa C" differencing scheme.
4. The horizontal time differencing is explicit whereas the vertical differencing is implicit. The latter eliminates time constraints for the vertical coordinate and permits the use of fine vertical resolution in the surface and bottom boundary layers.
5. The model has a free surface and a split time step. The external mode portion of the model is two-dimensional and uses a short time step based on the CFL condition and the external wave speed. The internal mode is three-dimensional and uses a long

time step based on the CFL condition and the internal wave speed. Complete thermodynamics have been implemented.

The basic equations have been cast in a bottom following, sigma coordinate system which is illustrated in Fig.2.2. The sigma coordinate system is probably a necessary attribute in dealing with significant topographical variability such as that encountered in estuaries or over continental shelf breaks and slopes. Together with the turbulence sub-model, the model produces realistic bottom boundary layers which are important in coastal waters (Mellor, 1985) and in tidally driven estuaries (Oey et al., 1985a, b), which the model can simulate since it does have a free surface.

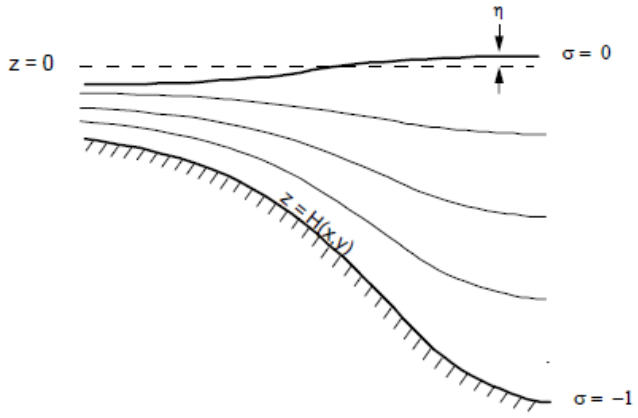

Fig.2.2. The sigma coordinate system applied in the POM model

The sigma coordinate equations are based on the transformation as follows:

$$x^* = x,\ y^* = y, \sigma = \frac{z-\eta}{H+\eta}, t^* = t \qquad (2.15)$$

Where x, y, z are the conventional cartesian coordinates; H (x, y) is the bottom topography and η(x, y, t) is the surface elevation. Thus, σ ranges from σ = 0 at z = η to σ = -1 at z = H. After conversion to sigma coordinates and deletion of the asterisks, the basic equations known as the continuity equation and Navier-Stokes equation may be written (in horizontal cartesian coordinates) as:

$$\begin{cases} \frac{\partial DU}{\partial x}+\frac{\partial DV}{\partial y}+\frac{\partial \omega}{\partial t}+\frac{\partial \gamma}{\partial T}=0 \\ \frac{\partial UD}{\partial t}+\frac{\partial U^2D}{\partial x}+\frac{\partial UVD}{\partial y}+\frac{\partial U\omega}{\partial \sigma}-fVD+gD\frac{\partial \gamma}{\partial x} \\ +\frac{gD^2}{\rho_0}\int_\sigma^0\left[\frac{\partial \rho'}{\partial x}-\frac{\sigma'}{D}\frac{\partial D}{\partial x}\frac{\partial \rho'}{\partial \sigma'}\right]d\sigma'=\frac{\partial}{\partial \sigma}\left[\frac{K_M}{D}\frac{\partial U}{\partial \sigma}\right]+F_x \\ \frac{\partial UD}{\partial t}+\frac{\partial UVD}{\partial x}+\frac{\partial V^2D}{\partial y}+\frac{\partial V\omega}{\partial \sigma}+fUD+gD\frac{\partial \gamma}{\partial y} \\ +\frac{gD^2}{\rho_0}\int_\sigma^0\left[\frac{\partial \rho'}{\partial y}-\frac{\sigma'}{D}\frac{\partial D}{\partial y}\frac{\partial \rho'}{\partial \sigma'}\right]d\sigma'=\frac{\partial}{\partial \sigma}\left[\frac{K_M}{D}\frac{\partial V}{\partial \sigma}\right]+F_y \end{cases} \quad (2.16)$$

Where U and V are the components of the horizontal velocity of tidal current, ω is the velocity component of the normal direction to the σ plain, f is the Coriolis coefficient, g is the acceleration of gravity, F_x and F_y are the horizontal viscosity diffusion coefficients, and K_M is the frictional coefficient of the sea bottom. The transformation to the Cartesian vertical velocity is:

$$W=\omega+U\left(\sigma\frac{\alpha_D}{\alpha_x}+\frac{\alpha_\eta}{\alpha_x}\right)+V\left(\sigma\frac{\alpha_D}{\alpha_y}+\frac{\alpha_\eta}{\alpha_y}\right)+\sigma\frac{\alpha_D}{\alpha_t}+\frac{\alpha_\eta}{\alpha_t} \quad (2.17)$$

The horizontal viscosity and diffusion terms are defined according to:

$$F_x\equiv\frac{\alpha}{\alpha_x}(H\tau_{xx})+\frac{\alpha}{\alpha_y}(H\tau_{xy}) \quad (2.18)$$

$$F_y\equiv\frac{\alpha}{\alpha_x}(H\tau_{xy})+\frac{\alpha}{\alpha_y}(H\tau_{yy}) \quad (2.19)$$

Where

$$\tau_{xx}=2A_M\frac{\alpha U}{\alpha_x},\quad \tau_{xy}=\tau_{yx}=A_M\left[\frac{\alpha U}{\alpha_y}+\frac{\alpha V}{\alpha_x}\right],\ \tau_{yy}=2A_M\frac{\alpha V}{\alpha_y} \quad (2.20)$$

Where the Smagorinsky Diffusivity A_M is:

$$A_M=C\Delta x\Delta y\frac{1}{2}|\nabla V+(\nabla V)^T|=C\Delta x\Delta y\left[\left(\frac{\alpha U}{\alpha_x}\right)^2+\frac{1}{2}\left(\frac{\alpha U}{\alpha_x}+\frac{\alpha V}{\alpha_y}\right)^2;\left(\frac{\alpha V}{\alpha_y}\right)^2\right] \quad (2.21)$$

2.2 Coastal Sea Areas

To construct a numerical ship navigation system, coastal sea areas such as the Osaka Bay of Japan and the East China Sea have been chosen to conduct numerical simulations of weather and ocean states. The reasons why these two regions are selected as well as the studies of these two areas are given as follows.

2.2.1 Osaka Bay Area

Acted as a busy shipping bay, the Osaka Bay of Japan is often attacked by strong typhoons coming from different directions, thus a need for high-resolution information on wind, wave and current has been brought to the attention of scientists and engineers. Besides, owning to the existed high-resolution topography (50M × 50M) data, as shown in Fig.2.3, the complex topography and higher ship density also calls for attention to find the different effects of weather and ocean in this area on ship navigation.

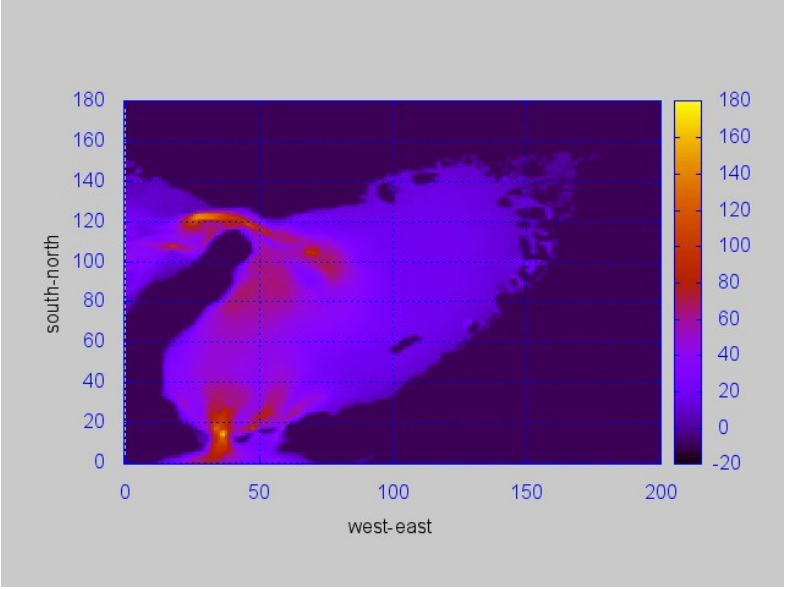

Fig.2.3. Topography of the Osaka Bay

Shiotani, S. studied about the influence of tidal current on a sailing ship (Shiotani, 2006), making the initial step of numerical ship navigation. Several numerical navigation experiments in the Japan coastal area were also carried out (Xia, Shiotani, et al, 2006), verifying the possibility to estimate ship position, however, the high-resolution weather

and ocean data was not utilized to improve the accuracy of ship simulation. In their research, the ship simulation model known as the Mathematical Model for Manoeuvring Ship Motion (MMG) was effectively verified to calculate the ship response to the ocean currents and waves, which has been studied in the 1980s (Yoshimura, 1989).

Other researchers have also studied about the influence of weather and ocean on a sailing ship in coastal area (Soda, Shiotani, et al, 2012), however, their simulation was conducted using a small vessel “Fukae Maru” only in one low pressure case without experiment verifying data, which is substituted by using a normal container ship model “SR108” in two symmetrical typhoon cases in this paper to further confirm the correctness of the proposed ship simulation method, while the next step is to implement a real navigation experiment based on the present feasibility confirmation.

Therefore, to find different effects on ship navigation as well as conduct the first step for constructing a numerical weather routing system, two representative typhoons were analyzed to make a ship navigation simulation with consideration of the tidal current, waves, and wind in Osaka Bay.

First, the mesoscale meteorological model of WRF-ARW version 3.4 (Weather Research & Forecasting Model) was used to generate high-resolution wind data, which was then put into SWAN (Simulating WAves Nearshore) and POM to get wave and tidal current data. Second, the numerical simulation data of wind, waves, and currents were applied to the navigational simulation of an oceangoing ship in Osaka Bay.

For the wind calculation, the simulation periods were from September 2, 00:00 UTC, to September 8, 00:00 UTC, 2004 (NO. 1) and October 3, 00:00 UTC, to October 9, 00:00 UTC, 2009 (NO. 2). Fig.2.4 shows the weather charts when these two typhoons were closest to Osaka Bay. In the case of NO. 1, the typhoon passed on the north side of Osaka Bay. In the case of NO. 2, the typhoon passed on the south side.

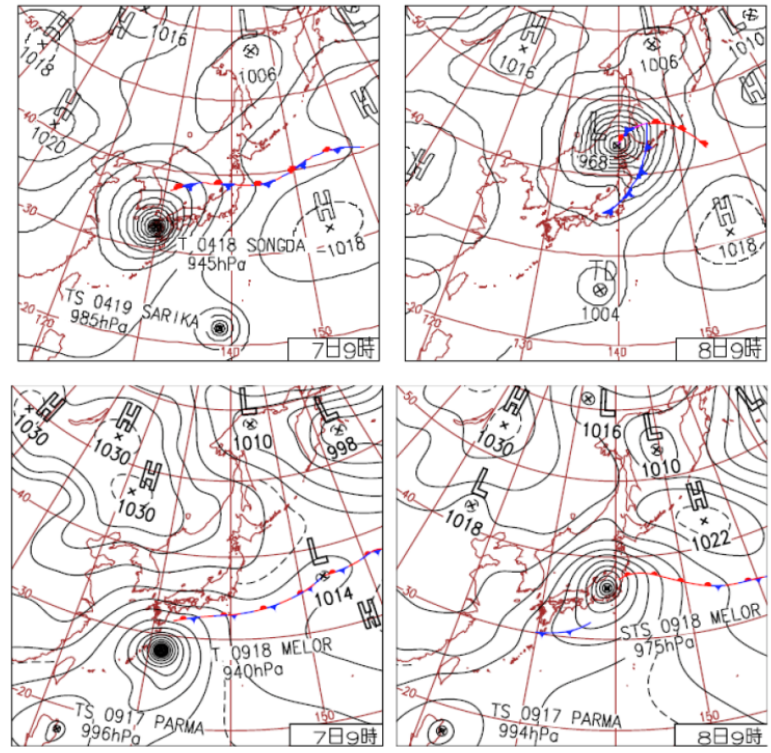

(Upper Weather Charts) NO. 1 Typhoon: September 7, 8, 00:00 UTC, 2004
(Lower Weather Charts) NO. 2 Typhoon: October 7, 8, 00:00 UTC, 2009

Fig.2.4. Weather charts of simulated typhoons

As shown in Fig.2.5, three domains for nesting were calculated in each case to simulate winds more accurately. In both cases, the vertical grid is 28 from top pressure to ground pressure. Detailed information calculated by WRF is shown in Table.1.

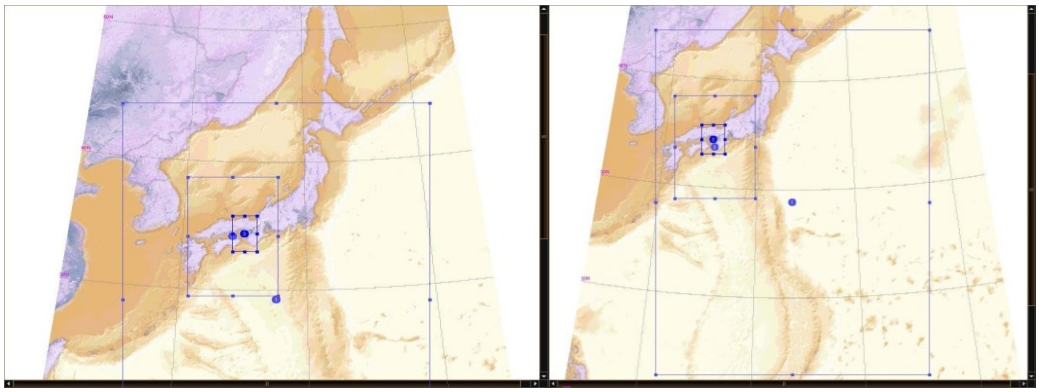

Fig.2.5. WRF Domain for wind calculation in Osaka Bay

Table.2.1. Calculation settings of WRF calculation in the Osaka Bay case

	NO. 1 typhoon			NO. 2 typhoon		
	d01	d02	d03	d01	d02	d03
Dimensio n	100x150x2 8	88x136x2 8	73x124x2 8	100x132x2 8	88x118x2 8	76x100x2 8
Mesh size	23.10 (km)	7.70 (km)	2.56 (km)	27.20 (km)	9.06 (km)	3.02 (km)
Time step	60(s)	20(s)	6.6(s)	60(s)	20(s)	6.6(s)
Start time	2004-09-02-00:00:00 UTC			2009-10-03-00:00:00 UTC		
End time	2004-09-08-00:00:00 UTC			2009-10-09-00:00:00 UTC		

As shown in the Fig.2.6, a strong south wind blew when the NO.1 typhoon was closest to Osaka Bay, while a strong north wind blew in the case of NO.2 typhoon. The calculated wind velocity and direction were compared with the observation data from JMA (Japan Meteorological Agency). They are mostly consistent when these two typhoons were closest to Osaka Bay, which was also the time period the simulation was conducted. Complicated topography, such as the mountains located around Osaka Bay and the artificial islands along the coastline, may contribute to the difference, as shown in Fig.2.7.

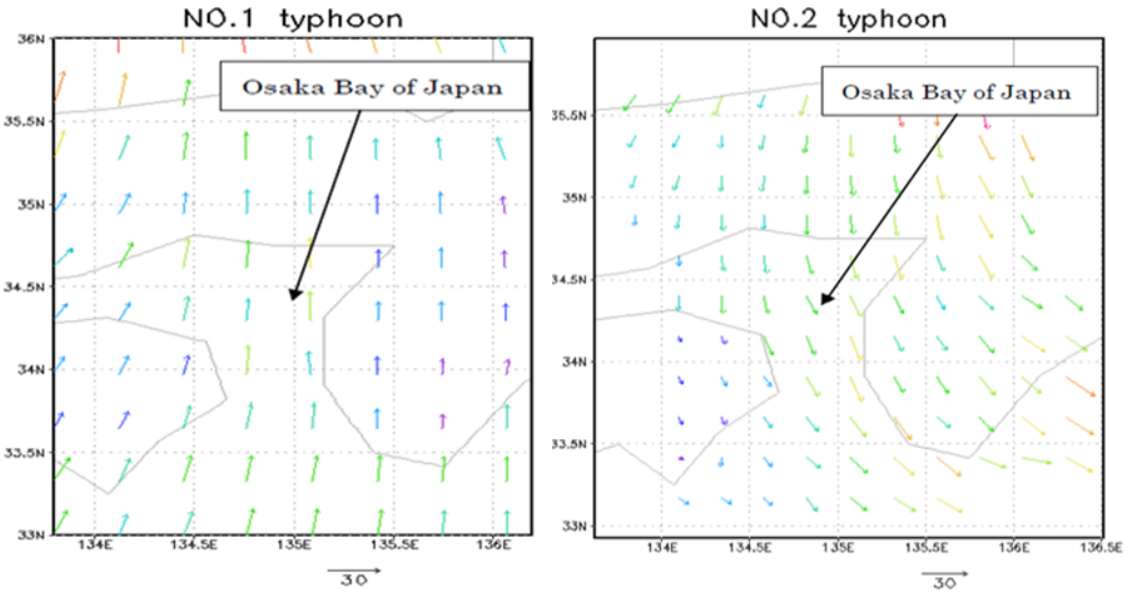

Fig.2.6. Surface wind distributions in Osaka Bay

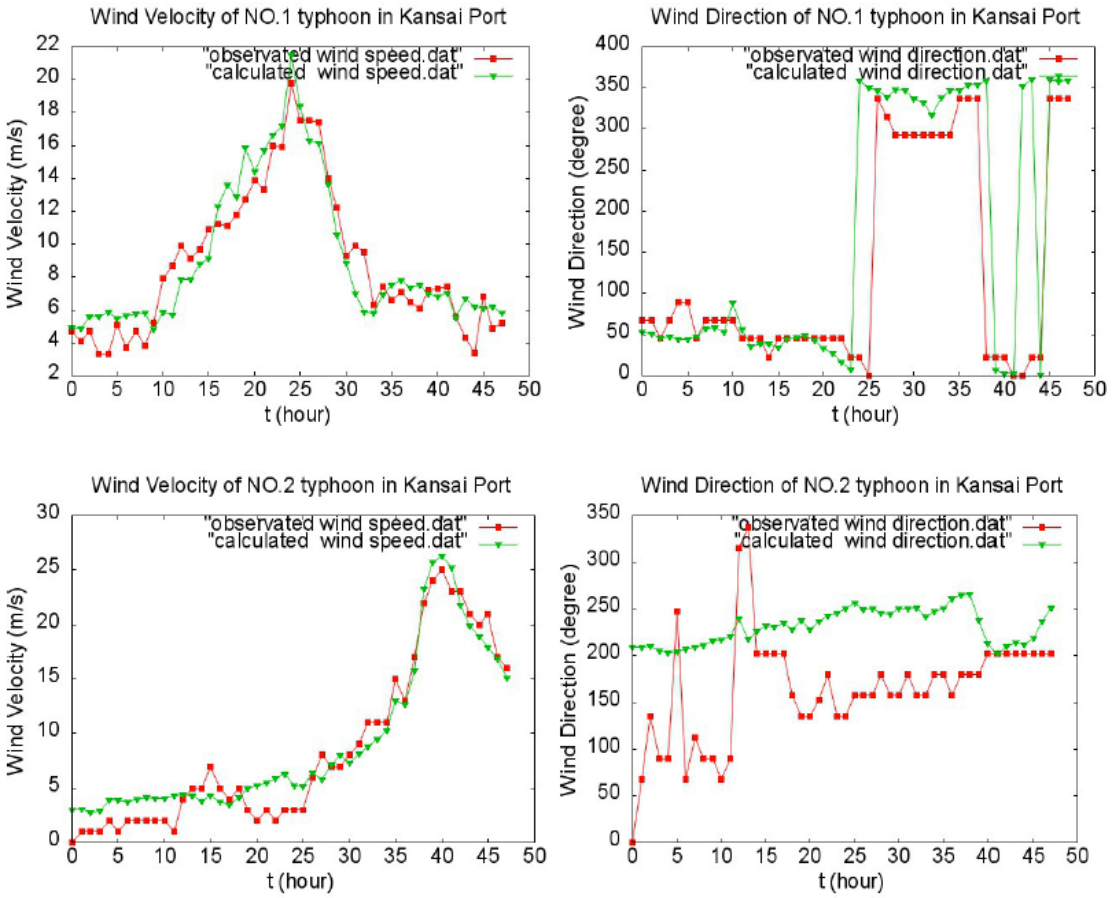

Fig.2.7. Comparisons of wind velocity and direction.

For calculation of tidal current in the Osaka Bay, the high-resolution wind speed and direction 10 meters above the sea surface calculated from the nesting WRF was put into the tidal simulation conducted by POM where the grid divisions in the x and y directions are the regular mesh while in the vertical direction is the sigma coordinate system. In these two typhoon cases, the grid number is 528 x901 (NO. 1 typhoon) and 648 x855 (NO. 2 typhoon) in the x-y axis. The horizontal grid interval of Δx and Δy is 50m in the calculation areas in both cases. The calculation time interval is 2 seconds for both cases.

The velocity distributions of the surface tidal current in Osaka Bay when these two typhoons were closest are shown in Fig.2.8. The sea level height between observation and POM calculation was compared in Fig.2.9. The change of surface current distribution, which is the main factor affecting ship navigation, was dramatic. The obvious influence of a typhoon on the tidal current can be found at the same time.

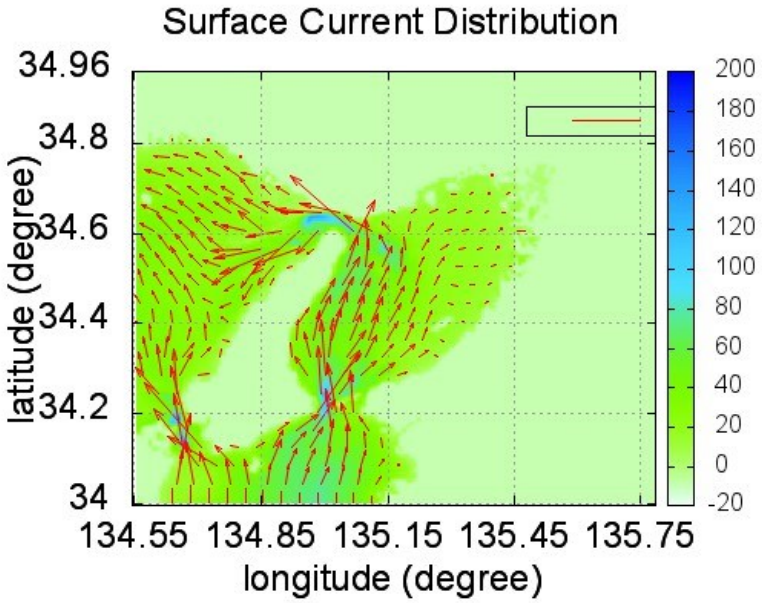

(A)

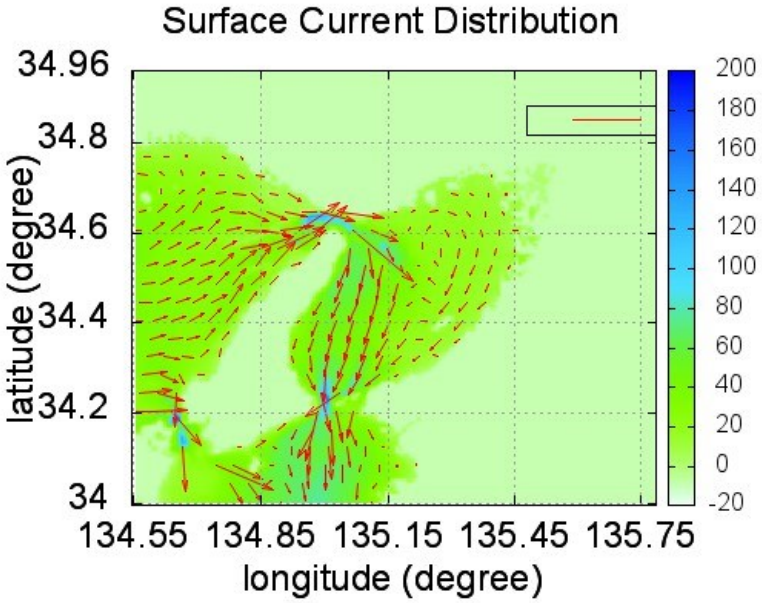

(B)

Fig.2.8-A, B. Surface current distributions in these two typhoon cases

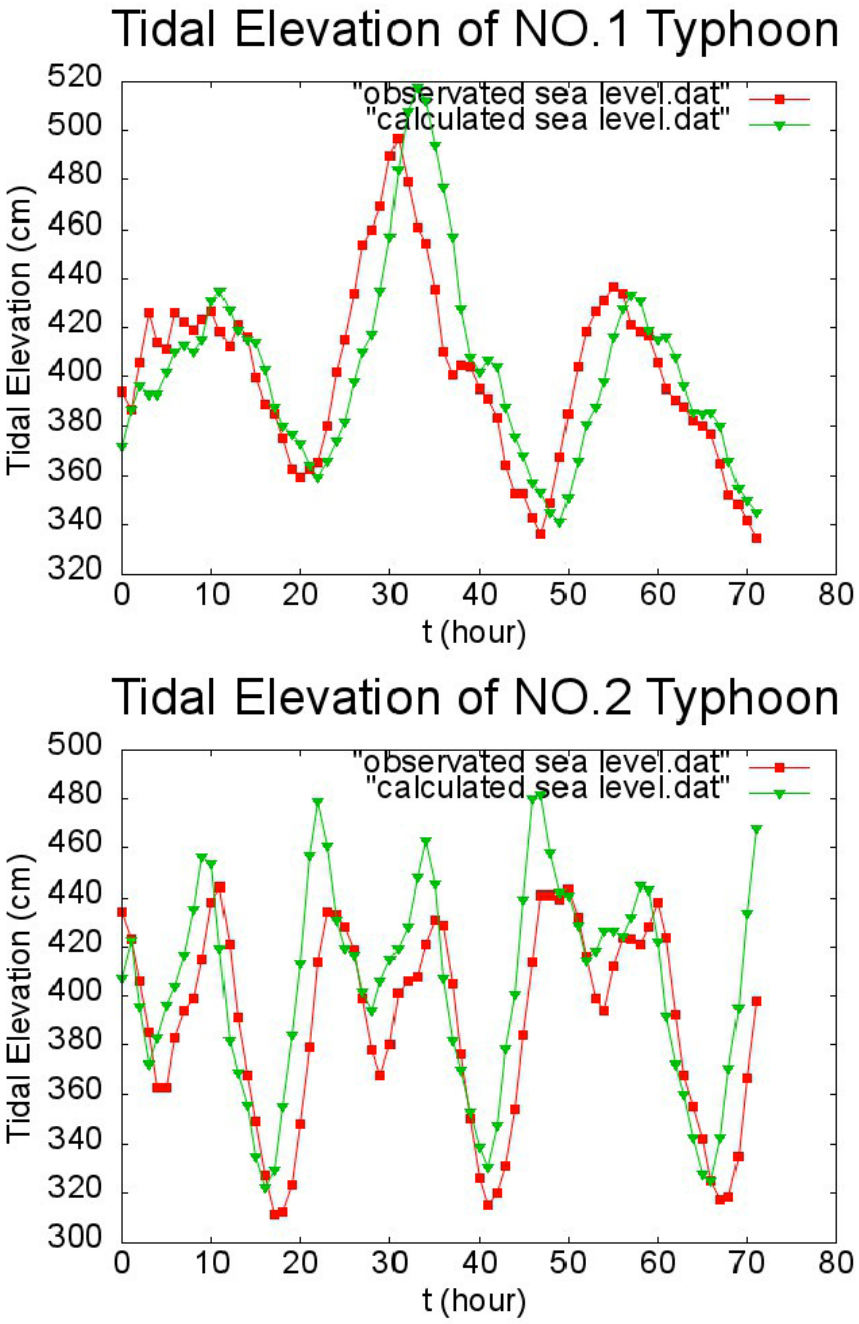

Fig.2.9. Comparison of sea level between observation and POM calculation

After the wind and tidal current data were generated, the wave calculation has become possible. Here, the wind data calculated by the weather simulation model WRF is put into SWAN as the surface wind stress, and the tidal current data is input as the boundary condition, which affects the wave height and period.

The maximum water depth of the regular grid interval of Δx and Δy is set to 300m. The mesh size is about 0.5 km, and the calculated time step is 10 seconds. The number of frequencies is 30 (0.04Hz-1Hz), and the number of meshes in θ is given 36 (every 10 degree). As shown in Fig.2.10, the calculated wave height was verified by the observed wave height of NOWPHAS (Nationwide Ocean Wave information network for Ports and HArbourS).

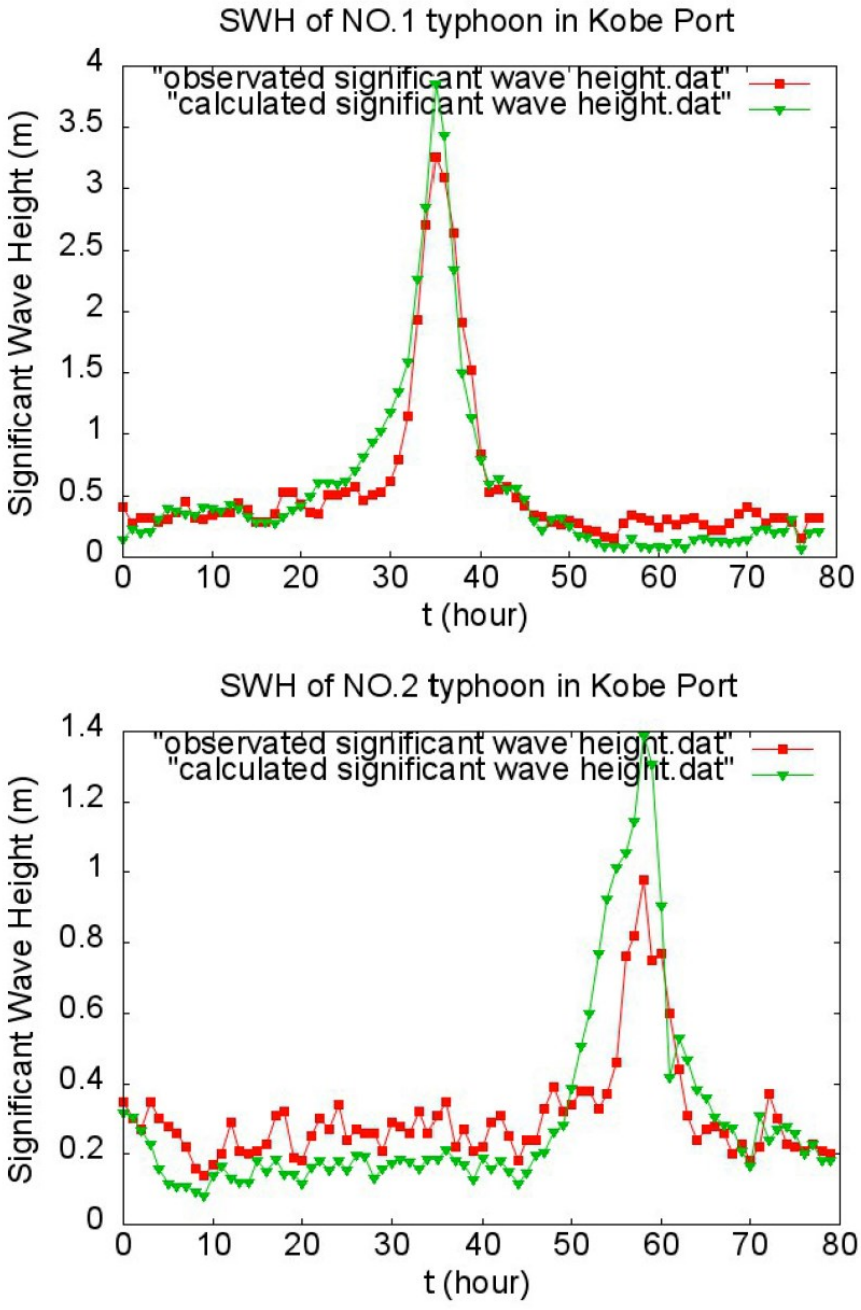

Fig.2.10. Comparison of calculated and observed significant wave height

The results of the wave calculation are shown in Fig.2.11-A, B. Comparing the simulation with observation data, it can be proven that the simulation by SWAN agrees with that of WRF. Regardless of the differences between the simulation and observation data, the larger simulation values should be owned to the larger calculated wind speed by WRF.

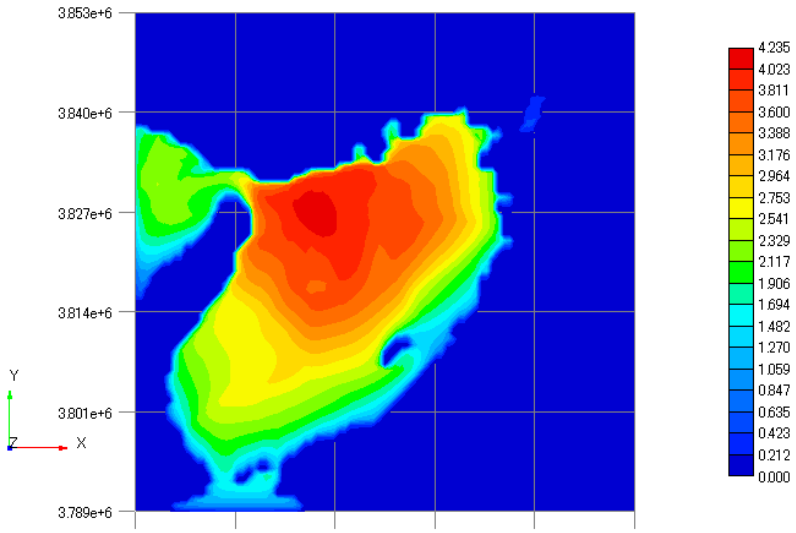

(A)

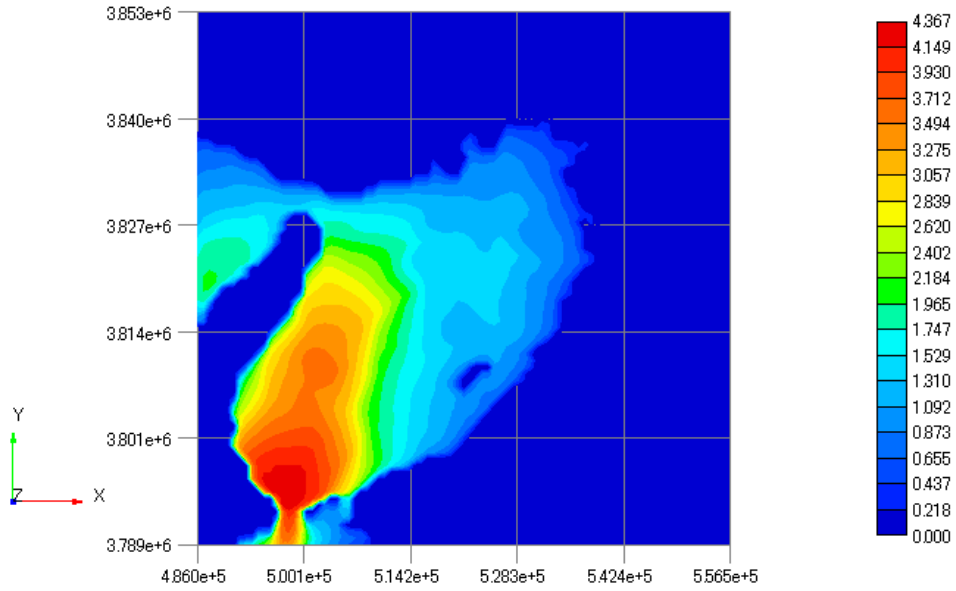

(B)

Fig.2.11-A, B. Distributions of significant wave height in two typhoon cases

2.2.2 The East China Sea Area (ECSA)

As an important area for ships such as tankers, LNG ships and cargo ships sailing from the East Asian countries to South Asian and also European countries through the Malacca Strait and the Suez Canal, the East China Sea is a busy shipping area, which has an important role on shipping, especially with the greatly increasing production effects of countries like China. The geography of the East China Sea Area and main shipping routes in the ECSA are shown in Fig.2.12 and Fig.2.13, respectively.

Fig.2.12. Geography of the East China Sea Area (ECSA)

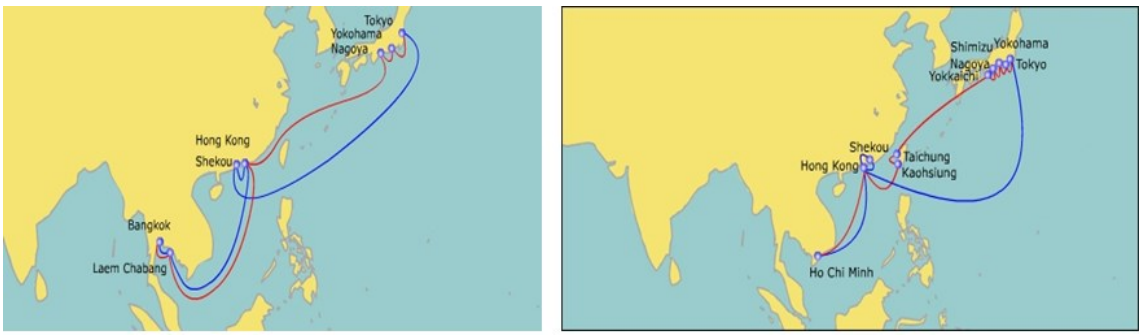

Fig.2.13. Main shipping routes in the ECSA

According to the relation between ship accidents and typhoons and he found that in the East China Sea by A.Toffolia. et al (A.Toffoli, et al., 2005), where approximately 15% of the accidents took place, is characterized by a mean significant wave height lower than 3 m and mean wave steepness larger than 0.025. Those regions (commonly tropical seas) are often prone to typhoons (as shown in Fig.2.15). With increasing fuel costs as well as environmental-protection requirements, the influence of ocean currents on ship navigation also calls for attention, especially for those areas heavily affected by strong ocean currents.

Additionally, with the increase of global warming influence, both the number and strength of those tropical storms happened in this area has become huger and more powerful in recent years. Besides, the Kuroshio Current can also affect shipping cost because of its high speed. Therefore, the strong western-boundary ocean current as well as the powerful typhoons which have a higher possibility to reduce fuel cost by using ocean current and a higher risk to keep safe in cases of typhoon-induced ocean waves., shown as Fig.2.14 and Fig.2.15, should also be paid attention to, considering about the economics and safety of ship navigation.. Therefore, to make safe and economical ship navigation here, the numerical ship navigation system is of great importance.

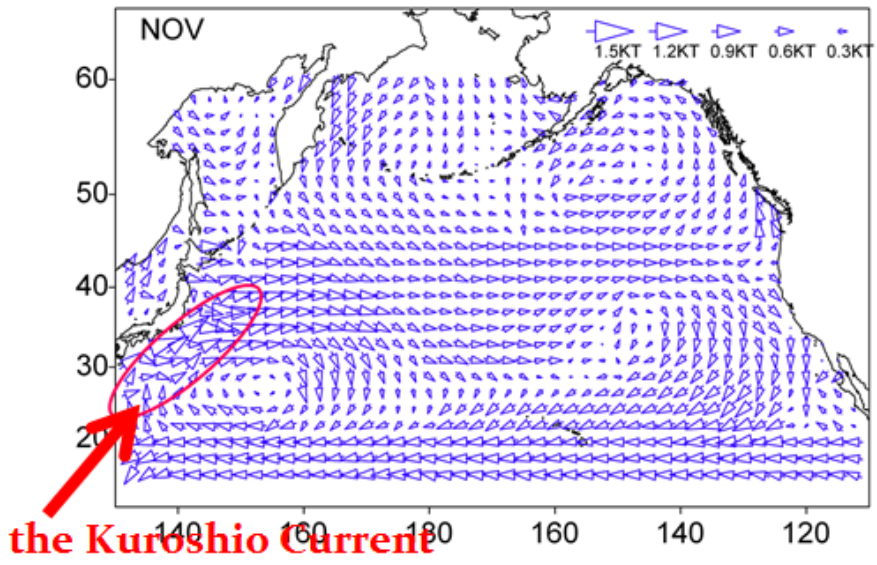

Fig.2.14. Ocean current data of the North Pacific (Current Chart data; long-time mean; November)

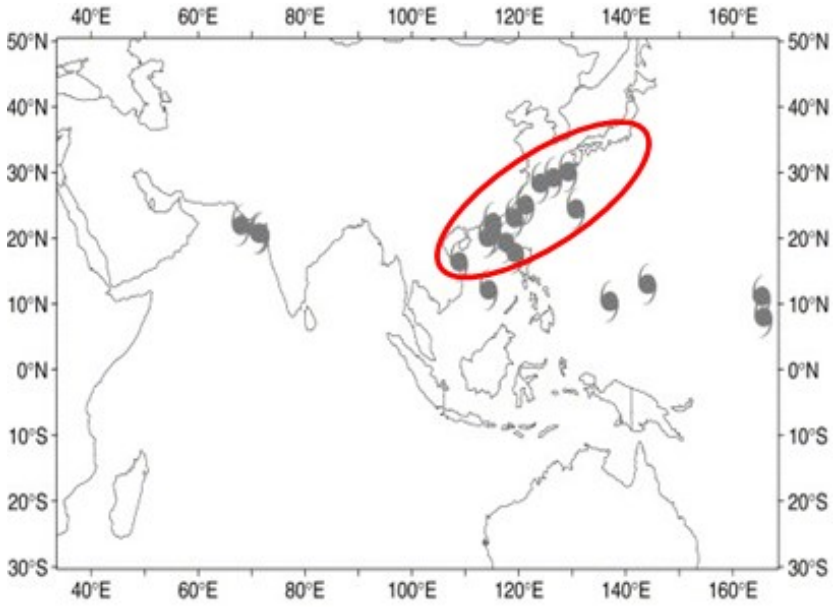

Fig.2.15. Locations of ship accidents that occurred during tropical typhoons

For wind calculation in the ECSA, a representative typhoon (SONGDA) observed in the East China Sea was selected. Having a lifetime of 186 hours, SONGDA had a minimum pressure of 920 hPa and maximum wind speed of 105 knots. Besides, it had a largest diameter of storm wind of 140 miles. WRF was run on 18 km horizontal resolution numerical grid with 28 vertical sigma levels. A 6km nested grid was initialized to provide higher resolution for the modeling of the low pressure. The grid numbers are respectively 180 x 150 x 28 for domain1, 286 x 283 x 28 for domain2 in the x-y-z axis. The Table.2.2 shows the detailed parameters of the WRF calculation. The simulated terms is 120 hours from 25th May, 2011, 00:00 UTC to 30th May, 2011, 00:00 UTC. Fig.2.16 shows the typhoon track and key information from the National Institute of Informatics (NII).

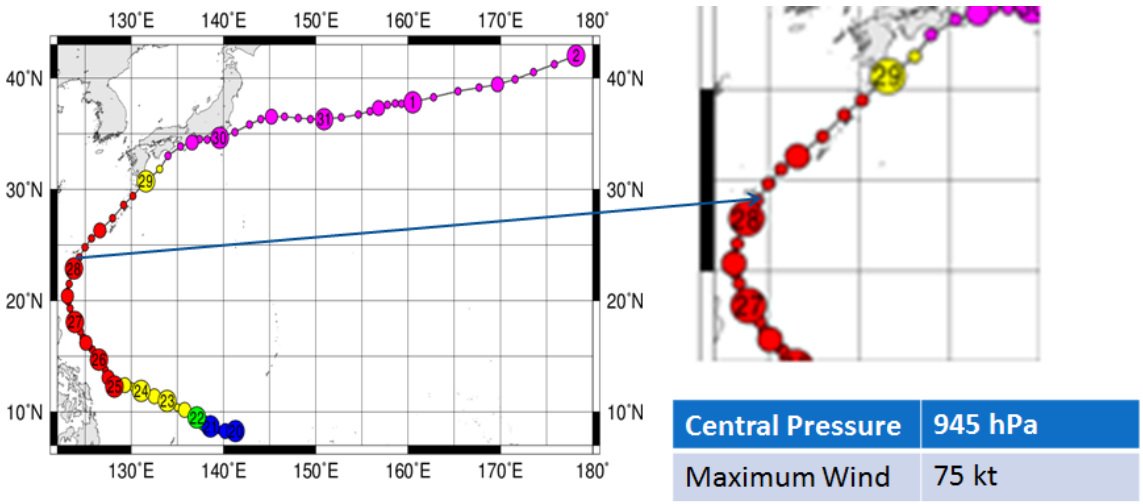

Fig.2.16. Typhoon track and key information from the National Institute of Informatics

Table2.2. Calculation settings of WRF calculation in the ECSA case

	Domain01	Domain02
Dimension	180 x 150 x 28	286 x 283 x 28
Mesh size	18km	6km
Time step	60 (s)	12 (s)
Microphysics	Lin et al. scheme	
Long wave Radiation	RRTM scheme	
Planetary Boundary layer	Yonsei University scheme	

In the calculation, the GFS-FNL data were used as boundary data for the WRF-pre-processing. The Global Forecast System (GFS) is operationally run four times a day in near-real time at NCEP. GFS-FNL (Final) Operational Global Analysis data are set on 1.0 x 1.0 degree grids every 6 hours. Full details of the NCEP/NCAR project and the dataset were given in Kalnay et al (Kalnay et al, 1996).

To verify the model accuracy, the simulated wind data were verified by the wind observed at Kitahara station and Naha station from the AmeDAS, the system of the Japan Meteorological Agency. The validation s of wind speed and direction are shown in Fig.2.17. The horizontal axis shows the time series in hours. The vertical axis shows

the wind speed and wind direction, respectively. Both wind speed of WRF and observation have same variation as time changes, however, WRF overestimated wind speed of about 2 m/s when the pressure reached its lowest value in the Kitahara station.

Fig.2.18 shows the 10-meter wind velocity distributions from WRF model at the same time and area with the simulation of ship navigation. Extreme low pressure generated strong anti-clockwise wind as the typhoon just arrived at its mature period.

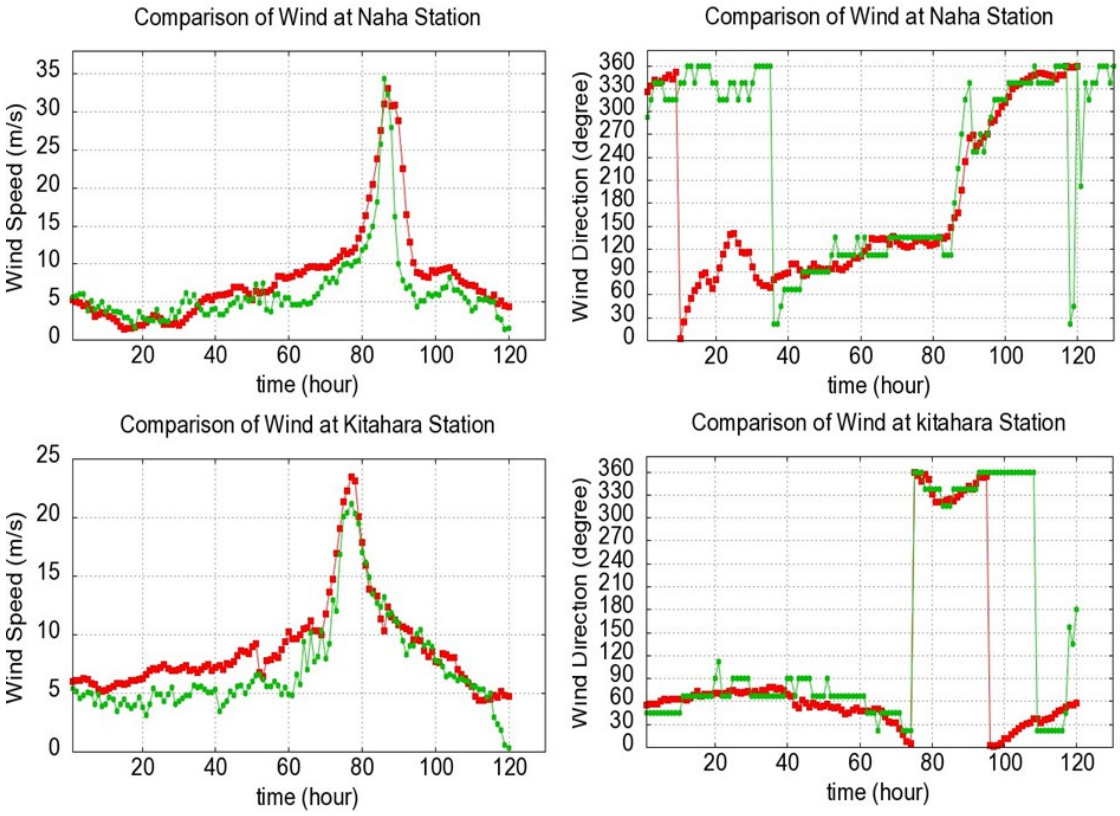

Fig.2.17. Comparison of WRF calculation and JMA observation

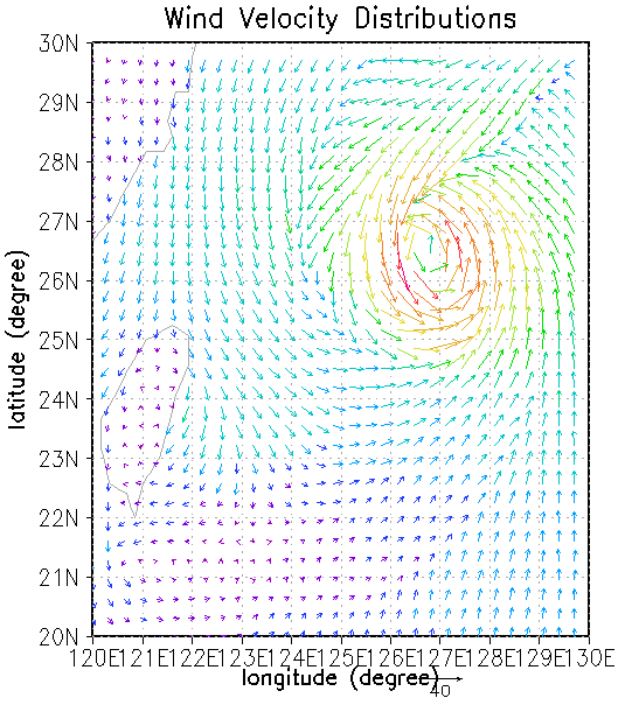

Fig.2.18. Wind velocity distributions from WRF model at 21:00, 28th, May, 2011 (UTC)

The 10 meter ocean surface wind generated by WRF has been used for wave calculation in the ECSA. Cubic spline data interpolation method was used to generate appropriate wind fields to match the spatial and temporal resolution of SWAN. The SWAN model was set to a resolution of 1km covering the ship navigation area. The minimum water depth in the model is 10 m and the time step is 5 min. The wavenumber grid is divided by 30 from 0.04 to 1 Hz and the wave direction spacing is 6. Table.3 gives the detailed parameters of wave calculation.

Table.2.3. Parameter Settings of Wave Calculation in the ECSA case

ECS Case	Parameter Setting
Dimension	1100*1100
Mesh size	1(km)
Time step	5(min)
Number of frequencies	30(0.04Hz-1Hz)
Number of meshes in θ	60

The distribution of significant wave height in the calculation area is also shown as Fig.2.19. The scale of the direction “from 0 to 1100” means the number of the mesh in the model simulation. A maximum value of about 12 meters can be found, affected by the low pressure of about 940 hPa.

In the Fig.2.20, the calculated significant wave height was verified by the observed significant wave height in the Nakagusuku-wan station (127°57′55″E, 26°14′32″N) every 20 minutes from NOWPHS. SWAN wave model well calculated the significant wave height when it reached peak value. However, the SWAN overestimated the significant wave height around the peak time at the Nakagusuku-wan station, which can be owed to the overestimation of wind speed from WRF at the nearby Naha station ($127^{o}41'1^{"}\mathrm{E}, 26^{o}12'4^{"}\mathrm{N}$), see Fig.33.

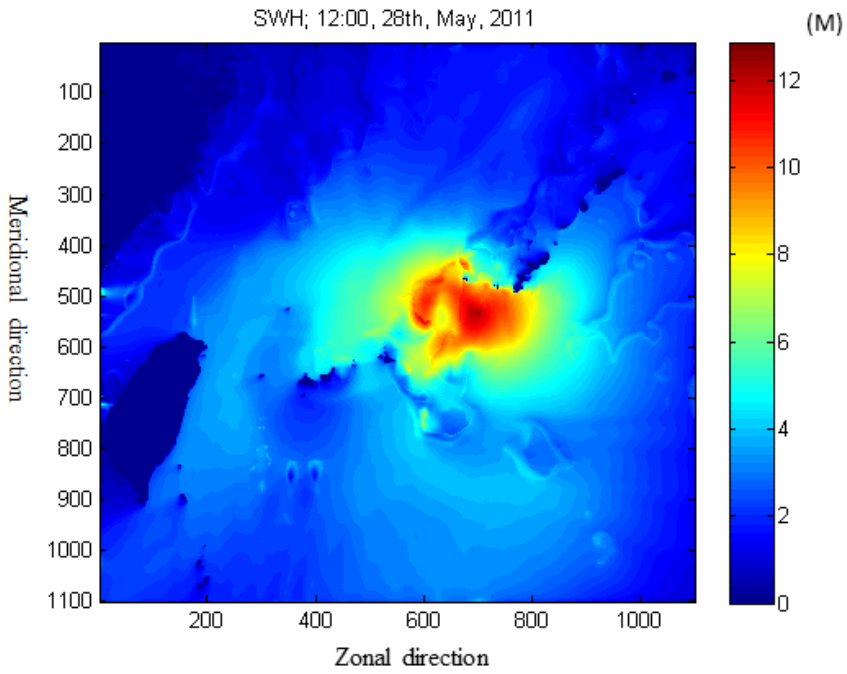

Fig.2.19. Distribution of significant wave height at 21:00, 28th, May, 2011 (UTC)

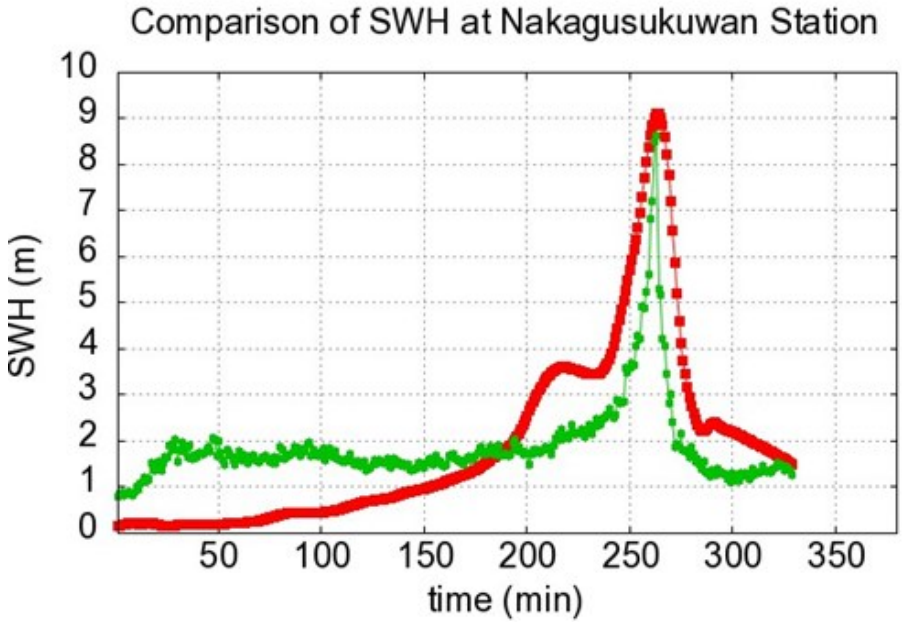

Fig.2.20. Comparison of Significant Wave Height between SWAN calculation and NOWPHAS observation

As for current routing, several studies have been made. Benjamin Franklin's chart of the Gulf Stream, made in 1796, has been beneficial for centuries (Bishop, 1984). In 1991, Lo et al. argued that by optimal ocean current routing, 10 million dollars (based on 1986 dollars and fuel costs) could be saved annually for the U.S. shipping industry—despite his underestimating special areas with strong currents, such as the western boundary currents, including the Gulf Stream; the Kuroshio Current and the Agulhas, Brazil, and East Australian currents. Another estimation made by Lo and McCord (1995) estimated that for a ship sailing at 16 knots, a 7.5% and 4.5% fuel saving could be achieved by riding favorable currents and avoiding unfavorable currents, respectively. Yu-Chia Chang et al. (2013) built a map of the Kuroshio Current axis in East Asia from the Surface Velocity Program (SVP) data and found that for ships sailing at a speed of 12 knots for approximately 1100 nm, the transit time could be shortened by 1.8% when riding favorable Kuroshio Currents.

For the model calculation of the Kuroshio Current, several studies have been conducted before.

Sekine and Kutsuwada (Sekine et al., 1994) used a primitive two-layer numerical model

with a rather coarse grid size of 1° × 1°, which illustrated that the model resolution appeared to be too coarse horizontally and vertically to resolve the details of the Kuroshio Current recirculation region.

Kagimoto and Yamagata (Kagimoto et al.,1997) ran a high-resolution eddy-resolving Pacific Ocean Model using a bottom-following vertical coordinate system to mimic the Kuroshio Current; they showed that in comparing model results with observations, a suitable model resolution is important for resolving locations of observations as well as essential dynamics related to the interaction between baroclinic ocean currents and bottom topography.

Guo and Yamagata (Guo, et al., 2003) applied a triply nested ocean general circulation model based on a POM to examine how the model's horizontal resolution influences the Kuroshio Current in the East China Sea (ECS) and the sea level variability. They argued that the higher-resolution model improves the baroclinic as well as the barotropic component of the Kuroshio Current and, thus, could reproduce more realistic density and current fields.

Other researchers have also made efforts to study the Kuroshio Current. Wakata (Wakata et al., 2006) employed an ocean general circulation model (OGCM) with a horizontal resolution of 0.25° × 0.25° and investigated the inter-annual variability of the Kuroshio Current volume transport. They found that, different from the time series with a timescale of several years, where the peaks and troughs of the Kuroshio Current volume transport are induced by wind stress curl locally and immediately eastward, the longer timescale variability was also induced by wind stress curl near the dateline.

Oey (Oey, et al., 2013) developed a data-assimilated Taiwan Ocean Prediction (ATOP) system based on two different forecast domains that covered the entire North Pacific Ocean at 0.1° × 0.1° horizontal resolution and 41 vertical sigma levels, and a smaller western North Pacific domain with the same horizontal resolution. The system showed that the simulations of the Kuroshio Current intrusion in the northern South China Sea and the subtropical counter current agreed well with observations of satellite altimetry data, which could also prove the high probability of the Kuroshio Current simulation using modern ocean models.

However, the quantitative effect of the Kuroshio Current on ship navigation based on

high-resolution ocean models has rarely been addressed in previous studies. Currently, owing to high-performance computers developed recently, a high-resolution numerical simulation of the Kuroshio Current has become available.

In this study, I will investigate how to quantitatively evaluate the effect of the Kuroshio Current on ship navigation in the East China Sea area. It is worth mentioning that the Kuroshio Current system sometimes experiences transitions from a relatively stable state to an unstable state in the areas south of Japan, including a period in late 2004. The areas of transition in the Kuroshio Current's dynamic state are not included in the present research.

The Princeton Ocean Model was used to calculate the Kuroshio Current in this study. As a three-dimensional, primitive equation ocean model, it includes thermodynamics and the level 2.5 Mellor-Yamada turbulence closure and uses a sigma coordinate in the vertical to resolve the variations of bottom topography (Blumberg et al., 1987; Mellor, 1998). Originally, the POM was designed for coastal waters, since the sigma-coordinate system can well resolve complex topography in the coastal region. However, it has also successfully simulated large-scale ocean circulations in recent years (Ezer, Mellor, 1997). For our purpose, which is to investigate the ocean surface current system, the POM model seems to be the proper model to select as our basic model.

The model covers the area from 30S to 65N and 100E to 70W in the meridional and zonal directions, respectively. The topography used in the simulation model was obtained by interpolating data from the ETOPO1 (1-min gridded elevation data) bathymetry database (Amante, B. W. Eakins, 2009), with a minimum and maximum depth of 10 m and 6000 m, respectively. The topography of the POM calculation area is given in Fig.2.21, with a contour interval of500 meters. The horizontal coordinate used here is the Mercator; with a horizontal resolution of 0.1×0.1degrees, 30 sigma vertical coordinates with a finer resolution in the upper layers are adopted. The sigma layers are as shown in Table.4.

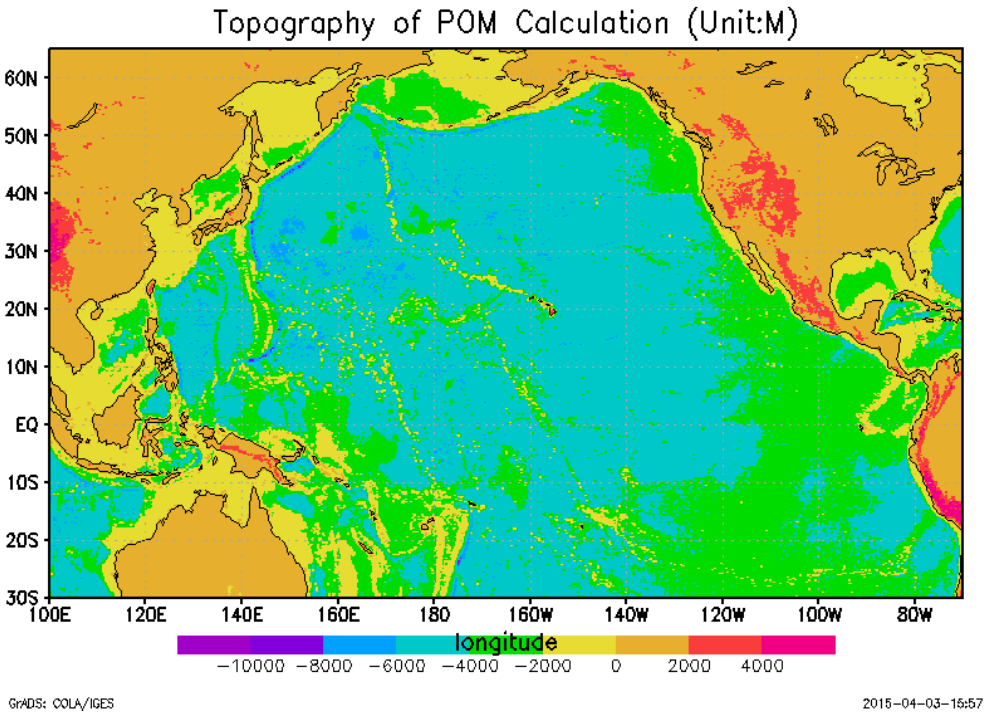

Fig.2.21. Bottom topography of the POM model. The contour interval is 500 m. The maximum depth is artificially fixed at 6000 m.

Table.2.4.Values of the vertical sigma coordinates used in the POM

Layer	Sigma coordinate value	Layer	Sigma coordinate value
1	0.0000	16	-0.4722
2	-0.0006	17	-0.5277
3	-0.0013	18	-0.5833
4	-0.0026	19	-0.6389
5	-0.0052	20	-0.6944
6	-0.0104	21	-0.7500
7	-0.0208	22	-0.8056
8	-0.0416	23	-0.8611
9	-0.0833	24	-0.9166
10	-0.1389	25	-0.9583
11	-0.1944	26	-0.9792
12	-0.2500	27	-0.9895
13	-0.3055	28	-0.9947
14	-0.3611	29	-0.9982
15	-0.4166	30	-1.0000

A smoothing of the topography was conducted following the criteria of 0.2 (see Mellor, et al., 1994):

$$\frac{|H_{i+1}-H_i|}{(H_{i+1}+H_i)} \leq \alpha \quad (1)$$

Where H_{i+1} and H_i are the depths at two adjacent grids, and α is a slope factor set as 0.2. The turbulent kinetic energy and a macroscale length of turbulence at the open boundaries are set to the value of (10^{-10}) in the POM.

The POM is driven by wind stresses, heat fluxes, and salt fluxes applied at the sea surface, with all lateral boundaries set to be solid boundaries for simplicity. This is acceptable because the southern boundary is set to be 30S, far away from the Kuroshio Current region.

The model is forced to run from a state of rest with the annual mean temperature and salinity of the World Ocean Atlas (WOA94) (Levitus, et al., 1994; Levitus, S., T. P. Boyer, 1994).

Additionally, a relaxation of the sea surface temperature and sea surface salinity was applied as described in Wakata (Wakata et al., 2006). The National Center for Environmental Prediction (NCEP)'s monthly mean wind stress data (Kistler, et al., 2001) were used for the surface boundary conditions in the 18-year spin-up process, considering the Rossby wave influence.

During the hindcast phase from January 1992 to December 2012, the daily mean wind stress and the SST data from the NCEP data are used instead of the monthly wind stress and SST data.

According to the CFL condition, the barotropic time step is set to 20 s, while the baroclinic time step is set to 1200 s. The other relevant parameters, such as HORCON and TPRNI, are set to 0.1 and 0.5, respectively (Mellor, 1998).

After the model spin-up, calculations are continuously carried out for the hydro- and thermodynamic parameters for the time period from January 1992 to December 2012. The key settings of POM model calculation can be found in Table.2.5.

Table.2.5. Key settings of POM model calculation

Area	80E~70W, 30S~65N
Time step	20 sec
Horizontal Mesh	0.1 × 0.1 degree
Vertical mesh	30 sigma layers
Calculation time period	Jan, 1992 to Dec, 2012
Boundary conditions	Etopo1; NCEP reanalysis; World Ocean Atlas SST &SSS

Before the POM results are used for numerical simulations of ship navigation, they are verified and compared with observations.

Fig.2.22.A, B show the time mean sea surface height in the Northwestern Pacific Ocean (NWPO) and in the ECSA, respectively. Fig.23 shows the time-mean surface current velocity distribution in the ECSA. As it illustrates, the Kuroshio Current flows northeastward along the continental slope in the ECS and turns eastward around 31°N somewhat northward near Japan.

The results agree well with the study of Chang, et al (Chang, et al. 2013), which applied the velocity of the Kuroshio Current from the SVP data, shown as Fig.2.24 and Fig.2.25. Its strength and path in the navigation simulation area are well reproduced, to some extent, considering the model resolution.

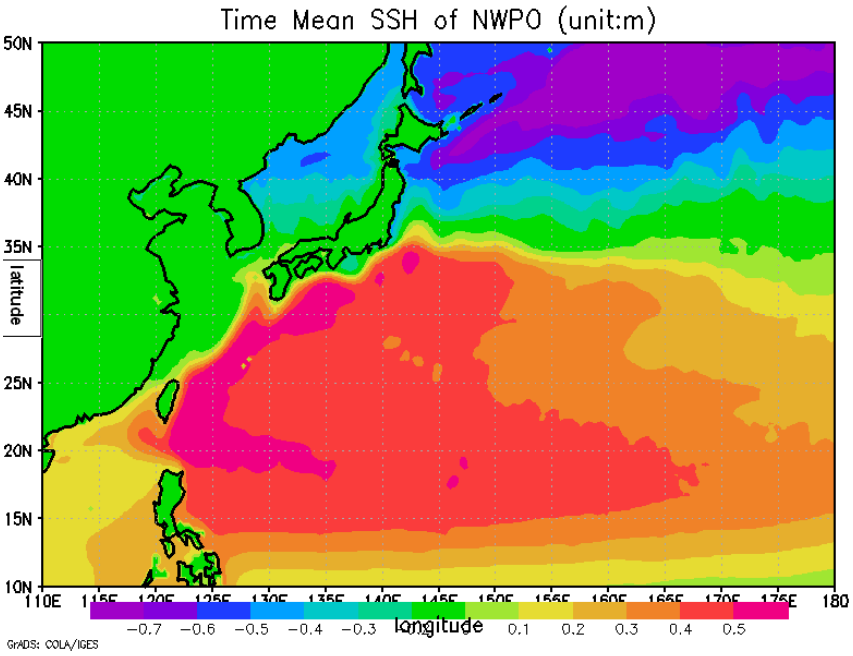

(A)

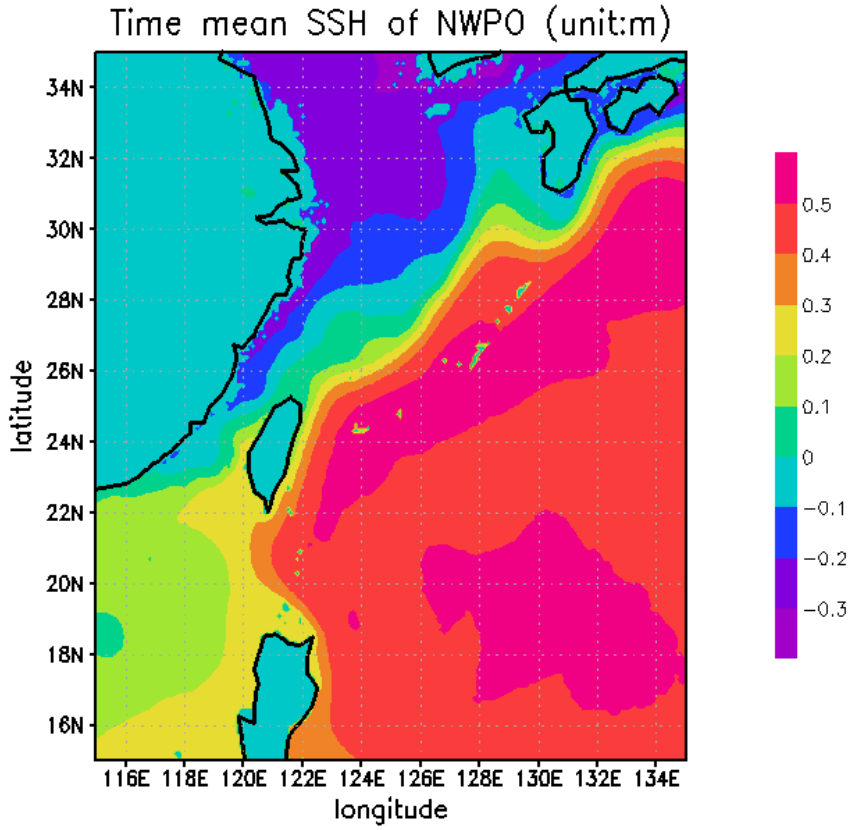

(B)

Fig.2.22-A, B. Time mean sea surface height in the hind cast process

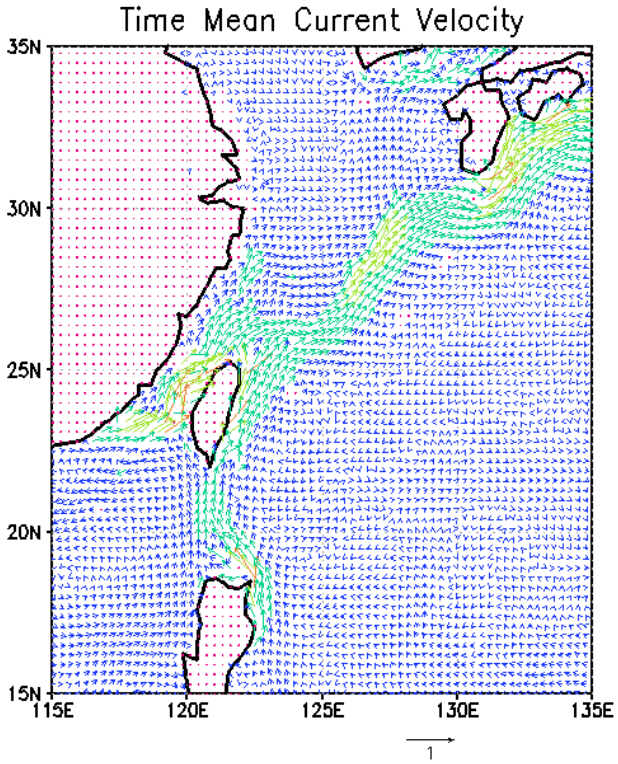

Fig.2.23. Averaged ocean surface current vector distribution of the calculation area by POM; 0.1*0.1 degree; 1992-2012.

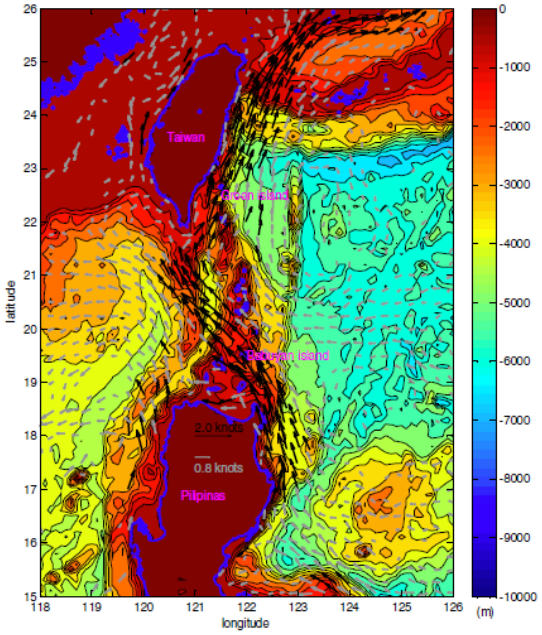

Fig.2.24. Enlargement of bin-averaged velocity east of Luzon and Taiwan.

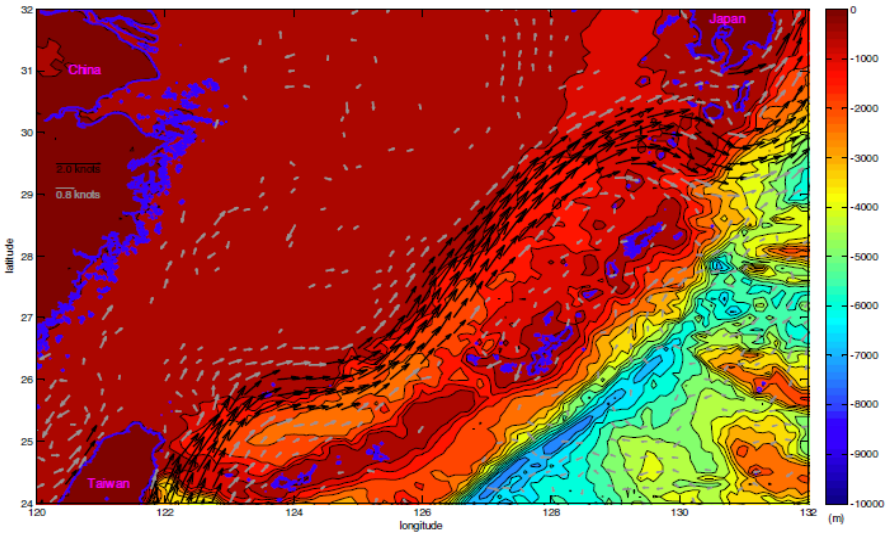

Fig.2.25. Enlargement of bin-averaged velocity in the East China Sea.

Additionally, Fig.2.26 A–C show a comparison of the Sea Surface Height Anomaly (SSHA) data from both the model results and the Japan Oceanographic Data Center (JODC) observation data at several representative stations northeastward along the continental slope in the ECS, including Ishigaki, Naha, and Tanegashima, with locations shown in Fig.2.27.

To avoid the influence of convection from spin-up to hind cast simulation, only the data from 2001 to 2010 is used in making the comparison. As the figures show, the X-axis is the time period with a unit of days, while the Y-axis is the SSHA data with a unit of meters.

The correlation coefficients of the SSHA in these three stations are calculated as 0.3821, 0.4341, and 0.5122, respectively. The low correlation coefficients may result from the locations of these three stations, which are rather far from the Kuroshio Current main path but close to the land area where the landscape has an influence.

However, all of these figures show a tendency of agreement about the peaks and troughs, simultaneously confirming the model results.

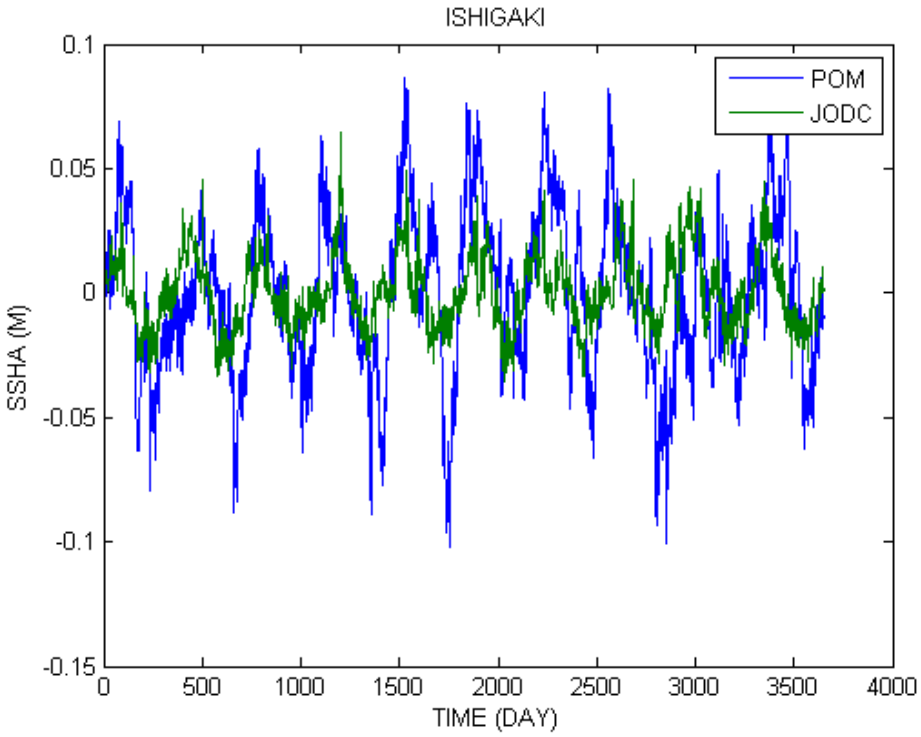

(A) ISHIGAKI

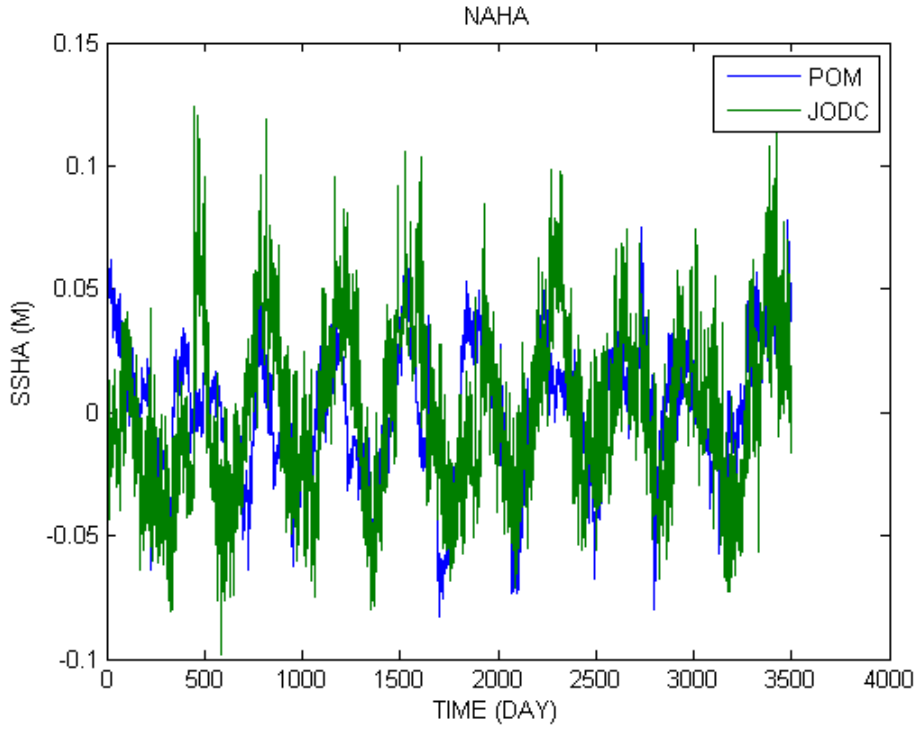

(B) NAHA

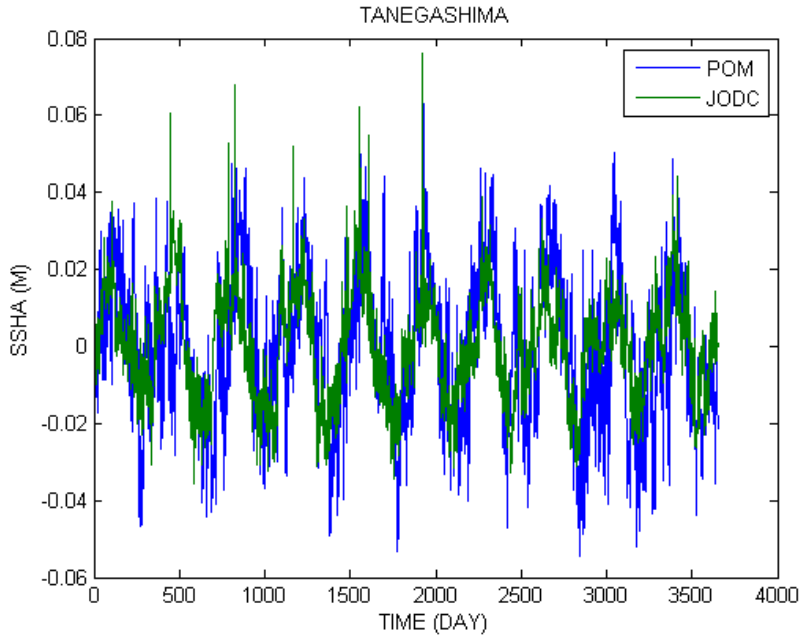

(C) TANEGASHIMA

Fig.2.26.A–C. Comparison of daily mean Sea Surface Height Anomaly (SSHA) data between the model calculation and the JODC observation in the hind cast process

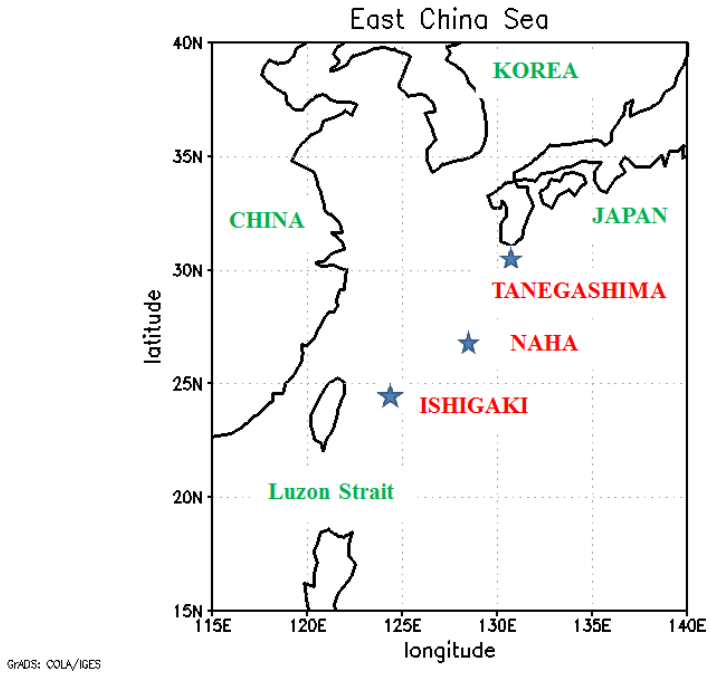

Fig.2.27. Locations of SSH observation stations along the continental slope in the ECSA

The above comparisons validate the simulations based on the POM numerical model, and the influence of the currents on ship navigation will be calculated based on a time period in the above POM hindcast process in the following section.

2.3 Global Scale

Instead of the above-applied regional models, global scale atmospheric and oceanic including the Multi-Scale Simulator for the Geoenvironment (MSSG-A & MSSG-O) and the state of the art wave model WAVEWATCH III are utilized here to generate the necessary high-resolution weather and ocean information to be used as the ocean states for numerical simulation of ship navigation.

2.3.1 Multi-Scale Simulator for the Geoenvironment (MSSG-A & MSSG-O)

As a coupled non-hydrostatic atmosphere-ocean-land model, Multi-Scale Simulator for the Geoenvironment (MSSG) has been developed in the Earth simulator Center of Japan (Takahashi, et al. 2007). To be optimized to run on the Earth simulator with high computational performance, both high performance computation and accurate calculation or precise discretization schemes are required for ultra-high resolution simulations. As it is designed for multi-scale Multiphysics simulations of weather/climate, MSSG is available with flexibility for different space and time scales of weather/climate phenomena as follows (Takahashi, et al. 2007):

(1). Global non-hydrostatic atmospheric circulation model: Global MSSG-A
(2). Regional non-hydrostatic atmospheric model: Regional MSSG-A
(3). Global non-hydrostatic/hydrostatic ocean model: Global MSSG-O
(4). Regional non-hydrostatic/hydrostatic ocean model: Regional MSSG-O
(5). Coupled Global MSSG-A Global MSSG-O: MSSG
(6). Coupled Regional MSSG-A Regional MSSG-O: Regional MSSG
(7). MSSG with Regional MSSG using nesting schemes

Because both Coriolis and metric terms have been introduced in the regional formulation, any regions in the global can be defined for the regional version models. And for regional version MSSG-A, MSSG-O and MSSG are utilized with one-way or two-way nesting schemes. And in our calculation, the one-way nesting scheme of type 5

(Coupled Global MSSG-A Global MSSG-O: MSSG), type 6 (Coupled Regional MSSG-A Regional MSSG-O: Regional MSSG) and therefore type 7 (MSSG with Regional MSSG using nesting schemes) mentioned has been utilized.

An atmospheric component of MSSG, which is called MSSG-A, is a non-hydrostatic global/regional atmosphere circulation model. Detailed compositions of MSSG-A can be found in Takahashi (Takahashi, et al. 2007).

The MSSG-A use the cloud-radiation scheme for long wave and shortwave interactions with both explicit cloud and clear-air based on the scheme in MM5. Over land, the ground temperature and ground moisture are computed by using a bucket model. As upper boundary condition, Rayleigh friction layer is set.

In the ocean component, which is called MSSG-O, detailed compositions of MSSG-A can be found in Takahashi (Takahashi, et al. 2007).

In both the atmospheric and ocean components, Yin-Yang grid system presented in Kageyama (Kageyama, and Sato, 2004) and Arakawa C grid is used. Conservation scheme was discussed in Peng (PENG, et al. 2006) and no side effects of over lapped grid system such as Yin-Yang grid were presented due to validations results of various benchmark experiments in Takahashi (Takahashi, et al., 2004a; 2004b) and Takahashi (Takahashi, et al. 2005).

Other studies by using the MSSG model can be referred to documents such as Takahashi (Takahashi, et al 2011) which studied the high performance computing of MSSG with ultra-high resolution, Takahashi (Takahashi, et al 2011) which conducted a world-highest resolution global atmospheric model and its performance on the Earth Simulator and Takahashi (Takahashi, et al 2013) which made a challenge toward the prediction of typhoon behavior and down pour.

2.3.2 WAVEWATCH III (WW3)

As a fully spectral third-generation ocean wind-wave model, WW3 has been developed at the Ocean Modeling Branch of the Environmental Modeling Center of NCEP for global and regional ocean wave prediction. WW3 was built on the base of WAVEWATCH-I and WAVEWATCH-II, which were developed at the Delft University

of Technology and NASA Goddard Space Flight Center, respectively (Tolman2009a, 2009b). However, WAVEWATCH III differs from its predecessors in all major aspects; i.e., governing equations, program structure, numerical and physical approaches.

WAVEWATCH III solves the random phase spectral action density balance equation for wavenumber-direction spectra. The implicit assumption of this equation is that properties of medium (water depth and current) as well as the wave field itself vary on time and space scales that are much larger than the variation scales of a single wave. With version 3.14 some source term options for extremely shallow water (surf zone) have been included, as well as wetting and drying of grid points. Whereas the surf-zone physics implemented so far are still fairly rudimentary, it does imply that the wave model can now be applied to arbitrary shallow water. A brief program flow chart of the WW3 model can be shown as Fig.2.28.

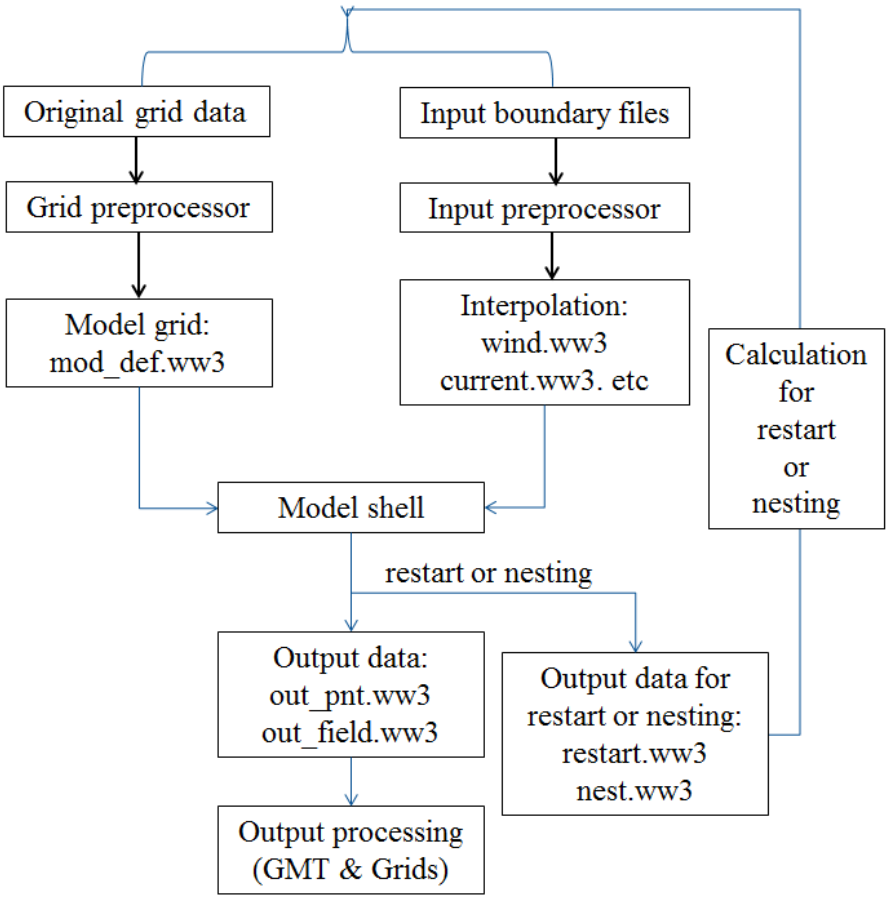

Fig.2.28. Brief program flow chart of the WW3 model

Main equations of WAVEWATCH III are described here following the WW3 user manual. And for more detailed information, the WAVEWATCH III user manual (Tolman, 1999) can be referred to.

(1) Governing Equation

As we know, phase parameters are the wavenumber vector K, the wavenumberk, the direction θ and several frequencies are generally used to describe waves or spectral wave components in water with limited depth and nonzero mean currents. A distinction between the relative or intrinsic (radian) frequency σ (= $2\pi f_r$), which is observed in a frame of reference moving with the mean current, and the absolute (radian) frequency ω(= $2\pi f_a$), which is observed in a fixed frame of reference are made when the effects of mean currents on waves are to be considered. The directionθ is by definition perpendicular to the crest of the wave (or spectral component), and equals the direction of k. Generally, scales of variation of depths and currents are assumed to be much larger than those of an individual wave.

The quasi-uniform (linear) wave theory then can be applied locally, giving the following dispersion relation and Doppler type equation to interrelate the phase parameters

$$\sigma^2 = gktanhkd \qquad (2.2.2.1)$$

$$\omega = \sigma + kU \qquad (2.2.2.2)$$

Where d is the mean water depth and U is the (depth- and time- averaged) current velocity. Wave direction can generally be ignored when the assumption of slowly varying depths and currents implies a large-scale bathymetry. The usual definition of k and ω from the phase function of a wave or wave component implies that the number of wave crests is conserved (see, e.g., Phillips, 1977; Mei, 1983)

$$\frac{\partial K}{\partial t} + \nabla\omega = 0 \qquad (2.2.2.3)$$

The rates of change of the phase parameters can be calculated by using equations from (2.2.2.1) through (2.2.2.3).

For monochromatic waves, the amplitude is described as the amplitude, the wave height, or the wave energy. For irregular wind waves, the (random) variance of the sea surface is described using variance density spectra (in the wave modeling community usually denoted as energy spectra). Within WAVEWATCH III TM the basic spectrum is the wavenumber-direction spectrum$\mathrm{F}(k,\theta)$, which has been selected because of its invariance characteristics with respect to physics of wave growth and decay for variable water depths. The output of WAVEWATCH III TM, however, consists of the more traditional frequency-direction spectrum$\mathrm{F}(f_r,\theta)$. The different spectra can be calculated from $\mathrm{F}(k,\theta)$ using straightforward Jacobian transformations

$$\mathrm{F}(f_r,\theta) = \frac{\partial k}{\partial f_r} F(k,\theta) = \frac{2\pi}{c_g} F(k,\theta) \tag{2.2.2.4}$$

$$\mathrm{F}(f_a,\theta) = \frac{\partial k}{\partial f_a} F(k,\theta) = \frac{2\pi}{c_g}\left(1+\frac{kU}{kc_g}\right)^{-1} F(k,\theta) \tag{2.2.2.5}$$

$$c_g = \frac{\partial \sigma}{\partial k} = n\frac{\sigma}{k}\ ,\ n = \frac{1}{2} + \frac{kd}{sinh2kd} \tag{2.2.2.6}$$

Where c_g is the so-called group velocity. From any of these spectra one dimensional spectrum can be generated by integration over directions, whereas integration over the entire spectrum by definition gives the total variance E (in the wave modeling community usually denoted as the wave energy).

Because of the wave action $A \equiv E / \sigma$ is conserved, the WW3 uses the wave action density spectrum $N(k,\theta) \equiv F(k,\theta) / \sigma$ within the model. The wave propagation then is described as

$$\frac{DN}{Dt} = \frac{S}{\sigma} \tag{2.2.2.7}$$

Where *D*/ *Dt* represents the total derivative of wave action density spectrum, and *S* represents the net effect of source and sinks for the spectrum *F.* Because the left side of Eq. (2.2.2.7) generally considers linear propagation, effects of nonlinear wave propagation (i.e., wave-wave interactions) arise in S. Propagation and source terms will be discussed separately in the following sections.

(2) Wave propagation

In a numerical model, a Eulerian form of the balance equation (2.2.2.7) is needed. This balance equation can either be written in the form of a transport equation (with velocities outside the derivatives), or in a conservation form (with velocities inside the derivatives).

In a large-scale application as the ECSA, the balance equation is transferred to a spherical grid, defined by longitude μ and latitude∅, but maintaining the definition of the local variance (i.e., per unit surface, as in WAMDIG, 1988)

$$\frac{\partial N}{\partial t} + \frac{1}{cos\emptyset}\frac{\partial}{\partial_\emptyset}\dot{\emptyset}Ncos\theta + \frac{\partial}{\partial_\mu}\dot{\mu}N + \frac{\partial}{\partial_k}\dot{k}N + \frac{\partial}{\partial_\theta}\dot{\theta}_g N \quad = \frac{S}{\sigma} \qquad (2.2.2.8)$$

$$\dot{\emptyset} = \frac{c_g cos\theta + U_\emptyset}{R} \qquad (2.2.2.9)$$

$$\dot{\mu} = \frac{c_g sin\theta + U_\mu}{Rcos\emptyset} \qquad (2.2.2.10)$$

$$\dot{\theta}_g = \dot{\theta} - \frac{c_g tan\emptyset cos\theta}{R} \qquad (2.2.2.11)$$

Where R is the radius of the earth and $U_\emptyset$ and U_μ are current components. Equation (2.2.2.11) includes a correction term for propagation along great circles, using a Cartesian definition of θ where θ = 0 corresponds to waves traveling from west to east. WAVEWATCH III TM can be run on either a Cartesian of spherical grid. Note that unresolved obstacles such as islands can be included in the equations.

(3) Source terms

In deep water, the net source term S is generally considered to consist of three parts, a wind-wave interaction termS_{in}, a nonlinear wave-wave interactions term S_{nl} and a dissipation (`whitecapping') termS_{ds}. The input term Sin is dominated by the exponential growth term, and this source term generally describes this dominant process only. For model initialization, and to provide more realistic initial wave growth and linear input term S_{ln} can also be considered in WAVEWATCH III TM.

In shallow water additional processes have to be considered, most notably wave-bottom interactions S_{bot} (e.g., Shemdin et al., 1978). In extremely shallow water, depth-induced breaking (S_{db}) and triad wave-wave interactions (S_{tr}) become important. Also available in WAVEWATCH III TM are source terms for scattering of waves by bottom features (S_{sc}) and a general purpose slot for additional, user defined source termsS_{xx}.

All this defines the general source terms used in WAVEWATCH III as

$$S = S_{ln} + S_{in} + S_{nl} + S_{ds} + S_{bot} + S_{db} + S_{tr} + S_{sc} + S_{xx} \qquad (2.2.2.12)$$

S_{ln} - linear input term
S_{in} - wind-wave interaction term
S_{nl} - nonlinear wave-wave interactions term
S_{ds} - a dissipation (`white-capping') term
S_{bot} - wave-bottom interactions term
S_{db}- depth-induced breaking term
S_{tr}- triad wave-wave interactions term
S_{sc} - scattering of waves by bottom features
S_{xx}- additional, user defined source terms

These source terms are defined for the energy spectra. In the model, however, most source terms are directly calculated for the action spectrum. The latter source terms are denoted as $S \equiv {}^{S}/_{\sigma}$. The source term packages used in this study are, the Tolman and Chalikov (Tolman and Chalikov, 1996) for both input and dissipation terms, the discrete interaction approximation (Hasselmann et al., 1985) method for nonlinear interaction, and the Joint North Sea Wave Project (JONSWAP) formulation for bottom friction (Hasselmann et al., 1973; Bouws and Komen, 1983).

2.3.3 Numerical Calculations of Weather and Ocean by MSSG and WW3

To complete a global scale optimum ship routing system, the numerical simulations of weather and ocean states has been conducted by utilizing the above-mentioned MSSG and WW3 models. Although the global scale optimum ship routing system is supposed to conduct optimum ship routing everywhere, the issue of ship routing from Osaka Bay

to Maraca strait (the ‘O-M route’ in following parts) has been chosen in this study.

As an important and busy shipping route, there are a large percentage of oil tankers travelling in the ‘O-M route’, connecting the Asian countries such as Japan, China and the Middle East countries where main oil suppliers exist. The distribution of tanker’s number in the world (Lloyd's List Intelligence) and the daily transit volumes through world maritime oil chokepoints from U.S. Energy Information Administration shown as Fig.2.2.9 and Fig.2.30, respectively.

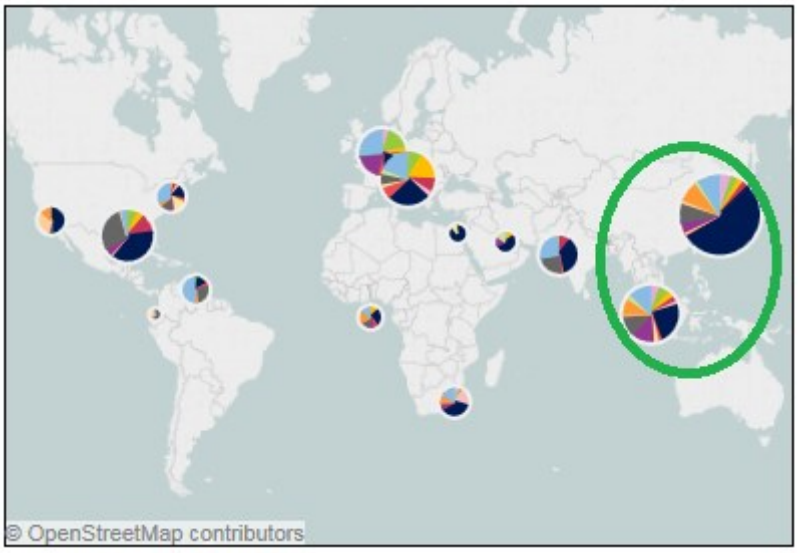

Fig.2.29. Distribution of tanker number in the world

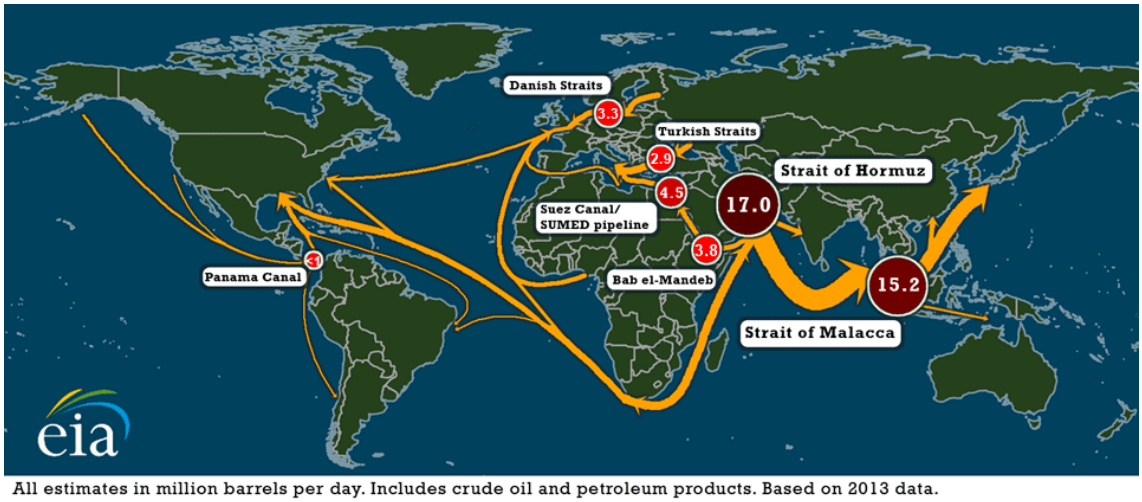

Fig.2.30. Daily transit volumes through world maritime oil chokepoints

Besides, compared with the route connecting the Indian Ocean and the South Atlantic

Ocean passing the South Africa sea area – the Cape Town, where ships have to both travel a longer distance and face the high winds and waves in the higher latitude, the Strait of Malacca, linking the Indian Ocean and the Pacific Ocean, is the shortest sea route between the Middle East and growing Asian markets, as shown in Fig.2.30.

Additionally, as described in part 2.2.2, the ECSA is nowadays a very busy shipping area with powerful typhoons and strong ocean current. Currently, over one-third of the world's maritime cargo is transported to and from Asian countries. Therefore, the optimum ship routing for 'O-M route' is of great importance for safer, more economical and environment-protection ship navigation.

In the coupled MSSG-A and MSSG-O calculation, the one-way nesting method has been chosen with the couple-time interval of 10 minutes from MSSG-A to MSSG-O. Two-month spin up from Static Ocean states are conducted at first, and then daily run has been started by using the restart data from the spin up process. The large nest coves the global area with a spatial resolution of 0.3×0.3 degree while the inner nest covers an area from 90E to 150E and 20S to 40N a spatial resolution of0.1×0.1 degree. The vertical levels for the MSSG-A and MSSG-O models are set to 55 and 42 layers from 1000 millibars to 10 millibars and sea surface to ocean bottom, respectively.

For input boundary data of MSSG-A, NCEP FNL (Final) Operational Global Analysis data with 1-degree by 1-degree grids prepared operationally every six are used while for MSSG-O, the four-times daily mean values of Gaussian Grid Data from the NCEP-DOE Reanalysis 2 database are utilized. To drive the MSSG-A model, Sea Surface Temperature, Sea Level Pressure, Soil Moisture/Water Content, Ice Extent, Topography, Tropospheric Ozone, Geopotential Height and Planetary Boundary Layer Height data are used, and to drive the MSSG-O, Ice concentration, Ground heat flux, Fresh water, Net short wave radiation, Momentum flux (zonal) and Momentum flux (meridional) are adapted beside the input data coming from MSSG-A coupling.

The MSSG-A and MSSG-O calculation results are shown as Fig. 2.31, where Sea Level Pressure, Sea Surface Wind distributions (10m above sea surface) and sea surface current distributions can be found.

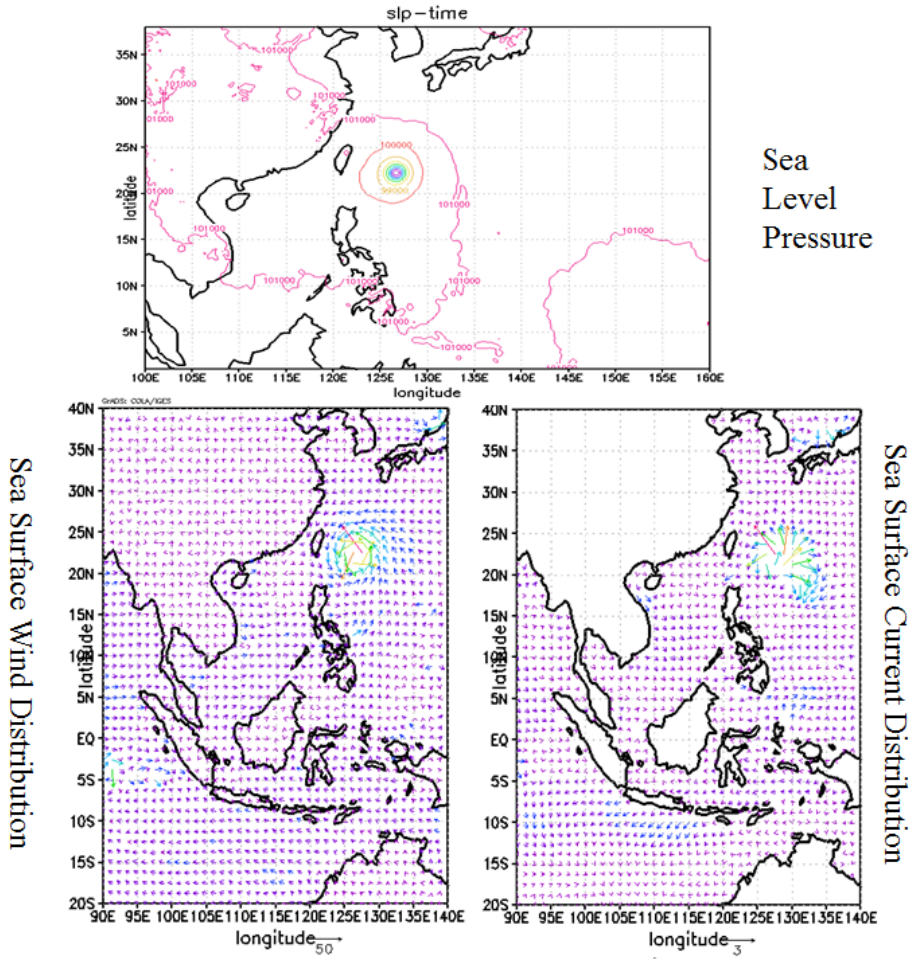

Fig.2.31. Calculation results of MSSG-A and MSSG-O for the Tokyo-Malacca route

In the WW3 calculation of ocean waves, to take the effects of swell into consideration, one-way nesting for three nests is applied to increase the accuracy and cost-efficiency of computerization. One-month spin up from Static Ocean states are conducted at first, and then daily run has been started by using the restart data from the spin up process. Topography data from ETOPO1 and wind data from NCEP-DOE Reanalysis 2 database are utilized to drive the wave model. The topography of these three nests is given as Fig.2.32. The largest nest covers an area from 0E to 359.5E and 75S to 75N with a spatial resolution of0.5 × 0.5 degree, and the middle-size nest covers an area from 60E to 280E and 50S to 60N with a spatial resolution of0.25 × 0.25 degree, while the inner-most nest covers an area from 90E to 150E and 20S to 40N with a spatial resolution of0.1 × 0.1 degree. Therefore, the high-resolution weather and ocean information generated by MSSG-A, MSSG-O and WW3 models of 0.1 × 0.1 degree can finally be utilized for the numerical simulation of ship navigation.

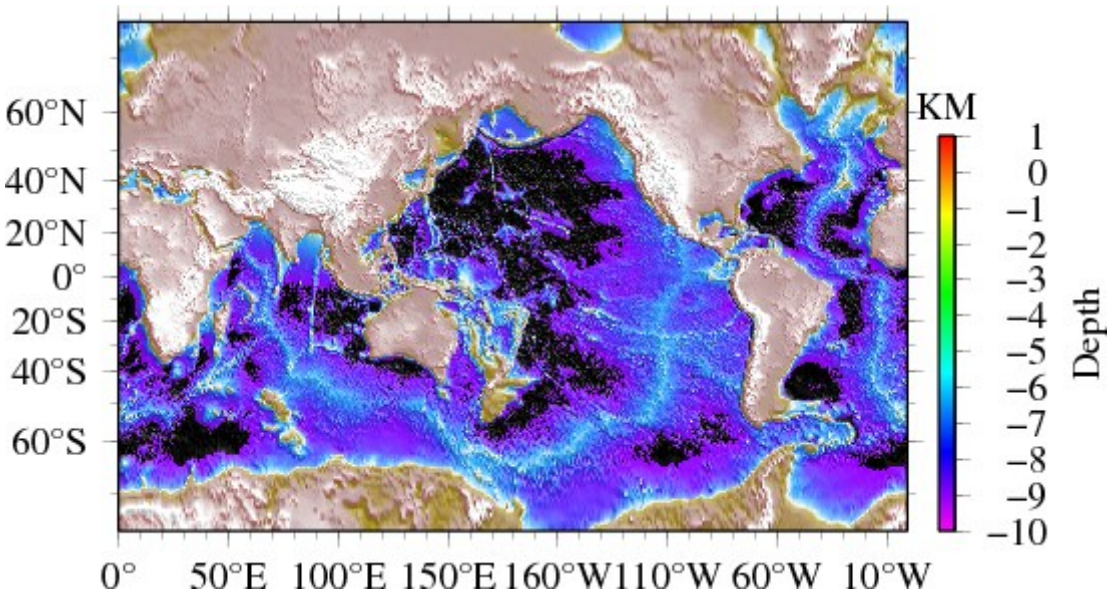
60°N
40°N
20°N
0°
20°S
40°S
60°S
0°
50°E
100°E
150°E
160°W
110°W
60°W
10°W
KM
1
0
−1
−2
−3
−4
−5
−6
−7
−8
−9
−10
Depth

(A)

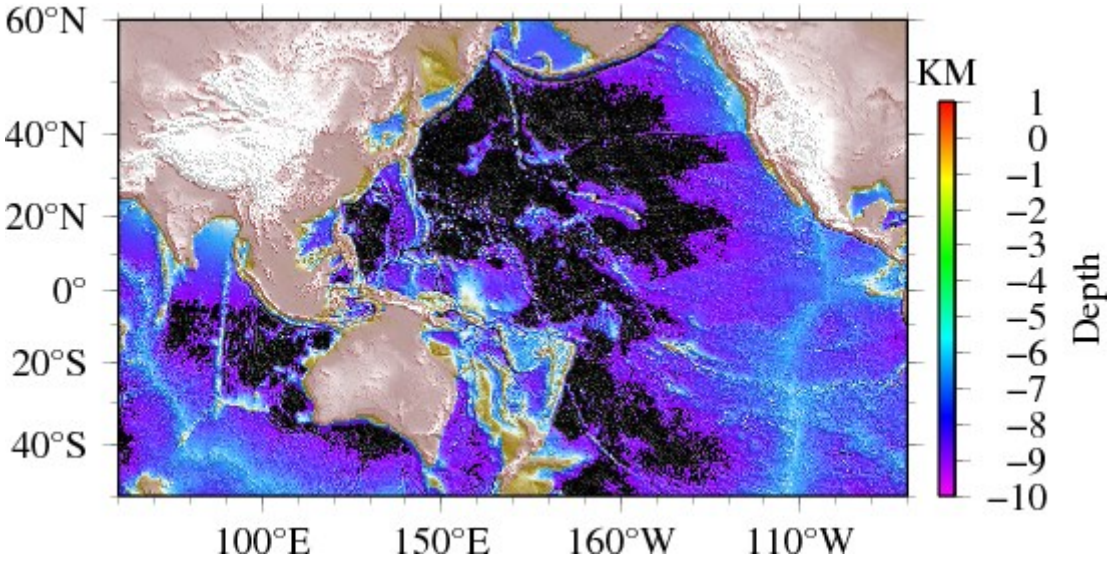
60°N
40°N
20°N
0°
20°S
40°S
100°E
150°E
160°W
110°W
KM
1
0
−1
−2
−3
−4
−5
−6
−7
−8
−9
−10
Depth

(B)

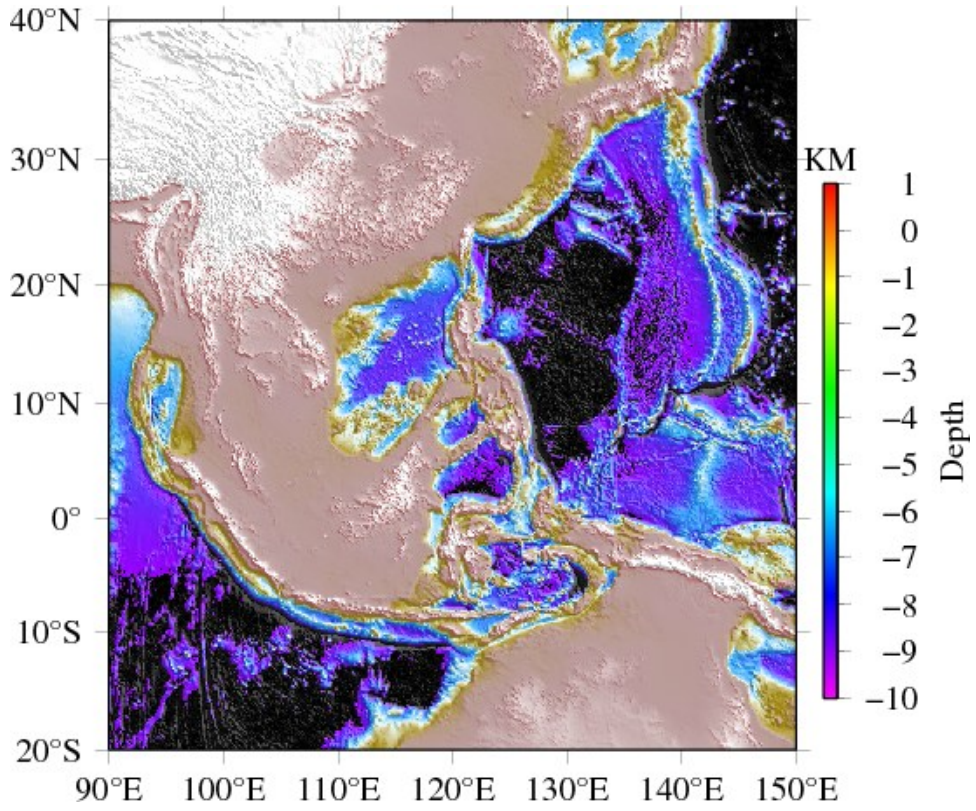

(C)

Fig.2.32. Topography of three nests in WW3 calculation. (A): Largest nest (0E-359.5E, 75S-75N); (B): Middle nest (60E-280E, 50S-60N); (C): Inner nest (90E-150E, 20S-40N)

Wave information necessary for numerical simulation of ship navigation such as the significant wave height, average wave period, and predominate wave direction of these three nests are shown as Fig.2.33, Fig. 2.34 and Fig. 2.35, respectively (Time period from 2011052700 to 2011052800 and time interval of every 6 hours for the largest nest; time 2011052800 for the other two nests as an example), for which the upper left figures are wind distributions, the lower left figures are average wave period, the upper right figures are significant wave height and the lower left figures are dominant wave direction, respectively. Compared the up two figures of these graphs, typhoon-induced ocean waves can be found clearly when the typhoon happens according to the wind information.

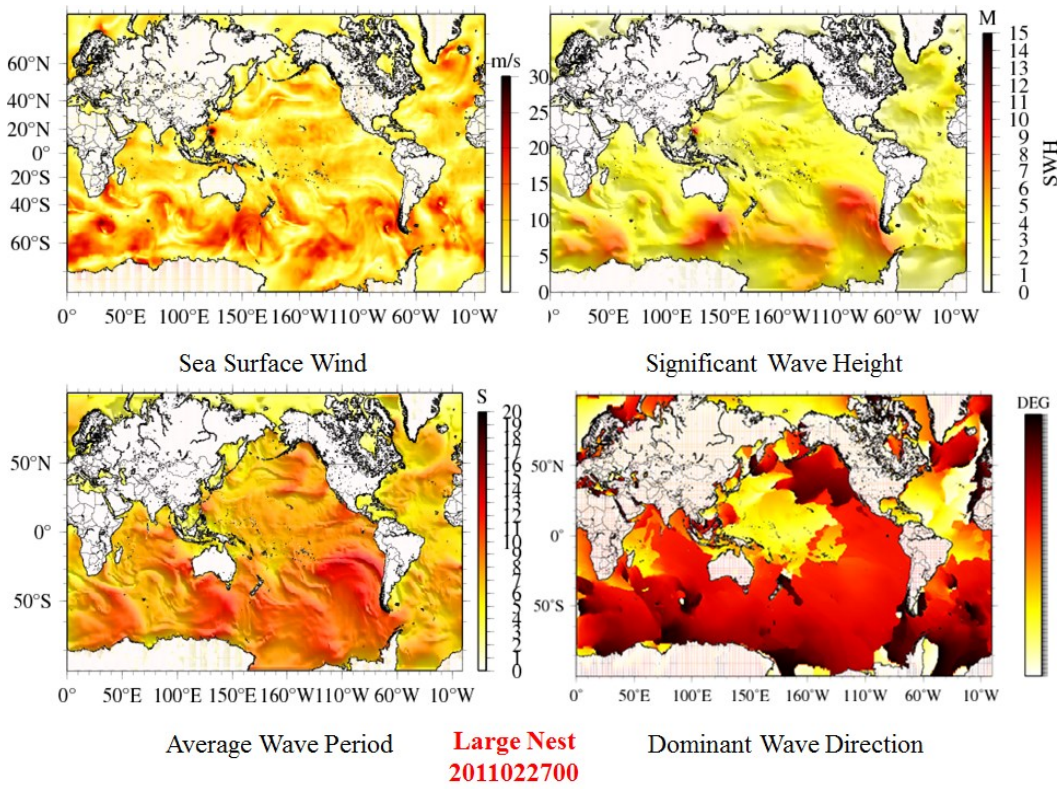
60°N
40°N
20°N
0°
20°S
40°S
60°S
0° 50°E 100°E 150°E 160°W 110°W 60°W 10°W
m/s
M
SWH
Sea Surface Wind
Significant Wave Height
50°N
0°
50°S
S
DEG
Average Wave Period
Large Nest
2011022700
Dominant Wave Direction

(A)

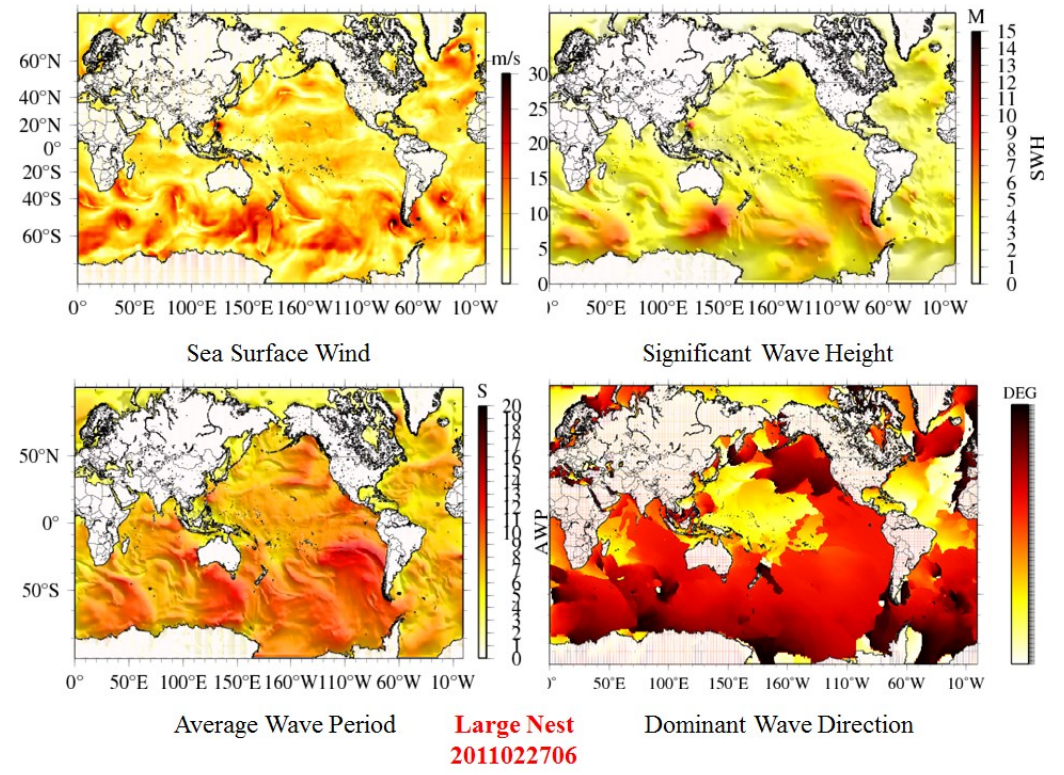
60°N
40°N
20°N
0°
20°S
40°S
60°S
0° 50°E 100°E 150°E 160°W 110°W 60°W 10°W
m/s
M
SWH
Sea Surface Wind
Significant Wave Height
50°N
0°
50°S
S
AWP
DEG
Average Wave Period
Large Nest
2011022706
Dominant Wave Direction

(B)

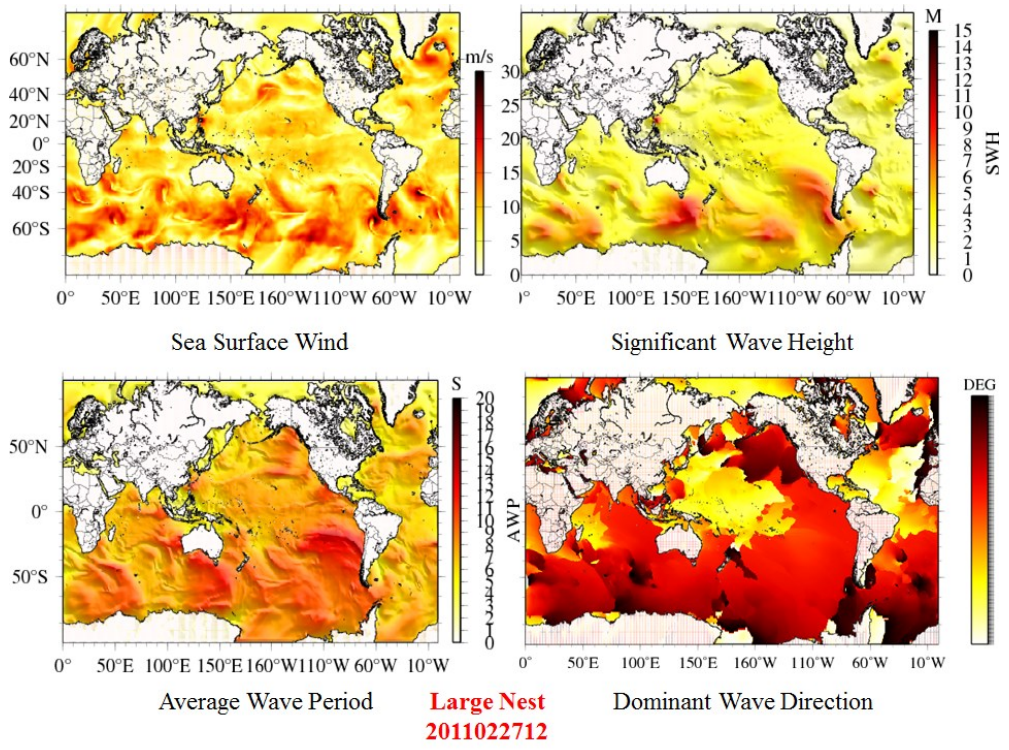
60°N
40°N
20°N
0°
20°S
40°S
60°S
0° 50°E 100°E 150°E 160°W 110°W 60°W 10°W
m/s
M
SWH
Sea Surface Wind
Significant Wave Height
50°N
0°
50°S
S
AWP
DEG
Average Wave Period
Large Nest
2011022712
Dominant Wave Direction

(C)

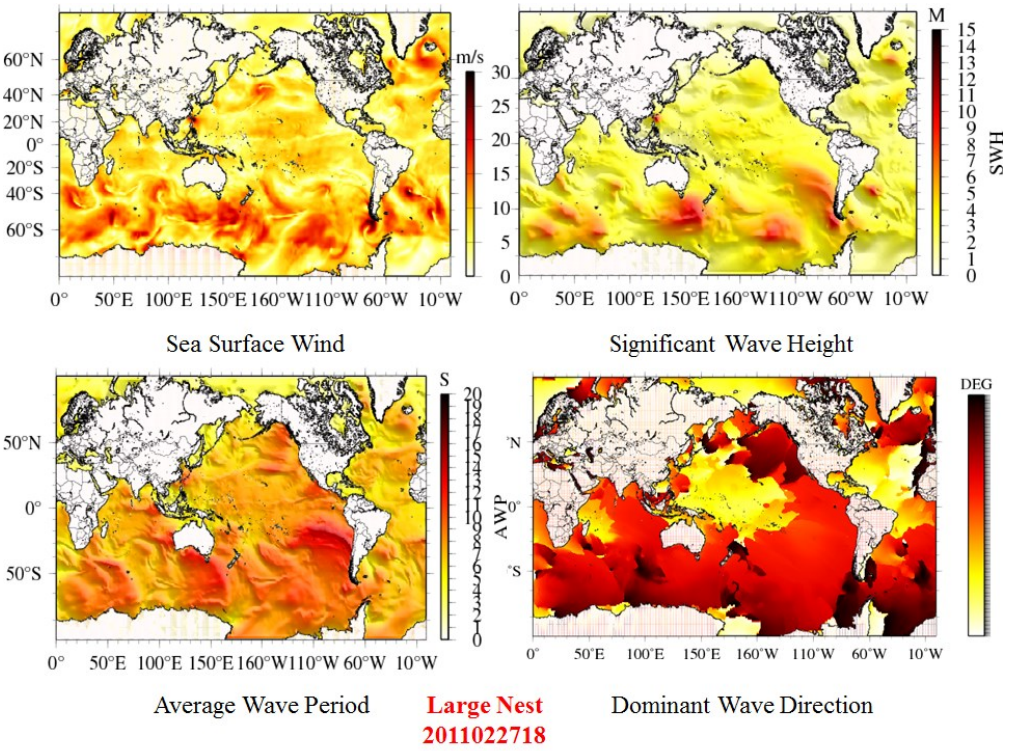
60°N
40°N
20°N
0°
20°S
40°S
60°S
0° 50°E 100°E 150°E 160°W 110°W 60°W 10°W
m/s
M
SWH
Sea Surface Wind
Significant Wave Height
50°N
0°
50°S
S
AWP
DEG
Average Wave Period
Large Nest
2011022718
Dominant Wave Direction

(D)

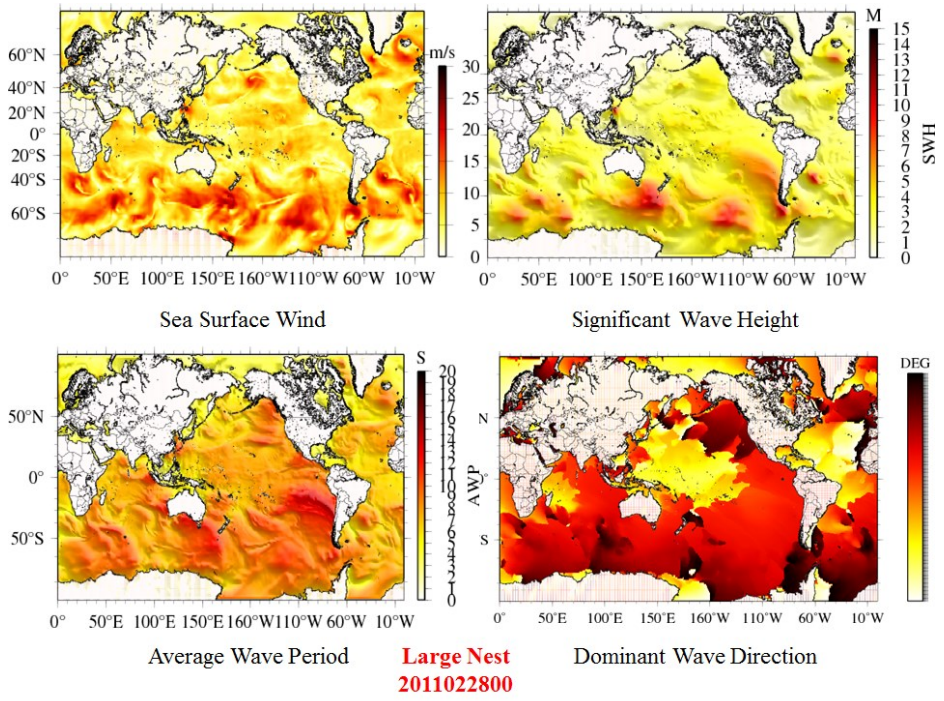

(E)

Fig. 2.33-A, B, C, D, E. Wave information generated by WW3 model for the largest nest. (Time period: 2011052700-2011052800; Time interval: 6 hours)

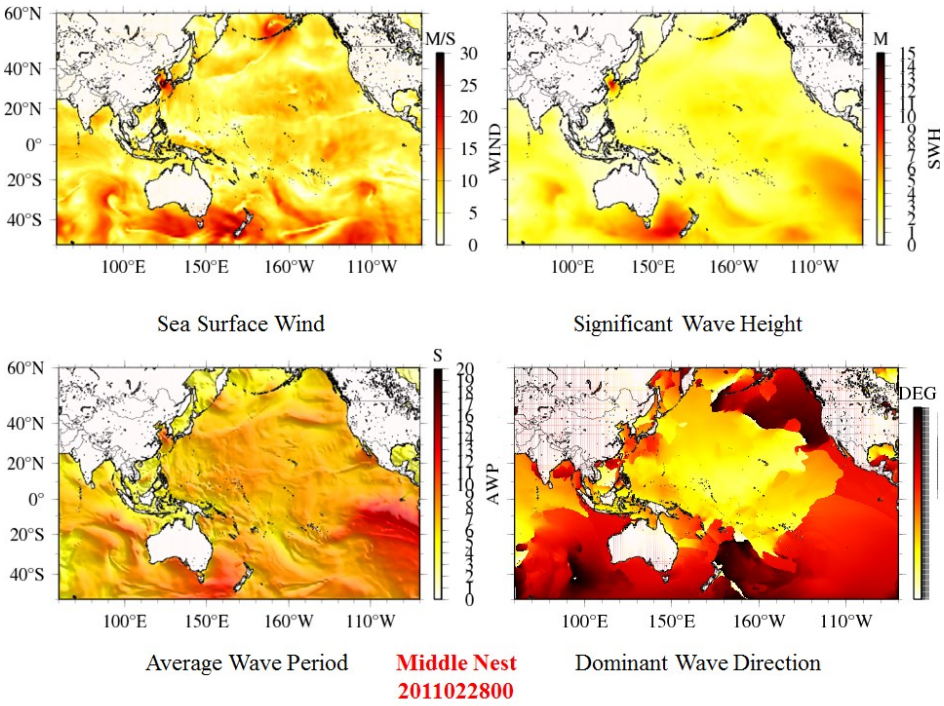

Fig.2.34. Wave information generated by WW3 model for the middle nest. (Time:

2011052800)

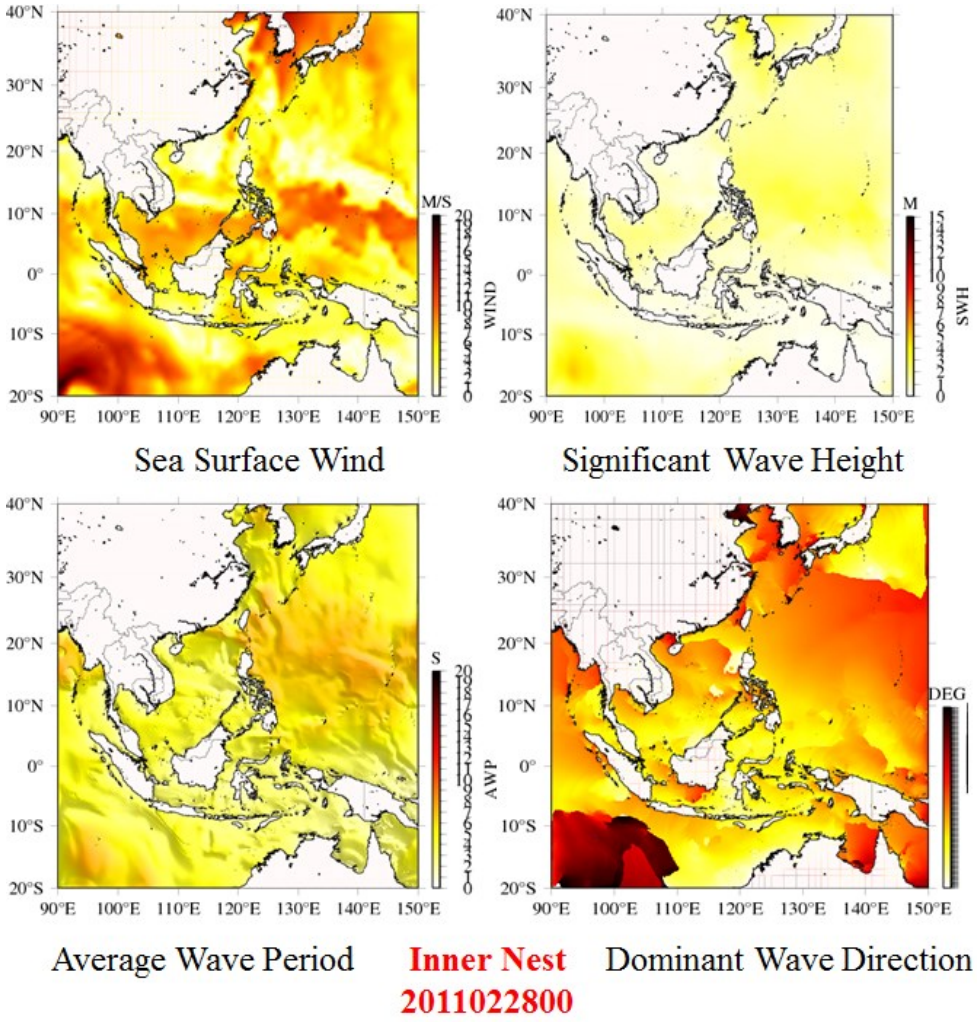

Fig.2.35. Wave information generated by WW3 model for the inner nest. (Time: 2011052800)

2.4. Summary

In this chapter, numerical calculation of weather and ocean in coastal sea areas such as the Osaka Bay area and the East China Sea Area as well as the Ocean Sea area have been studied by using modernized regional and global scale atmospheric and oceanic models. Detailed information of numerical calculation settings based on those models has been given. Results are firstly given and then verified by comparisons with observation data as well as other researchers' studies. It has been proved that those

atmospheric and oceanic models can be used to generate necessary high-resolution weather and ocean information, which can be utilized in the numerical simulation of ship navigation to be given in next chapter.

However, variations between model results and observation data as well as the errors existing in long-period weather prediction also illustrates that more studies should be made to clearly understand the problems to be solved in the complex atmospheric sciences such as understanding of the basic processes and their modeling which may relates to observations and data assimilation, those covered within the traditional disciplines (atmospheric physics and chemistry, atmospheric dynamics and weather forecasting), those concerned with the interactions between the atmosphere and its boundaries, and those related to the atmospheric component of climate studies.

References

Alan F. Blumberg and George L. Mellor. (1987). A Description of a Three-Dimensional Coastal Ocean Circulation Model.

Amante, C., B. W. Eakins, 2009. ETOPO1 1 Arc-Minute Global Relief Model: Procedures, Data Sources and Analysis. NOAA Technical Memorandum NESDIS NGDC-24, March, p. 19.

A. Toffolia, , , J.M. Lefèvreb, E. Bitner-Gregersenc, J. Monbaliua. (2005). Towards the identification of warning criteria: Analysis of a ship accident database. Applied Ocean Research, Volume 27, Issue 6, Pages 281–291

Arakawa, Chuichi, et al. "Large-eddy Simulation of Wind for Numerical Site Calibration Technology Phase I: Basic Study of Numerical Simulation on Complex Terrain." Annual Report of the Earth Simulator Center April 2008 (2007).

Blumberg, et al., 1987.A description of a three-dimensional coastal ocean circulation model.Three-Dimensional Coastal Ocean Models, 1–16.

Booij, N., R. C. Ris, and Leo H. Holthuijsen. "A third‐generation wave model for coastal regions: 1. Model description and validation." Journal of Geophysical Research: Oceans (1978–2012) 104.C4 (1999): 7649-7666.

Bouws, E. and G. J. Komen, 1983: On the balance between growth and dissipation in an extreme depth-limited wind-sea in the southern North Sea. J. Phys. Oceanography., 13, 1653-1658.

Choi, Youngjin, et al. "Simulation of Deepwater Horizon Oil Spill Using Coupled Atmosphere-Ocean Model." マリンエンジニアリング 48.1 (2013): 105-109.

Dingemans, M. W., Water Wave Propagation Over Uneven Bottoms, part 1, Linear Wave Propagation, Adv. Ser. Ocean Eng., vol. 13, 471 pp., World Sci., River Edge, N. J., 1997.

Ezer, T., G. L. Mellor, 1997. Simulations of the Atlantic Ocean with a free surface sigma coordinate ocean model.Journal of Geophysical Research: Oceans (1978–2012) 102(C7),15647–15657.

Guo,Xinyu, et al., 2003. A triply nested ocean model for simulating the Kuroshio-Roles of horizontal resolution on JEBAR. Journal of Physical Oceanography 33 (1), 146–169.

Hasselmann, K., et al., Measurements of wind-wave growth and swell decay during the Joint North Sea Wave Project (JONSWAP), Dtsch. Hydrogr. Z. Suppl., 12(A8), 1–95, 1973.

Hasselmann, S. and K. Hasselmann, 1985: Computations and parameterizations of the

nonlinear energy transfer in a gravity-wave spectrum, Part I: A new method for efficient computations of the exact nonlinear transfer integral. J. Phys. Oceanography., 15, 1369-1377.
Kageyama, A. and Sato, T., 2004: The Yin-Yang Grid: An Overset Grid in Spherical Geometry. Geochem.Geophys.Geosyst., 5, Q09005, doi:10.1029/2004GC000734.
Kagimoto, etal., 1997. Seasonal transport variations of the Kuroshio: An OGCM simulation. Journal of Physical Oceanography 27 (3), 403–418.
Kalnay, Eugenia, et al. "The NCEP/NCAR 40-year reanalysis project." Bulletin of the American meteorological Society 77.3 (1996): 437-471.
Kamio, Takeshi, Makoto Iida, and Chuichi Arakawa. "Analysis on Turbulent Flows using Large-eddy Simulation on the Seaside Complex Terrain." Journal of Physics: Conference Series. Vol. 555. No. 1. IOP Publishing, 2014.
Kistler, R., et al., 2001. The NCEP-NCAR 50-Year Reanalysis:Monthly means CD-ROM and documentation. Bulletin of the American Meteorological Society 82 (2), 247–267.
Komen, G. J., S. Hasselmann, and K. Hasselmann, On the existence of a fully developed wind-sea spectrum, J. Phys. Oceanogr., 14, 1271– 1285, 1984.
Levitus, S., et al.,1994: Salinity. Vol. 3, World Ocean Atlas 1994, NOAA Atlas NESDIS 3, p. 99.
Levitus, S., T. P. Boyer, 1994.Temperature. Vol. 4, World Ocean Atlas 1994, NOAA Atlas NESDIS 4, p. 117.
Mellor, G.L., and A.F. Blumberg, Modeling vertical and horizontal diffusivities with the sigma coordinate system, Mon. Wea. Rev, 113, 1380-1383, 1985.
Mellor, G. L., et al., 1994. The pressure gradient conundrum of sigma coordinate ocean models. Journal of Atmospheric and Oceanic Technology11 (4),1126–1134.
Mellor, G. L., 1998. Users Guide for a Three-dimensional, Primitive Equation, Numerical Ocean Model. Princeton, NJ 08544-0710.Program in Atmospheric and Oceanic Sciences, Princeton University.
Mei, C. C., 1983: The applied dynamics of ocean surface waves. Wiley, New York, 740 pp.
Oey, L.-Y., G.L. Mellor, and R.I. Hires, A three-dimensional simulation of the Hudson-Raritan estuary. Part I: Description of the model and model simulations, J. Phys. Oceanogr., 15, 1676-1692, 1985a.
Oey, L.-Y., G.L. Mellor, and R.I. Hires, A three-dimensional simulation of the Hudson-Raritan estuary. Part II: Comparison with observation, J. Phys. Oceanogr., 15, 1693-1709, 1985b.

Oey, L. Y., et al., 2013. ATOP—the Advanced Taiwan Ocean Prediction System based on the mpiPOM Part 1: Modeldescriptions, analyses and results. Terrestrial Atmospheric and Oceanic Sciences 24 (1), 137–158.
Peng, X., Feng Xiao, F. and Takahashi, K., Conservation constraint for quasi-uniform overset grid on sphere, Quarterly Journal Royal Meteorology Society. (2006), 132, pp.979–996.
Phillips, O. M., 1977: The dynamics of the upper ocean, second edition. Cambridge Univ. Press, 336 pp.
Rene Laprise. (1992). The Euler Equations of Motion with Hydrostatic Pressure as an Independent Variable, Monthly Weather Review. JANUARY 1992, 197- 207
Ou, Shan-Hwei, et al. "Simulating typhoon waves by SWAN wave model in coastal waters of Taiwan." Ocean Engineering 29.8 (2002): 947-971.
Sekine, et al., 1994.Seasonal variation in volume transport of the Kuroshio south of Japan. Journal of Physical Oceanography 24 (2), 261–272.
Takahashi, K. et al., 2004a: Proc. 7th International Conference on High Performance Computing and Grid in Asia Pacific Region, 487–495.
Takahashi, K., et al., 2004b. "Non-hydrostatic Atmospheric GCM Development and its computational performance", http://www.ecmwf.int/newsevents/meetings/ workshops/2004/ high_performance_ computing-11th/ presentations.html.
Takahashi, K, et al. 2005: Non-hydrostatic atmospheric GCM development and its computational performance", Use of High Performance computing in meteorology, Walter Zwieflhofer and George Mozdzynski Eds., World Scientific, 50–62.
Takahashi, Keiko, et al. "Multi-Scale Simulator for the Geoenvironment: MSSG and Simulations." Use of High Performance computing in meteorology (2007).
Takahashi, Keiko, et al. "Multi-scale weather/climate simulations with multi-scale simulator for the geoenvironment (MSSG) on the Earth Simulator." Annual Report of the Earth Simulator Center April 2007 (2006).
Takahashi, Keiko, et al. "High performance computing of MSSG with ultra-high resolution." Parallel Computing Technologies. Springer Berlin Heidelberg, 2011. 484-498.
Takahashi, Keiko, et al. "World-highest resolution global atmospheric model and its performance on the Earth Simulator." State of the Practice Reports. ACM, 2011.
Takahashi, Keiko, et al. "Challenge toward the prediction of typhoon behavior and down pour." Journal of Physics: Conference Series. Vol. 454. No. 1. IOP Publishing, 2013.
Tolman, H. L. and D. V. Chalikov, 1996: Source terms in a third-generation wind-wave

model. J. Phys. Oceanogr., 26, 2497-2518.
Tolman, H. L., 2009a: User manual and system documentation of WAVEWATCH III TM version 3.14 . Environmental Modeling Center Marine Modeling and Analysis Branch, U. S. Department of Commerce National Oceanic and Atmospheric Administration National Weather Service National Centers for Environmental Prediction 5200 Auth Road, Camp Springs, MD 20746.
Tolman, H. L., 2009b: User manual and system documentation of WAVEWATCH III(TM) version 3.14 . Environmental Modeling Center Marine Modeling and Analysis Branch.
TROSELJ, Josko, Yosuke YAMASHIKI, and Kaoru TAKARA. "Ocean Circulation Response to Inflow from Abukuma River Outlet." (2013).
Shemdin, O., K. Hasselmann, S. V. Hsiao and K. Heterich, 1978: Nonlinear and linear bottom interaction effects in shallow water in turbulent fluxes through the sea surface, wave dynamics and prediction, pp. 347-365. NATO Conf. Ser. V, Vol 1.
Shiotani Shigeaki, Haibo Xia. "A Basic Study on the Numerical Estimation of Ship Positioning for Weather Routing in Coastal Water." The Sixteenth International Offshore and Polar Engineering Conference. International Society of Offshore and Polar Engineers, 2006.
Soda, Taisuke, Shigeaki Shiotani, and Kenji Sasa. "Basic Study on Numerical Navigation System with Numerical Weather and Ocean." Journal of the Japan Society of Naval Architects and Ocean Engineers 16 (2012).
Yu-Chia Chang, Ruo-Shan Tseng, Guan-Yu Chen, Peter C Chu and Yung-Ting Shen (2013). Ship Routing Utilizing Strong Ocean Currents. Journal of Navigation, 66, pp 825-835.
WAMDIG, 1988: The WAM model - a third generation ocean wave prediction model. J. Phys. Oceanography., 18, 1775-1809.
Wakata, etal., 2006.Interannual variability of the Kuroshio transport passing through the 137 E meridian in an OGCM related to the North Pacific windstress. Journal of Oceanography 62 (1), 25–[52]. Whitham, G. B., Linear and Nonlinear Waves, 636 pp., John Wiley, New York, 1974.
Xia H., Shiotani S., et al. (2006). Estimation of Ship’s Course for Sailing on Route by Navigation Simulation in Coastal Water, The Journal of Japan Institute of Navigation, No. 115, pp. 51-57.

CHAPTER 3

CONSTRUCTION OF THE NUMERICAL SHIP NAVIGATION SYSTEM

3.1 Description of ship model (SR108), wave resistance model (RIOS) and ship maneuvering model (MMG)

3.1.1 Ship Model SR108

The numerical calculations of ship navigation were based on the characteristics of the SR108 as a container ship, shown in Table.3.1. The data of the hull lines and main characteristics of this ship were used for the calculation.

Data of the hull lines and main characteristics of this ship were used for calculations. The hydrodynamic forces and external forces were simplified. Considering that the objective is to study the effects of the current on ship navigation, only the advance, drift, and rotation motions in smooth water were considered.

Table3.1. Principal Properties of the SR108

Symbol	*Ship*
Length (P.P)	175.00m
Length (W.L)	178.21m
Beam (M.L.D)	25.40m
Draught (M.L.D)	9.50m
LCG realative to midships	-2.48m
Block coefficient	0.572
Displaced volume	24,801ton
Wetted surface	5,499m^2
Diameter of propeller	6.507m
Ratio of propeller pitch	0.7348
A_R (m^2)	32.46m^2

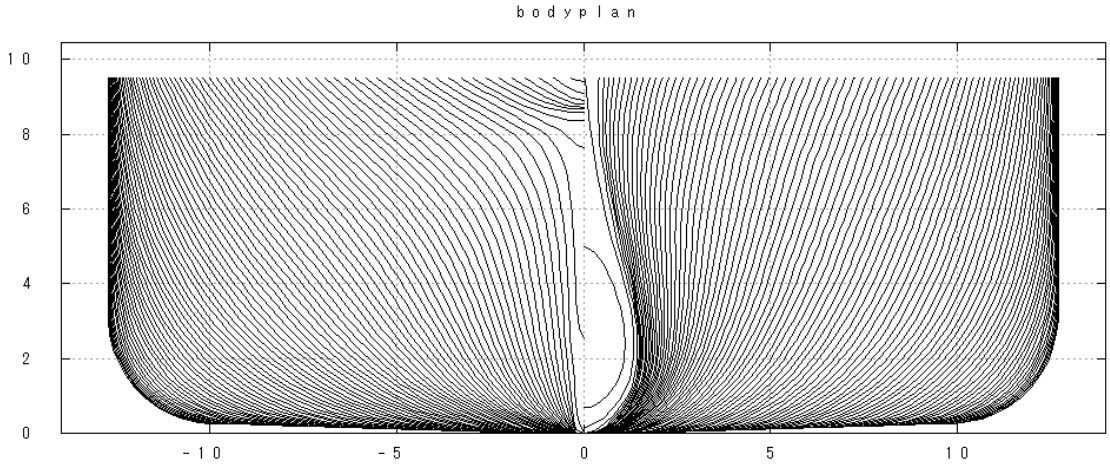

Fig.3.1. Body plan of the ship mode SR108

3.1.2 Ship response to ocean waves

In a rough sea state, the high wind and waves can increase the ship resistance by producing wave reflection or diffraction, generating vertical ship motions like heave and pitch as well as wind resistance on the superstructure, which will lead to speed loss of the sailing ship.

As shown in the Fig.3.2, the short-time forecasted added resistance, side force and turn moment of the model SR108 in ocean waves were calculated by using the Enhanced United Theory built in Research Initiative on Oceangoing Ships system (Kashiwagi, Mizokami, and Tasukawa, 1999), where the horizontal and vertical axis show the average wave period in second and the values of ship response in KN, respectively.

Here the Froude number of the ship is 0.2, ship speed is 16 knots and the significant wave height was set to 1m. In the ship response calculation, the sea waves were selected as the ITTC type and the swell was set to the JONSWAP option. For the wind pressure, the widely used Fujiwara method was adopted (Fujiwara, Ueno, Nimura, 1998). The numbers from 0 to 180 of every 30 represent the directions of encountering waves from the ship stern to bow.

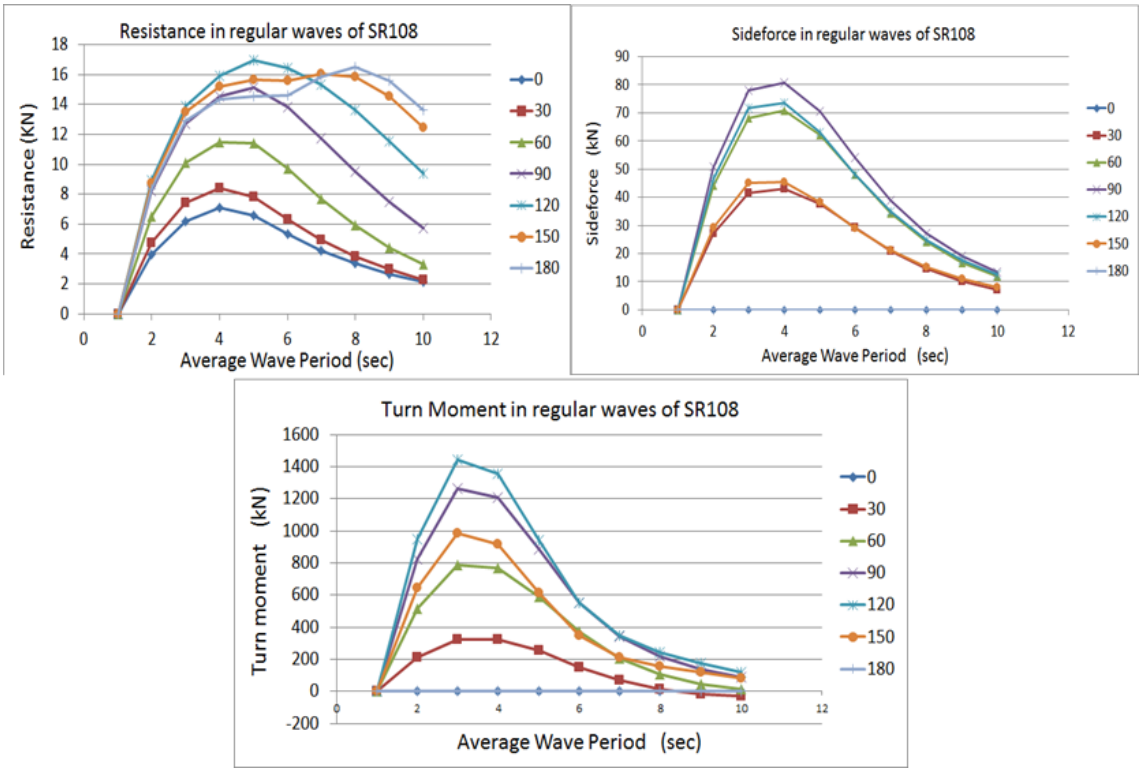

Fig.3.2. Responses of the ship model SR108 in ocean waves

3.1.3 Ship maneuvering model

The accurate estimation of a ship's position is very important for optimum ship routing. Such estimations can be obtained when hydrodynamic forces and moments affecting the hull are known in advance. The ship maneuvering model MMG (Kose, et al., 1981;Ogawa, 1981; Yoshimura, 1986), widely used to describe a ship's maneuvering motion, was adopted for the estimation of a ship's location by simulation based on the characteristics of a container ship model,SR108, with detailed information and a body plan shown in Table.3.1 and Fig.3.1, respectively. The primary features of the MMG model are the division of all hydrodynamic forces and moments working on the vessel's hull, rudder, propeller, and other categories, as well as the analysis of their interaction.

The body-fixed coordinate system of the MMG model and the equation of the ship's motion in the body-fixed coordinate system adopted in the MMG are given in Fig.3.3 and equation 3.1, respectively

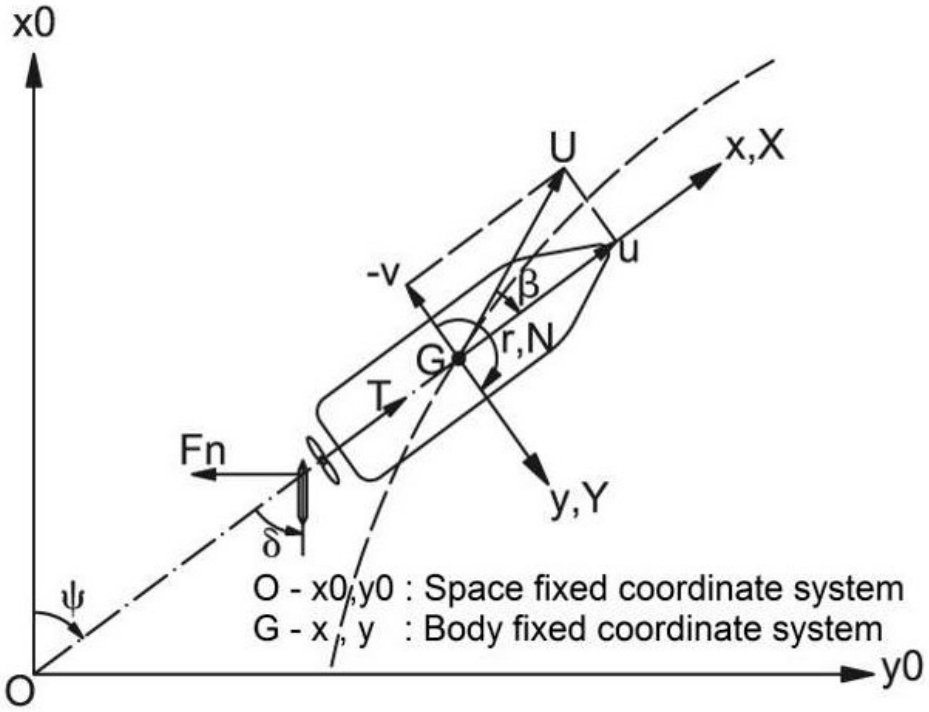

Fig.3.3. Coordinate system of the MMG model

$$\begin{cases} (\mathrm{m}+\mathrm{m_x})\mathrm{u}-(\mathrm{m}+\mathrm{m_y})\mathrm{vr}=\mathrm{X} \\ (\mathrm{m}+\mathrm{m_y})\mathrm{v}+(\mathrm{m}+\mathrm{m_x})\mathrm{ur}=\mathrm{Y} \\ (\mathrm{I_{zz}}+\mathrm{J_{zz}})\mathrm{r}=\mathrm{N} \end{cases} \tag{3.1}$$

where m is the mass, $\mathrm{m_x}$ and $\mathrm{m_y}$ are added mass, u and v are components of the velocity in the directions of the x-axis and the y-axis, respectively, and r is the angular acceleration; $\mathrm{I_{zz}}$ and $\mathrm{J_{zz}}$ are the moment of inertia and the added moment of inertia around G, respectively; X and Y are hydrodynamic forces, and N is the moment around the z-axis.

According to the MMG model, the hydrodynamic forces and the moment in the above equation can be written as:

$$\begin{cases} X = X_H + X_P + X_R + X_T + X_A + X_W \\ Y = Y_H + Y_P + Y_R + Y_T + Y_A + Y_W \\ N = N_H + N_P + N_R + N_T + N_A + N_W \end{cases} \tag{3.2}$$

Where the subscripts H, P, R, T, A, and W denote the hydrodynamic force or moment induced by the hull, the propeller, the rudder, the thruster, the air, and the wave, respectively.

Among those subscripts, the computation of the hydrodynamic forces caused by the wind is given as equation 3.3.

$$\begin{cases} X_A = \frac{\rho_A}{2} V_A^2 A_T C_{XA}(\theta_A) \\ Y_A = \frac{\rho_A}{2} V_A^2 A_L C_{YA}(\theta_A) \\ N_A = \frac{\rho_A}{2} V_A^2 L A_L C_{NA}(\theta_A) \end{cases} \tag{3.3}$$

Where the subscripts are given as follows:

ρ_A : density of the air
θ_A : relative wind direction
V_A : relative wind velocity
A_L , A_T : frontal projected area and lateral projected area, respectively
C_{XA}, C_{YA}, and C_{NA} are the coefficients (Fujiwara, T. 1998)

Among those subscripts, the computation of the hydrodynamic forces caused by the wave is given as equation 3.4.

$$\begin{cases} X_W = \rho g h^2 B^2 / L \overline{C_{XW}}(U, T_V, \aleph - \varphi_0) \\ Y_W = \rho g h^2 B^2 / L \overline{C_{YW}}(\omega_0, \aleph - \varphi_0) \\ N_W = \rho g h^2 B^2 / L \overline{C_{NW}}(\omega_0, \aleph - \varphi_0) \end{cases} \tag{3.4}$$

Among those subscripts, the computation of the hydrodynamic forces caused by the currents is given as equation 3.5.

$$\begin{aligned} X_H &= -R + \frac{\rho}{2} L d U^2 \left(X'_{\beta r} r' \sin\beta + X'_{uu} cos^2\beta \right) \\ Y_H &= \frac{\rho}{2} L d U^2 \left(Y'_\beta \beta + Y'_r r' + Y'_{\beta\beta} \beta|\beta| + Y'_{rr} r'|r'| + Y'_{\beta\beta r} \beta^2 r' + Y'_{\beta rr} \beta r'^2 \right) \\ N_H &= \frac{\rho}{2} L^2 d U^2 \left(N'_\beta \beta + N'_r r' + N'_{\beta\beta} \beta|\beta| + N'_{rr} r'|r'| + N'_{\beta\beta r} \beta^2 r' + N'_{\beta rr} \beta r'^2 \right) \end{aligned} \tag{3.5}$$

Where ρ is the water density, L is the ship length, d is the ship draft, U is the ship's speed, and R is the resistance of the hull:

$$\mathrm{R} = \frac{\rho}{2} S u^2 C_t \tag{3.6}$$

where S is the wetted surface area, u is the speed component at X direction, and

$$C_t = \{(1+k)C_{f_0} + \Delta C_f\} + C_w \tag{3.7}$$

Where$k$ is the ship form factor, ΔC_f is the roughness factor, C_w is the wave drag factor, and

$$C_{f0} = 0.463(log_{10}R_n)^{-2.6} \tag{3.8}$$

WhereR_n is the Froude number. The other parameters, such as $X'_{\beta r}$, X'_{uu},Y'_{β}, $Y'_{\beta\beta,}Y'_{rr}$, $Y'_{\beta\beta r}$, $Y'_{\beta rr}$andN'_{β},N'_{r}, $N'_{\beta\beta}$, N'_{rr}, $N'_{\beta\beta r}$, $N'_{\beta rr}$, are various coefficients calculated from several ship model experiments (Kijima, et al., 1990; Hasegawa, 1980).

3.2 Numerical simulations of ship navigation

3.2.1 Osaka Bay Area

For the case of numerical simulation of ship navigation in the Osaka Bay Area, the numerical navigation was carried out with a fixed propeller revolution of 12.3kn in still water. For all of these simulations, a straight-heading direction was used for about one hour of courses 045 and 225 and for about half an hour of courses 090 and 270 as shown in Fig.3.4. The hydrodynamic forces as well as external forces were simplified. Only the advance, drift, and rotation motions in smooth water were considered. In all cases, autopilot was utilized.

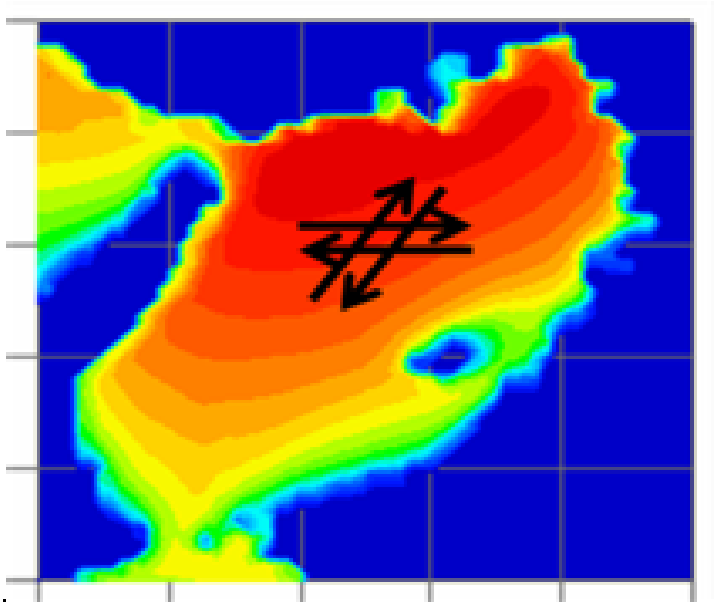

Fig.3.4. Course settings for numerical navigation in the Osaka Bay Area case

The six groups of figure in Fig.3.5-A, B, C and Fig3.6-A, B, C show the ship's tracks in the numerical simulation on the effects of the wind wave, tidal currents, wind-wave currents, and set course. The coordinate system in these figures is longitude (E) and latitude (N).

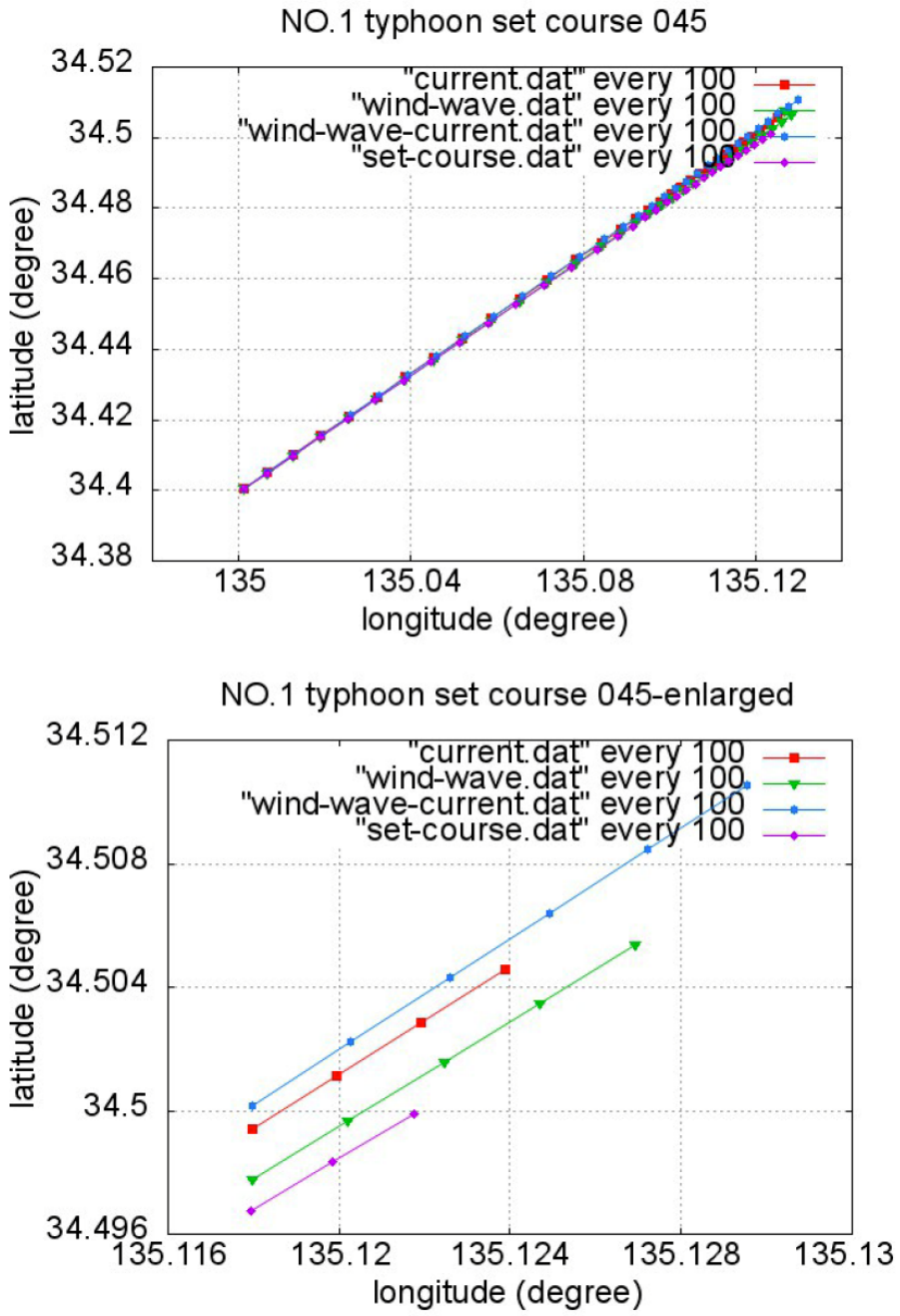
NO.1 typhoon set course 045
"current.dat" every 100
"wind-wave.dat" every 100
"wind-wave-current.dat" every 100
"set-course.dat" every 100
34.52
34.5
34.48
34.46
34.44
34.42
34.4
34.38
latitude (degree)
135
135.04
135.08
135.12
longitude (degree)
NO.1 typhoon set course 045-enlarged
"current.dat" every 100
"wind-wave.dat" every 100
"wind-wave-current.dat" every 100
"set-course.dat" every 100
34.512
34.508
34.504
34.5
34.496
latitude (degree)
135.116
135.12
135.124
135.128
135.13
longitude (degree)

(A)

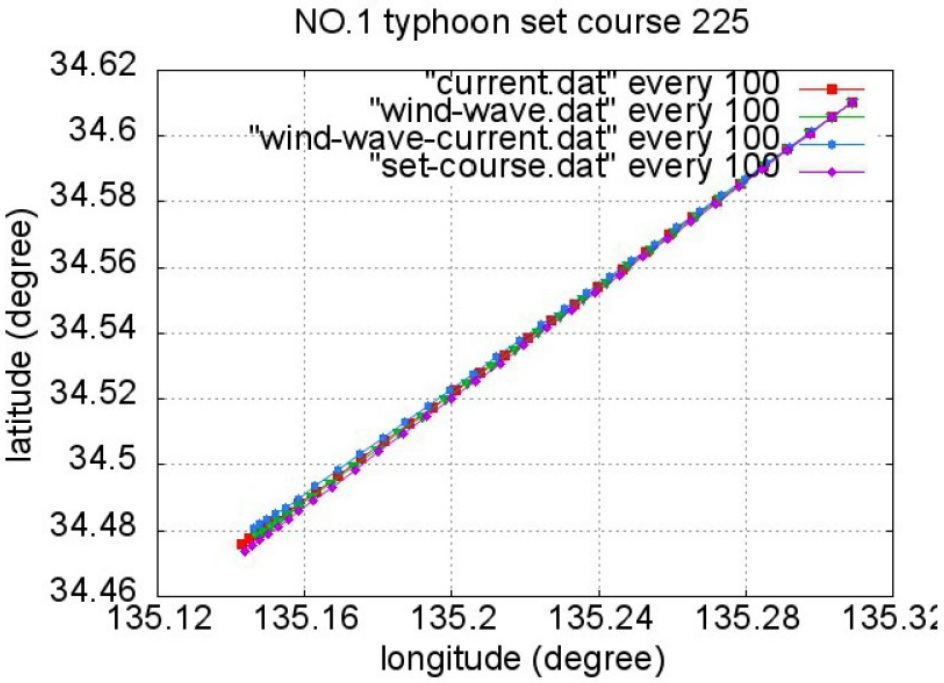
NO.1 typhoon set course 225
"current.dat" every 100
"wind-wave.dat" every 100
"wind-wave-current.dat" every 100
"set-course.dat" every 100
34.62
34.6
34.58
34.56
34.54
34.52
34.5
34.48
34.46
135.12
135.16
135.2
135.24
135.28
latitude (degree)
longitude (degree)

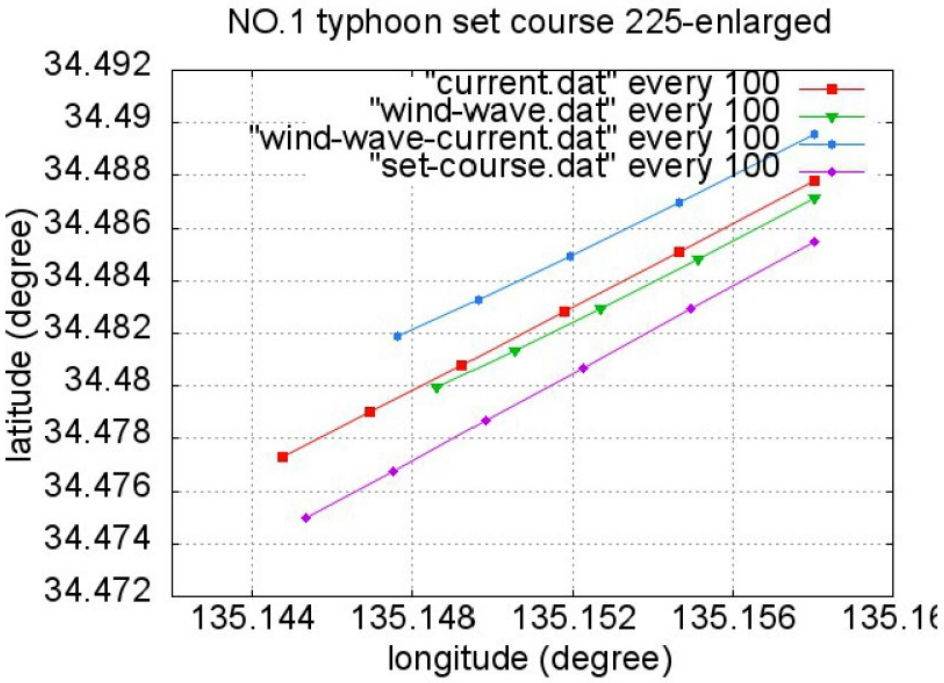
NO.1 typhoon set course 225-enlarged
"current.dat" every 100
"wind-wave.dat" every 100
"wind-wave-current.dat" every 100
"set-course.dat" every 100
34.492
34.49
34.488
34.486
34.484
34.482
34.48
34.478
34.476
34.474
34.472
135.144
135.148
135.152
135.156
latitude (degree)
longitude (degree)

(B)

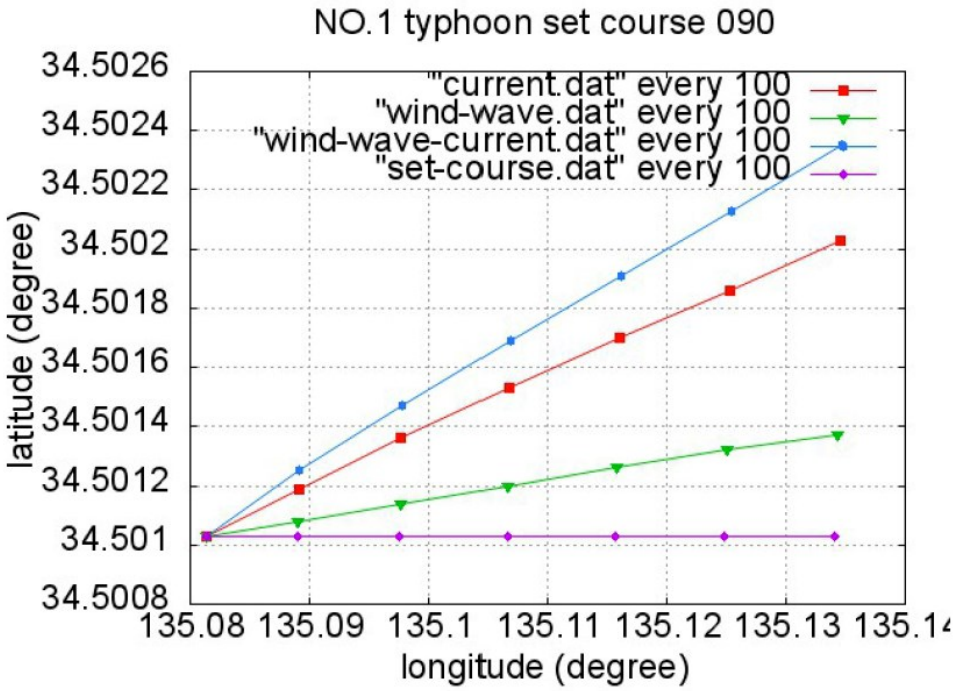

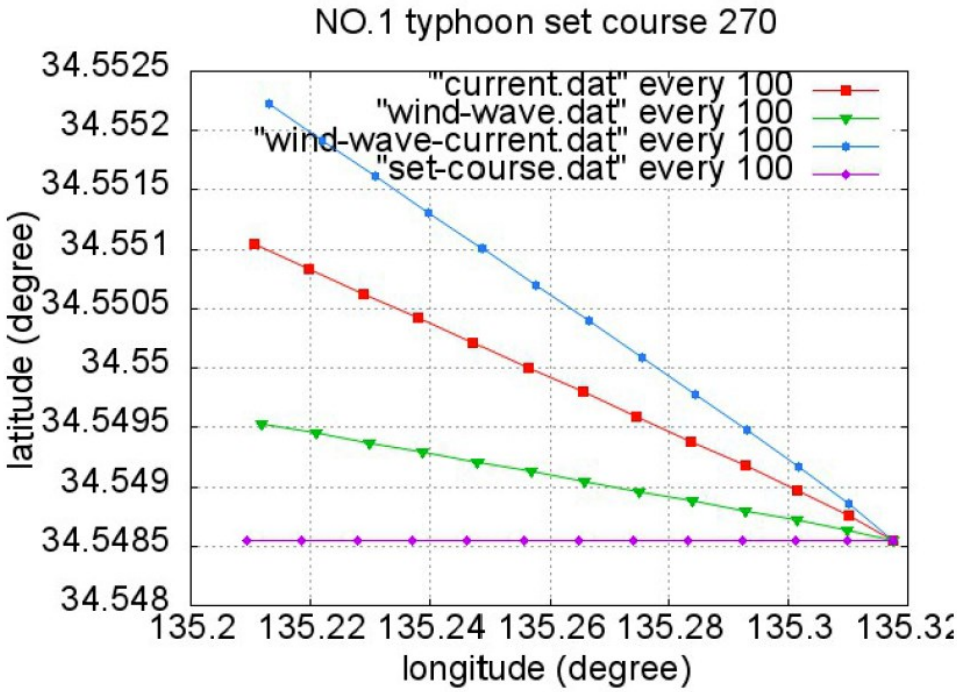

(C)

Fig.3.5-A, B, C. Numerical simulations of ship navigation by SR108 in Osaka Bay of No.1 typhoon

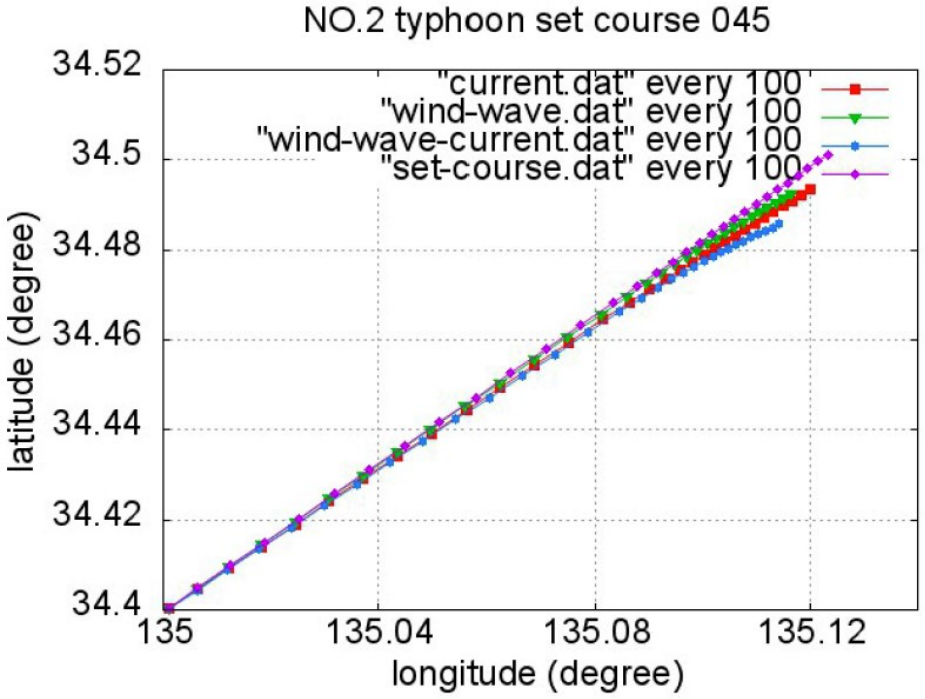
NO.2 typhoon set course 045
"current.dat" every 100
"wind-wave.dat" every 100
"wind-wave-current.dat" every 100
"set-course.dat" every 100
34.52
34.5
34.48
34.46
34.44
34.42
34.4
latitude (degree)
135
135.04
135.08
135.12
longitude (degree)

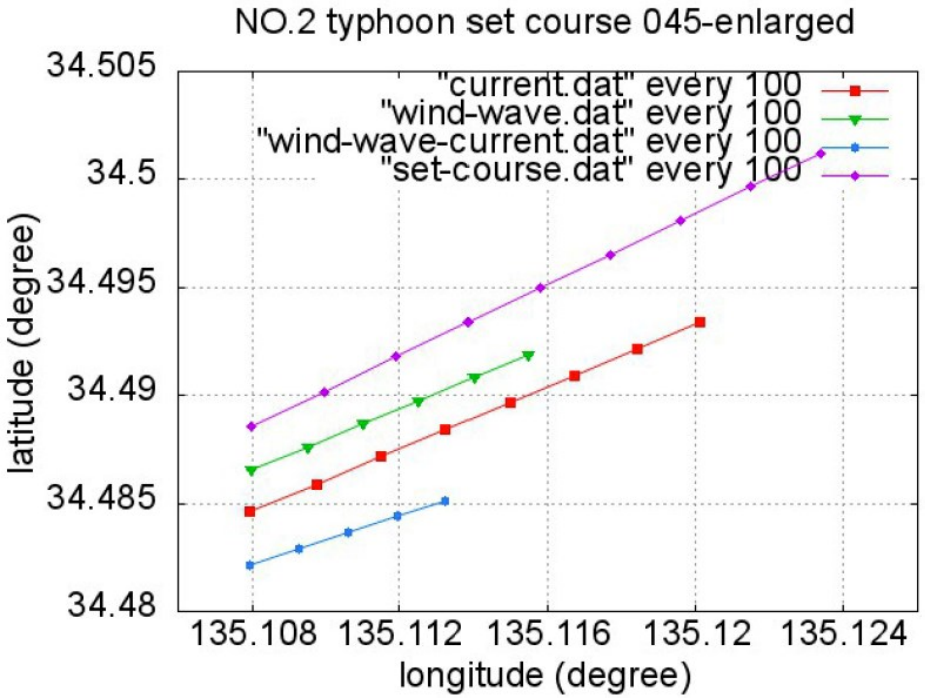
NO.2 typhoon set course 045-enlarged
"current.dat" every 100
"wind-wave.dat" every 100
"wind-wave-current.dat" every 100
"set-course.dat" every 100
34.505
34.5
34.495
34.49
34.485
34.48
latitude (degree)
135.108
135.112
135.116
135.12
135.124
longitude (degree)

(A)

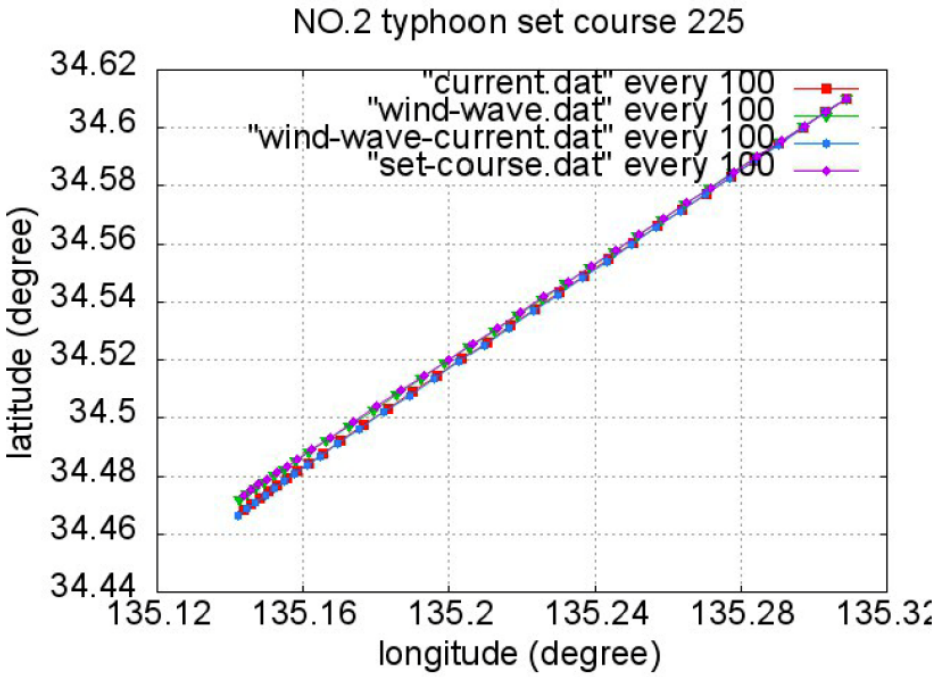
NO.2 typhoon set course 225
"current.dat" every 100
"wind-wave.dat" every 100
"wind-wave-current.dat" every 100
"set-course.dat" every 100
34.62
34.6
34.58
34.56
34.54
34.52
34.5
34.48
34.46
34.44
latitude (degree)
135.12
135.16
135.2
135.24
135.28
135.32
longitude (degree)

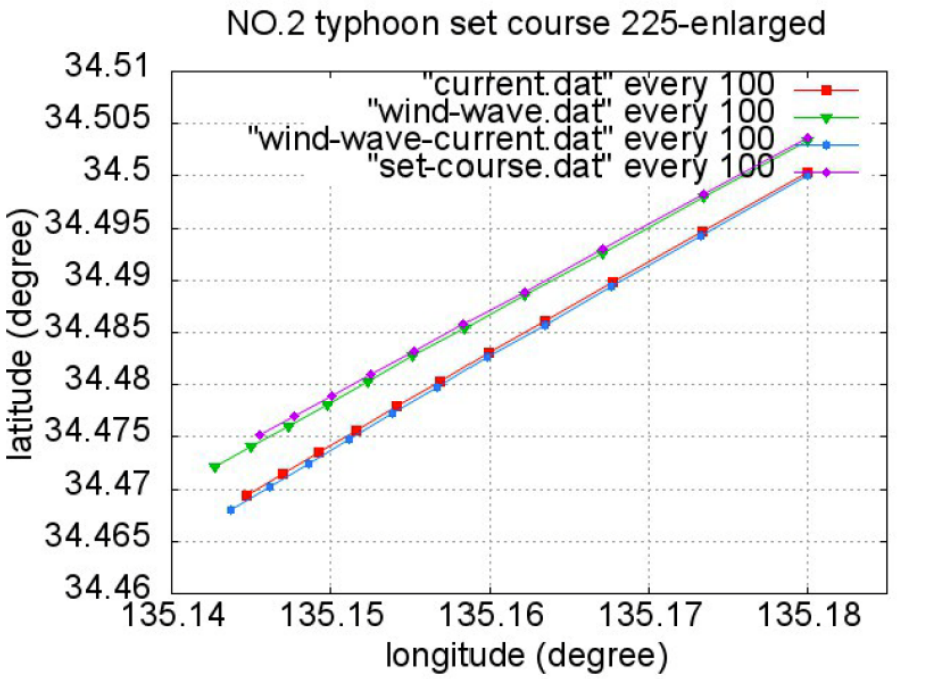
NO.2 typhoon set course 225-enlarged
"current.dat" every 100
"wind-wave.dat" every 100
"wind-wave-current.dat" every 100
"set-course.dat" every 100
34.51
34.505
34.5
34.495
34.49
34.485
34.48
34.475
34.47
34.465
34.46
latitude (degree)
135.14
135.15
135.16
135.17
135.18
longitude (degree)

(B)

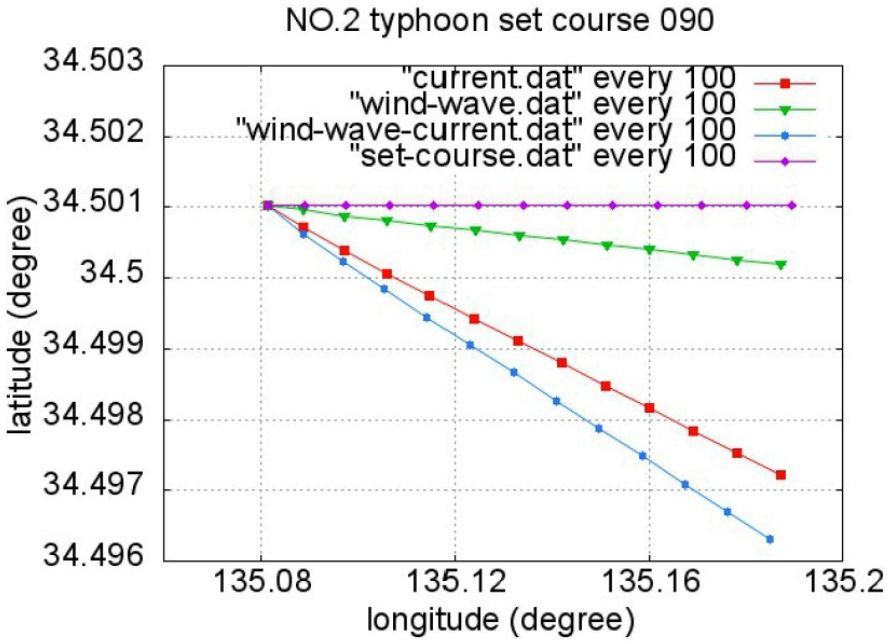

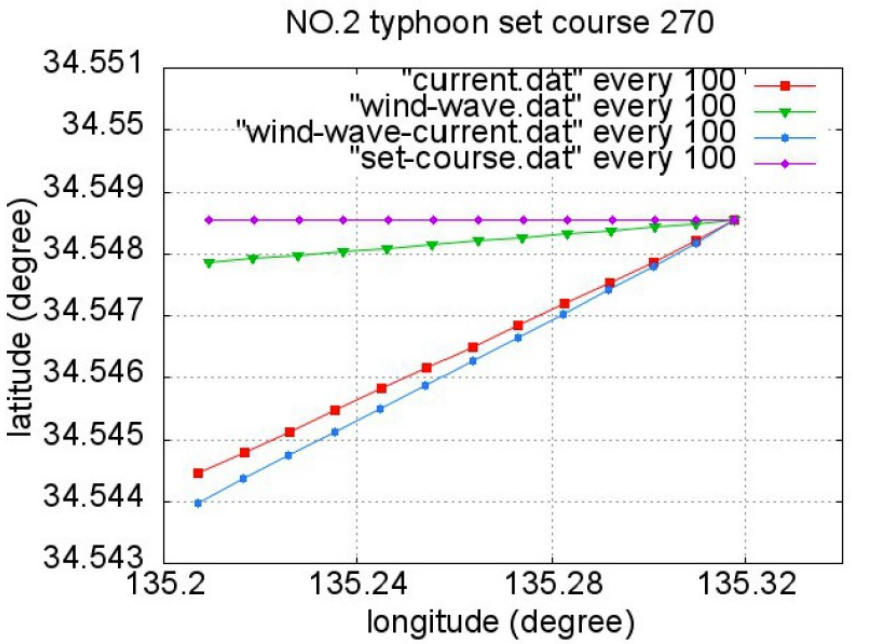

(C)

Fig.3.6-A, B, C. Numerical simulations of ship navigation by SR108 in Osaka Bay of No.2 typhoon

The course line marked with diamond shapes indicates the dead-reckoning track. The line marked with squares tracks the effects of tidal currents. The line marked with triangles shows the effect of wind and wave, while the line marked with circles shows

the influence of a combination of wind, wave, and tidal currents. The enlarged versions of 045 and 225 degrees are also given to illustrate the differences more clearly. Obvious influences by these factors can be found by noting the difference of coordinate intervals of longitude (E) and the latitude (N).

By comparing the actual tracks affected by two different typhoons in four virtual courses, it can be found that the strong south wind of NO. 1 typhoon has an effective influence on moving the ship northward, while the ship tends to move southward in the NO. 2 typhoon. In the cases of navigating in incline following waves, shown as the Fig.3.5-A and Fig.3.6-B respectively, the ship has a tendency to move a longer-than-normal distance, but in the other two figures of the Fig. 3.5-B and Fig. 3.6-A, moving in a headwind can make the real distance shorter. Additionally, when ship movement is influenced by lateral wave, shown in the Fig.3.5-C and Fig.3.6-C, lateral displacements are relatively large.

Considering the drift tracks above, it can be confirmed that wind has a major effect on drift distance, while current has more influence on drift angle. By comparing the drift angles, the tidal current is found to have a greater effect on a moving ship than waves and wind do.

3.2.2 East China Sea Area

To quantitatively investigate the effects of the Kuroshio Current on ship navigation, several experiments (riding favorable currents and unfavorable currents) were calculated in the ship navigation simulation area, respectively. Detailed information of course settings for numerical navigation in the East China Sea Area case can be found in Fig.3.7 and Table.3.2, respectively. As shown in Fig.3.7 and Table.3.2, four groups with course settings of 045, 090, 225, and 270 were simulated. Chosen for their distances from the Kuroshio Current main path, three start points (SP) were chosen for each group to make the simulations. For all of these cases, the numerical navigation was carried out in a fixed propeller revolution of 16 knots for 36 hours.

For the numerical simulation, ship speed of 16 knots as well as navigation time of 36 hours has been set. Considering that the objective is to study the effects of the current, only the advance, drift, and rotation motions in smooth water were considered. The hydrodynamic forces as well as external forces were simplified. In all cases, autopilot

was utilized.

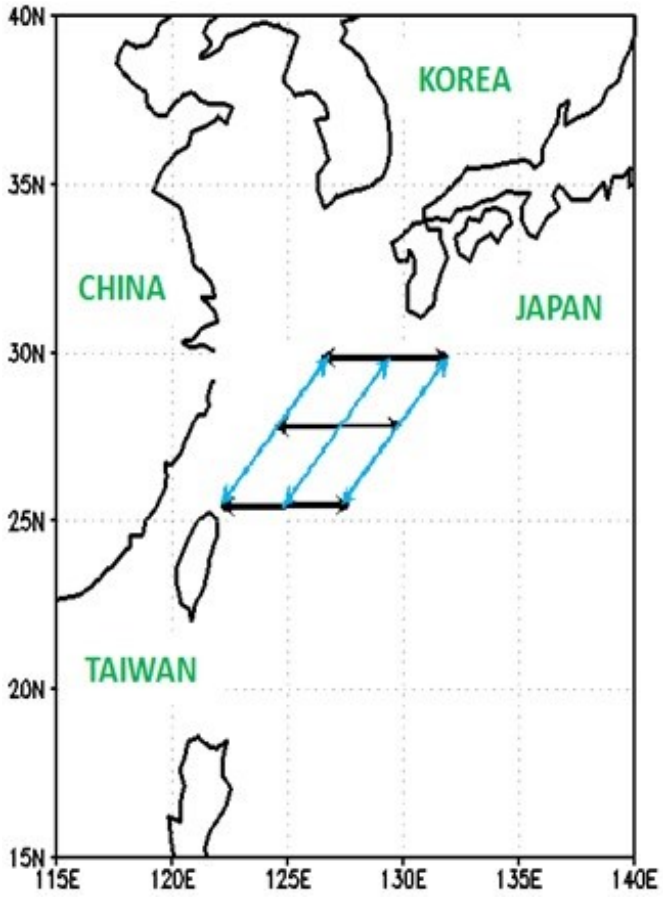

Fig.3.7. Course settings for numerical navigation in the East China Sea Area case

Table.3.2. Simulation designs for different cases in the East China Sea Area case

Set Course (SC)	Ship Start Point (SP)	Set Course (SC)	Ship Start Point (SP)
045	West (121E,26N)	090	South (121E,26N)
	Middle (124E,26N)		Middle (123E,28N)
	East (127E,26N)		North (125E,30N)
225	West (125E,30N)	270	South (126E,26N)
	Middle (128E,30N)		Middle (128E,28N)
	East (131E,30N)		North (130E,30N)

In Fig.3.8–Fig.3.11, the numerical ship tracks affected by the Kuroshio Current are given. The drift angle, drift distances, and speed variations in these simulation cases are given in Table.3.3 and Fig.3.12. The drift angles were calculated by the start point and end point, with the positive and negative drift angles representing angles to the left and right of the initial courses, respectively.

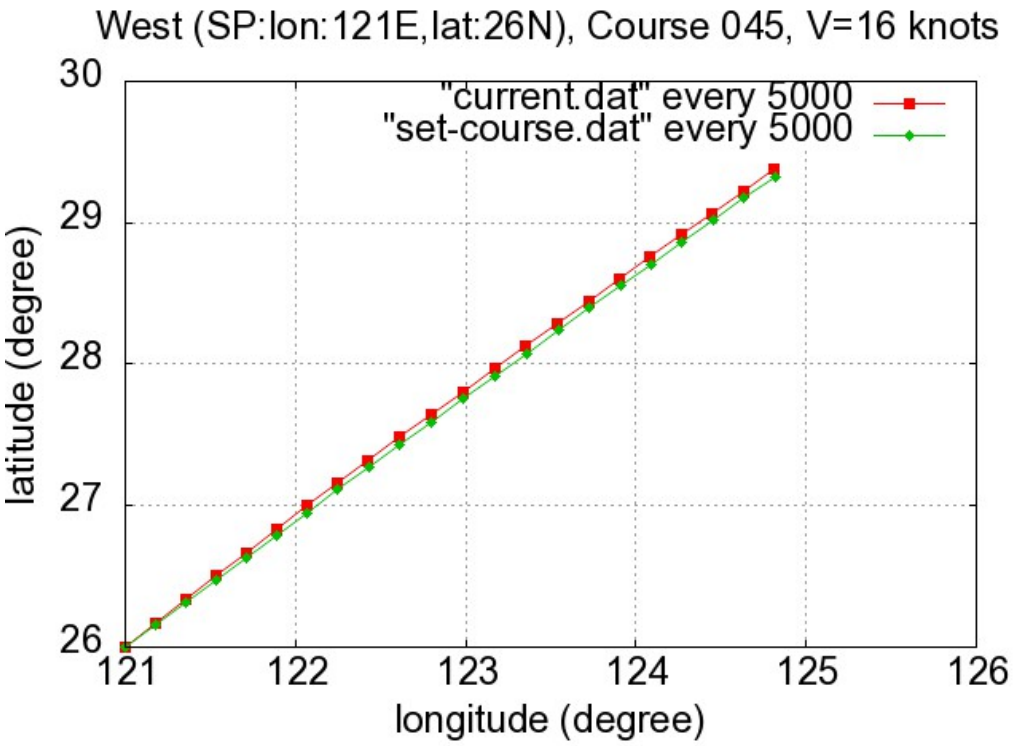

(A)Start point 121E, 26N

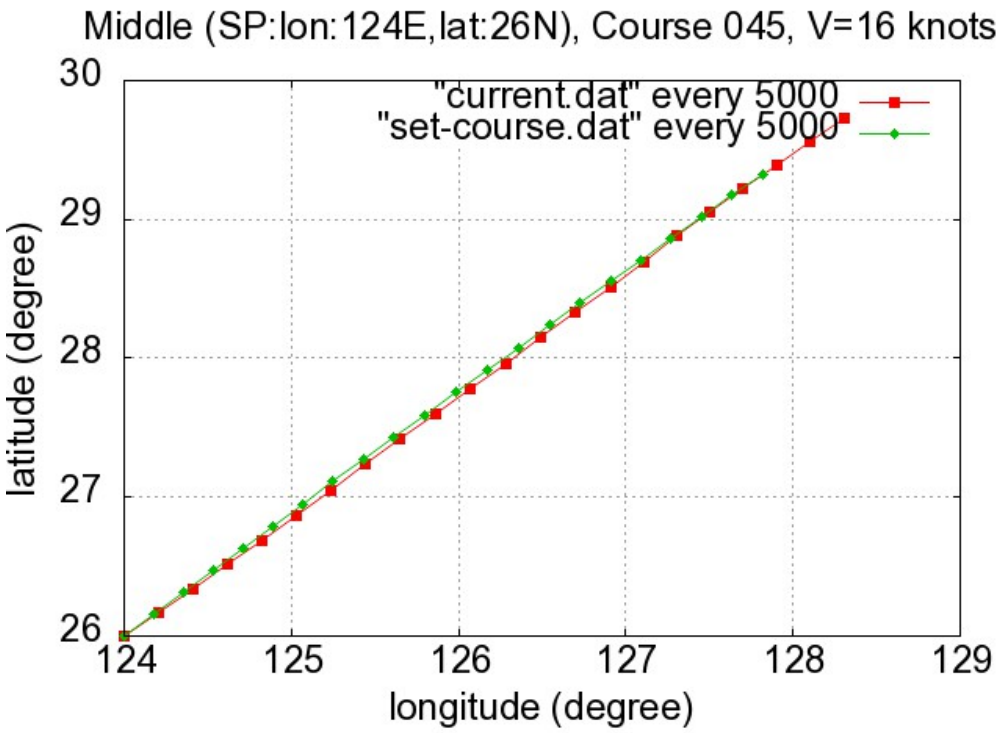

(B)Start point 124E, 26N

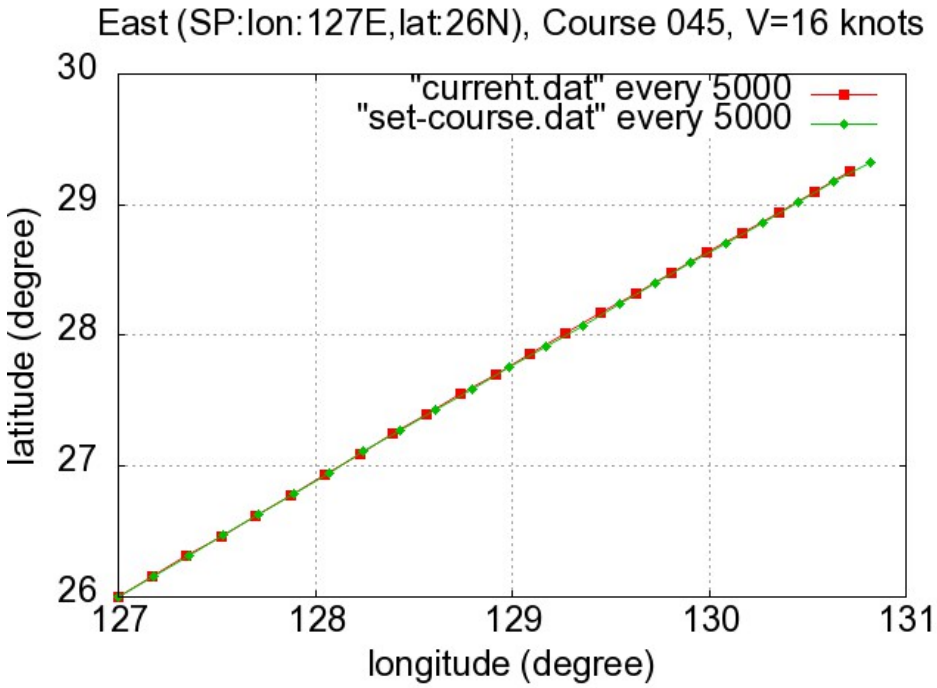

(C)Start point 127E, 26N

Fig.3.8. Numerical ship tracks in the Course 045 group

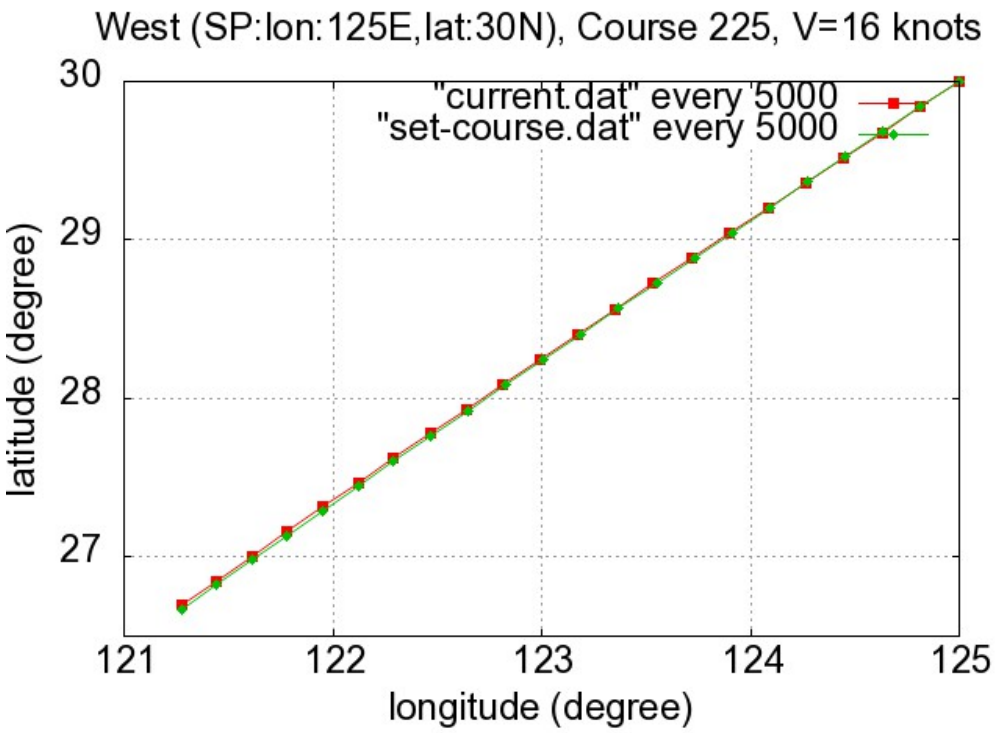

(A)Start point 125E, 30N

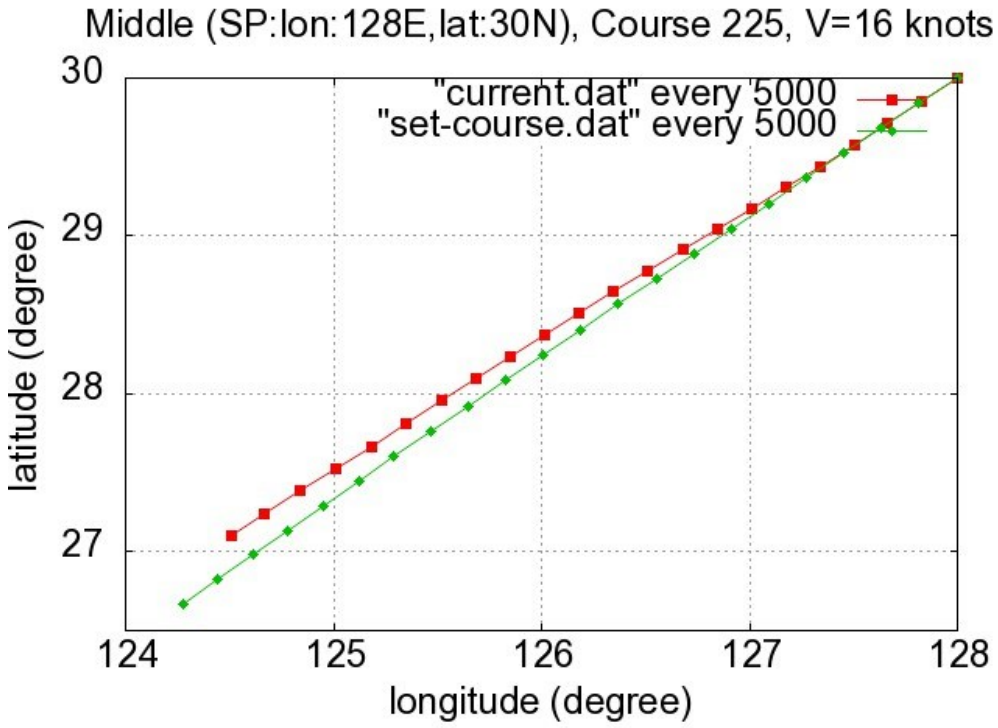

(B)Start point 128E, 30N

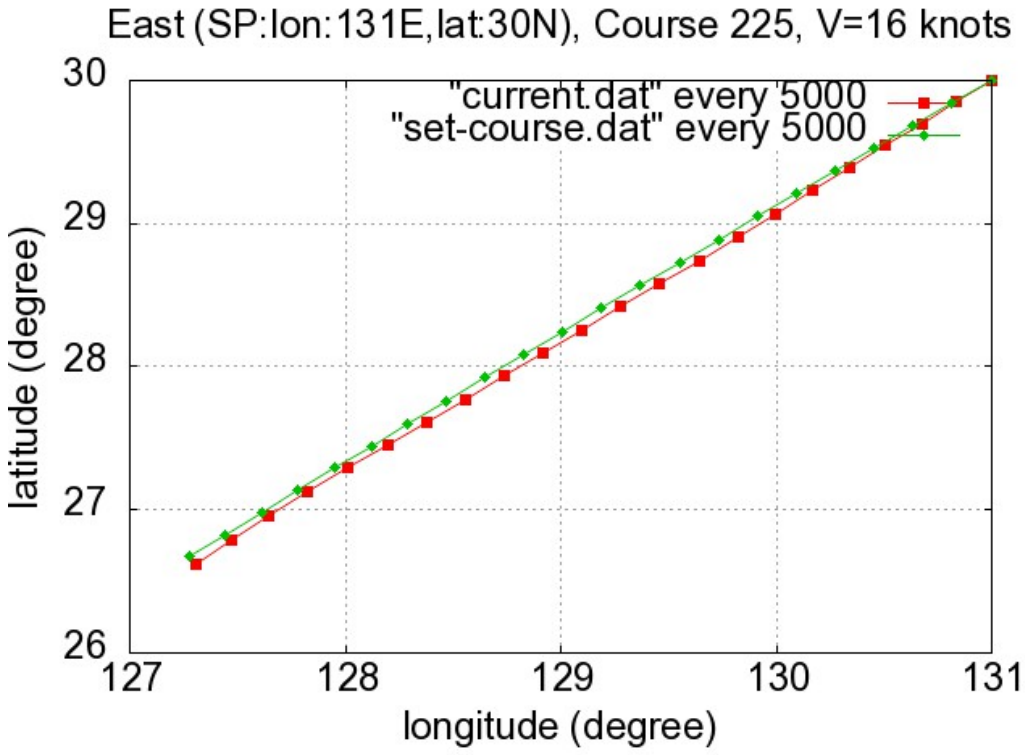

(C) Start point 131E, 30N

Fig.3.9. Numerical ship tracks in the Course 225 group

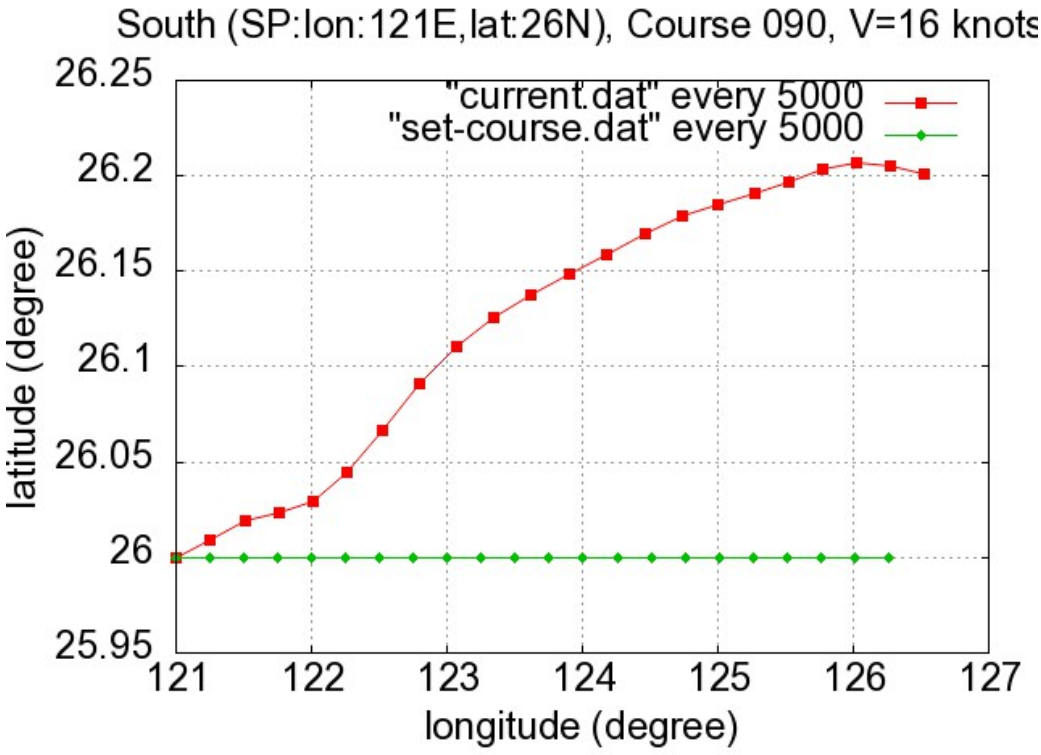

(A)Start point 121E, 26N

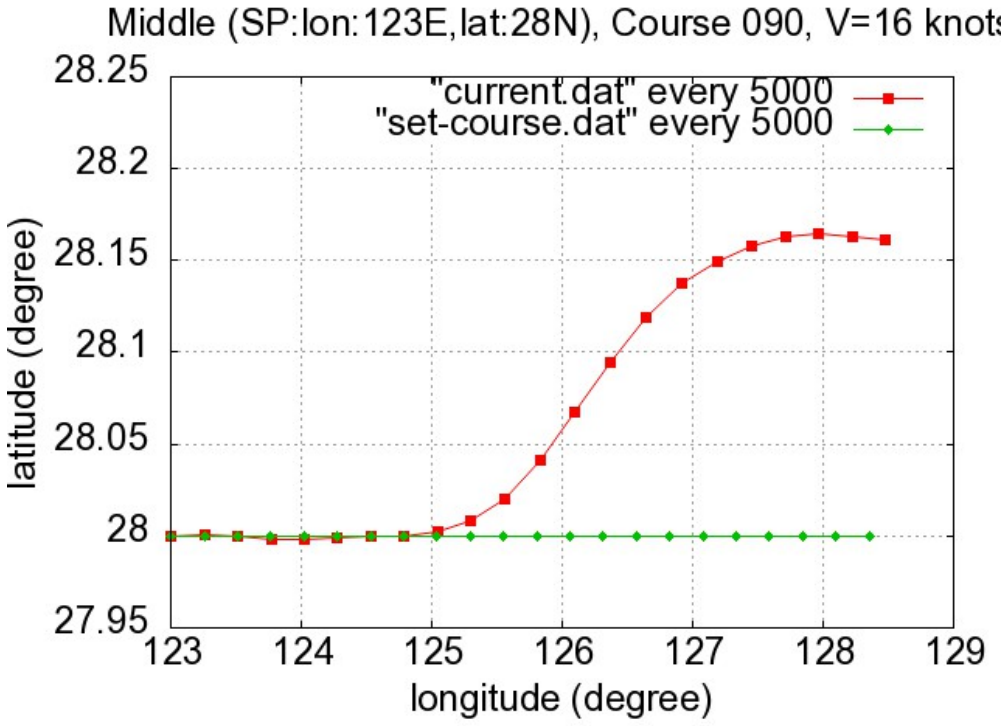

(B)Start point 123E, 28N

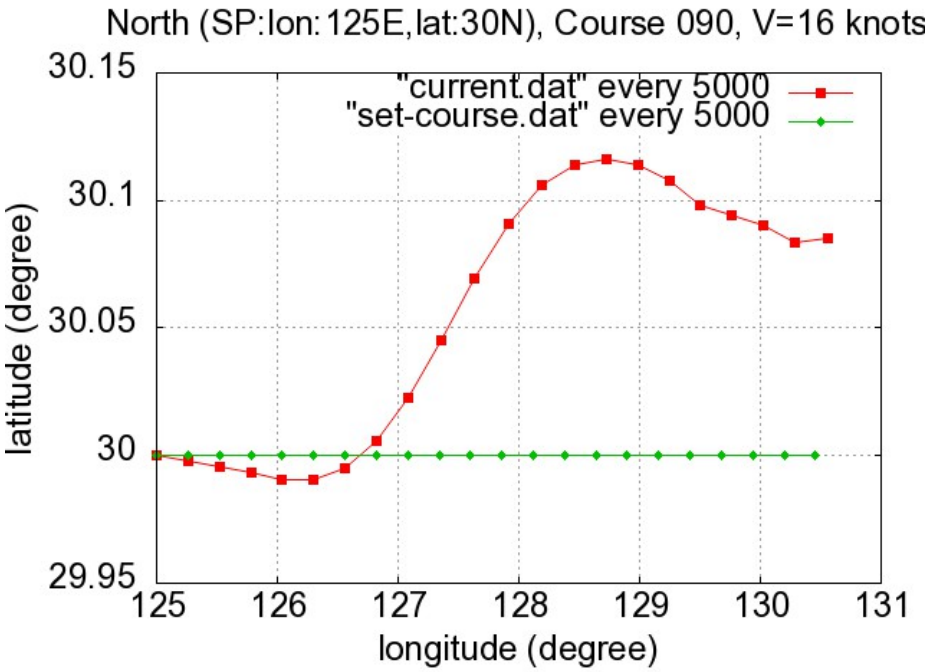

(C) Start point 125E, 30N

Fig.3.10. Numerical ship tracks in the Course 090 group

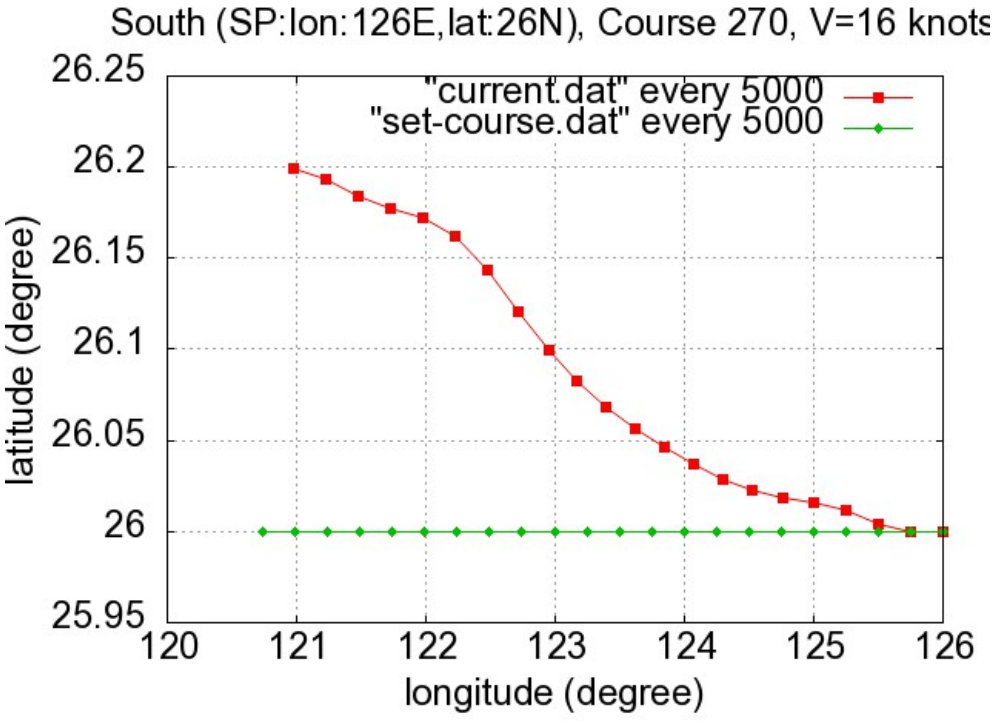

(A) Start point 126E, 26N

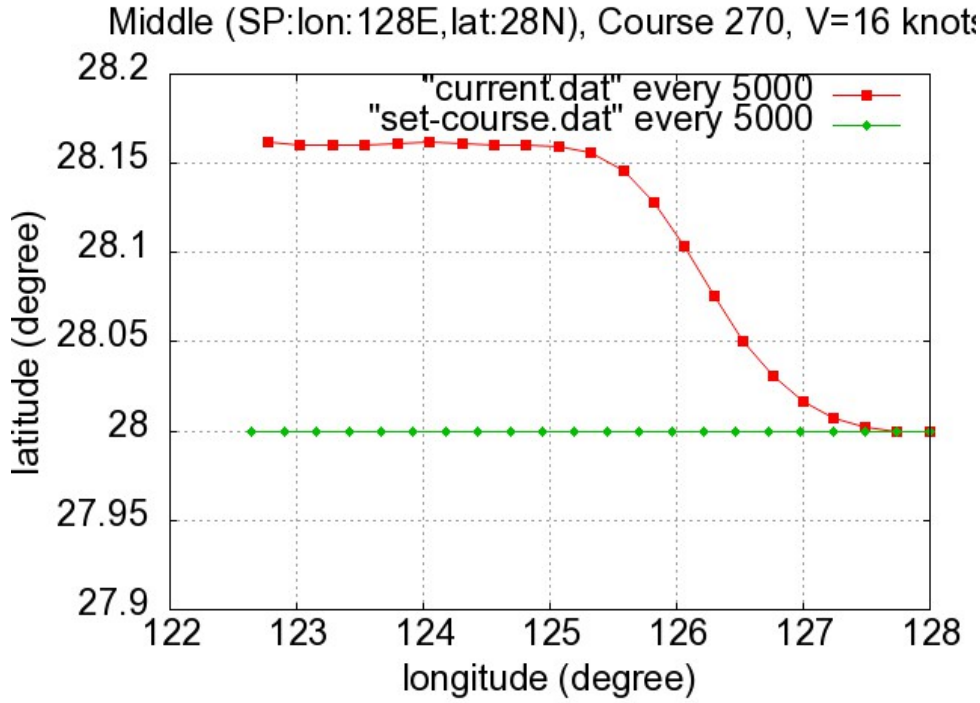

(B)Start point 128E, 28N

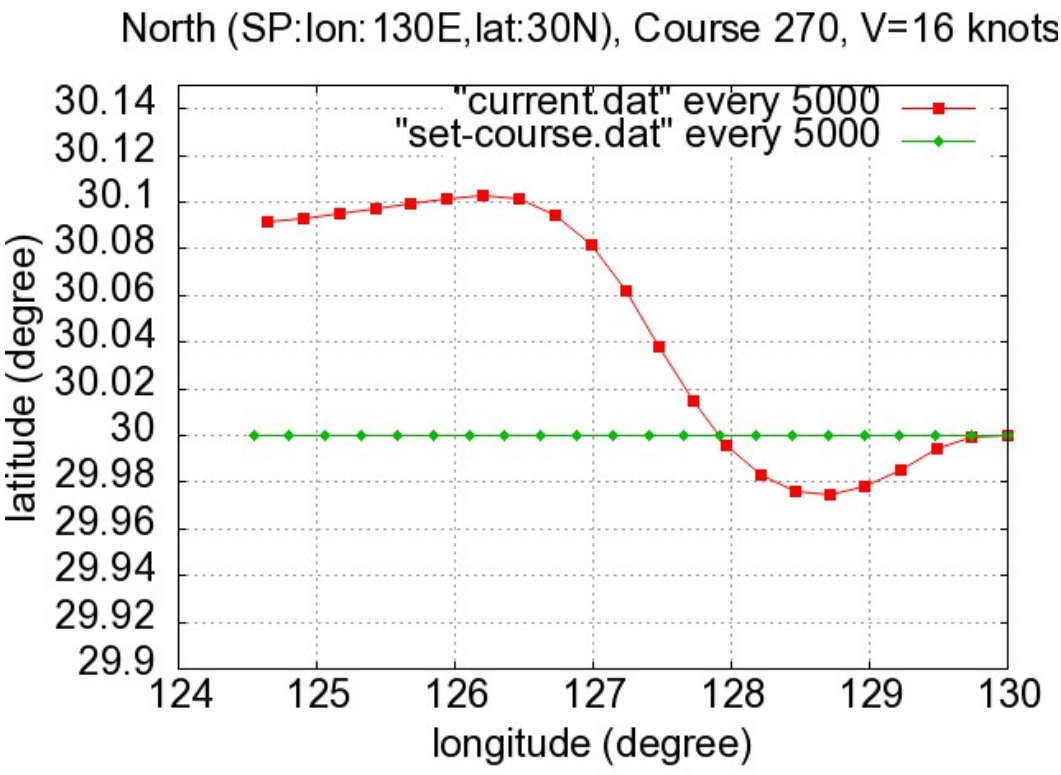

(C)Start point 130E, 30N

Fig.3.11. Numerical ship tracks in the Course 270 group

Table.3.3.Drift angles, drift distances, and speed variations in all cases

Set Course (SC)	Ship Start Point (SP)	Drift Angle (degree)	Drift Distance (km)	Ship Speed Change (%)
045	West (121E,26N)	0.45	3.38	0.09
	Middle (124E,26N)	-0.04	64.96	1.67
	East (127E,26N)	0.08	-12.69	-0.33
225	West (125E,30N)	-0.20	-1.86	-0.05
	Middle (128E,30N)	-1.95	-52.34	-1.36
	East (131E,30N)	0.65	2.67	0.07
090	South (121E,26N)	2.23	26.47	0.68
	Middle (123E,28N)	1.84	11.87	0.31
	North (125E,30N)	1.05	9.53	0.25
270	South (126E,26N)	-2.47	-23.85	-0.61
	Middle (128E,28N)	-1.97	-12.80	-0.33
	North (130E,30N)	-1.09	-10.16	-0.26

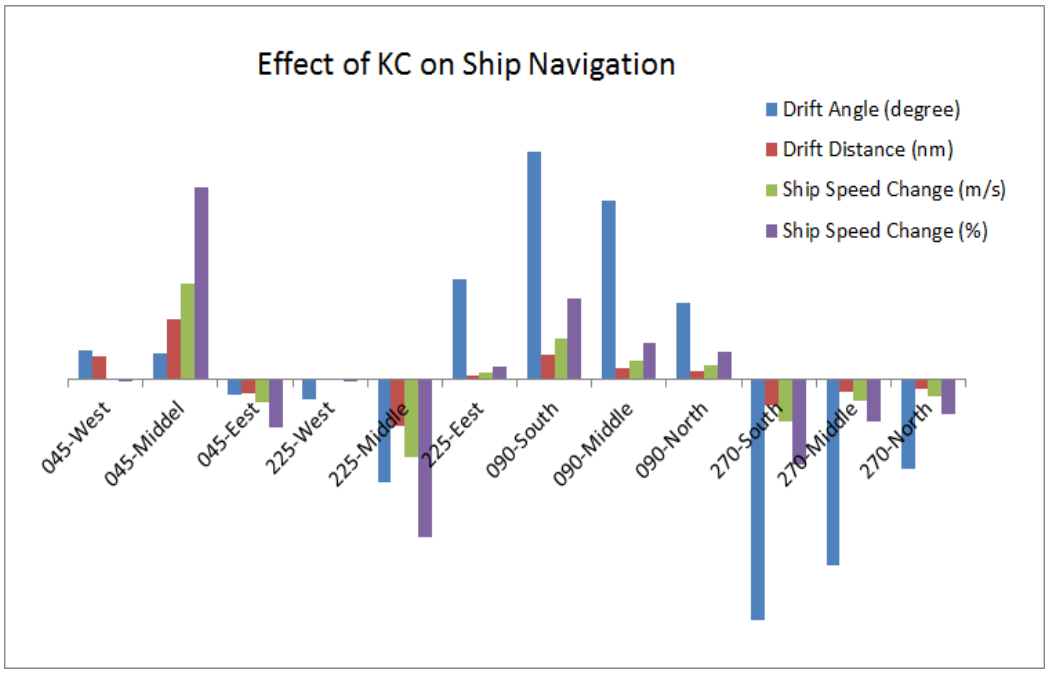

Fig.3.12. Effect of the Kuroshio Current on ship's drifting and speed variations in all cases

Comparing the data of groups 045 and 225, we can say that the Kuroshio Current main path can affect fuel and time costs significantly, as shown in the cases of 045-Middle and 225-Middle, where the ship navigates along and against the Kuroshio Current main path, respectively. When the ship navigates along the Kuroshio Current main path (case 045-Middle), the maximum drift distance and ship speed increase can be 64.96 km and 1.67%, respectively. Conversely, in the case of 225-Middle, the ship will have a maximum drift distance shortage and speed loss of 52.34 km and 1.36% percent, respectively. The results agree well with the study of Chang, et al (Chang, et al. 2013) (1.8%), which applied the velocity of the Kuroshio Current from the Surface Velocity Program data.

In the 090 and 270 cases, it can be seen that the earlier the ship is affected by the Kuroshio Current main path the bigger the drift angle and the distance become. This also verifies that the velocity of the Kuroshio Current main path is much larger than the current in the nearby ocean area.

As illustrated by all of these cases, it may be quantitatively confirmed that navigating along the Kuroshio Current main path may save time as well as fuel costs due to the effect of the Kuroshio Current's velocity; conversely, navigating in the opposite direction will increase the navigational cost significantly.

Additionally, aiming to construct the numerical ship navigation system taking all the weather and ocean into consideration, beside of the Kuroshio Current, influences of ocean wind and ocean waves have also been studied. To quantitatively investigate the effect of wind, wind-induced waves as well as ocean current on ship navigation, several experiments were calculated when the typhoon (SONGDA; for detailed calculation, please refer to Chapter.2.2.2) was approaching, arriving and leaving the ship navigation simulation area, respectively. Simulation results of wind, current and wind-induced waves were verified by utilizing observation data. Influences of strong wind, wind-induced ocean waves and ocean current on ship's track were also studied by calculating several different cases.

According to the wind speed variations from the typhoon eye on the meridional and zonal directions, see Fig.3.13, the distance of ship location to the typhoon eye was focused on in the first case to find the different effects of locations on ship navigation, shown as Fig.3.14-a. While in the second case, given as Fig.31.4-b, the moment when

the typhoon approached, arrived at as well as left the ship navigation area were studied to search for typhoon-avoidance conditions.

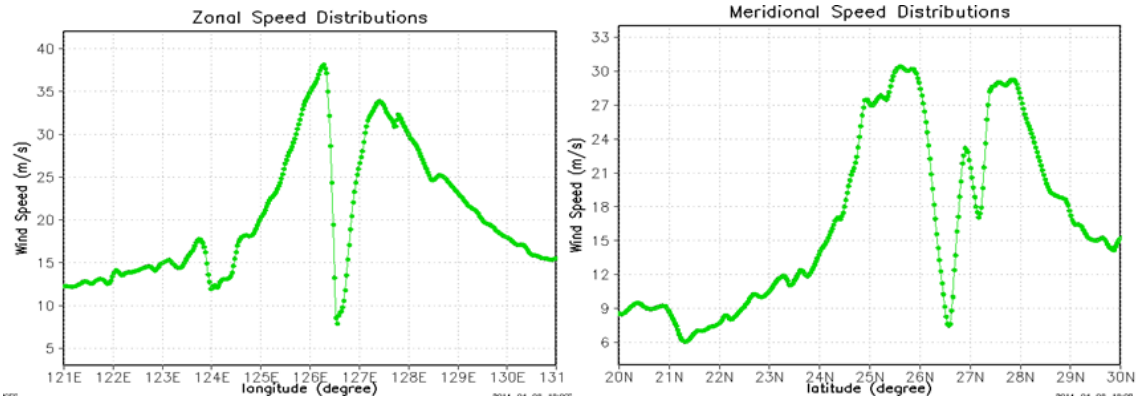

Fig.3.13. Meridional and zonal wind speed around the typhoon eye (126.6 E; 26.3 N)

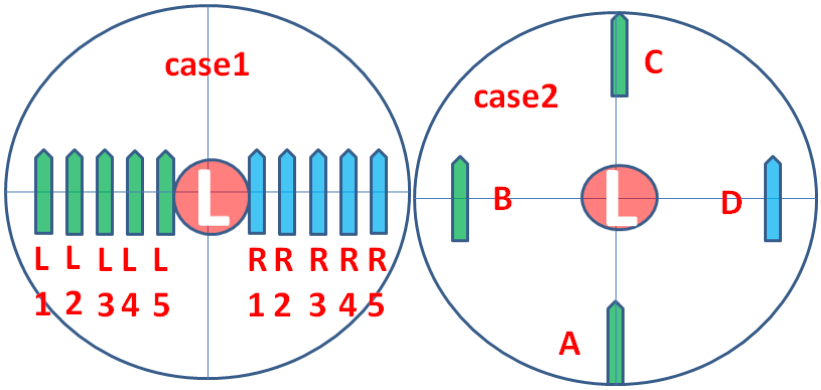

Fig.3.14. Graph descriptions of the two simulation cases

A distance interval of 0.8 degree of both left and right side from the typhoon eye in the zonal direction was set in the case 1. In the case2, 0.6 degree in the zonal direction was applied in the zonal direction while the closet distance of about 0.5 degree was set in the meridional direction.

The detailed settings were given as Table.3.4. Relative locations of ship and typhoon, Kuroshio Current in two cases are given as the top two and below two figures of Fig.3.15, respectively.

The wind speed, wind direction, significant wave height, average wave period and current velocity were input to the ship maneuvering model with a spatial resolution of

every 0.01 degree. The numerical navigation was carried out for about 10 hours at a corresponding ship speed as 16 knots in calm water with the fixed propeller rotation.

Table.3.4. Simulation designs for different cases in the East China Sea Area case

Typhoon eye		126.6 E & 26.6 N			
Ship routes	Course	Start location			
		Left quadrant		Right quadrant	
Case.1	000	L1	125.8 E & 25N	R1	127.4 E & 25N
		L2	125 E & 25N	R2	128.2 E & 25N
		L3	124.2 E & 25N	R3	129 E & 25N
		L4	123.4 E & 25N	R4	129.8 E & 25N
		L5	122.6 E & 25N	R5	130.6 E & 25N
Case2	000	A		126.6 E & 22 N	
		B		126.6 E & 27 N	
		C		126 E & 25N	
		D		127.2 E & 25 N	

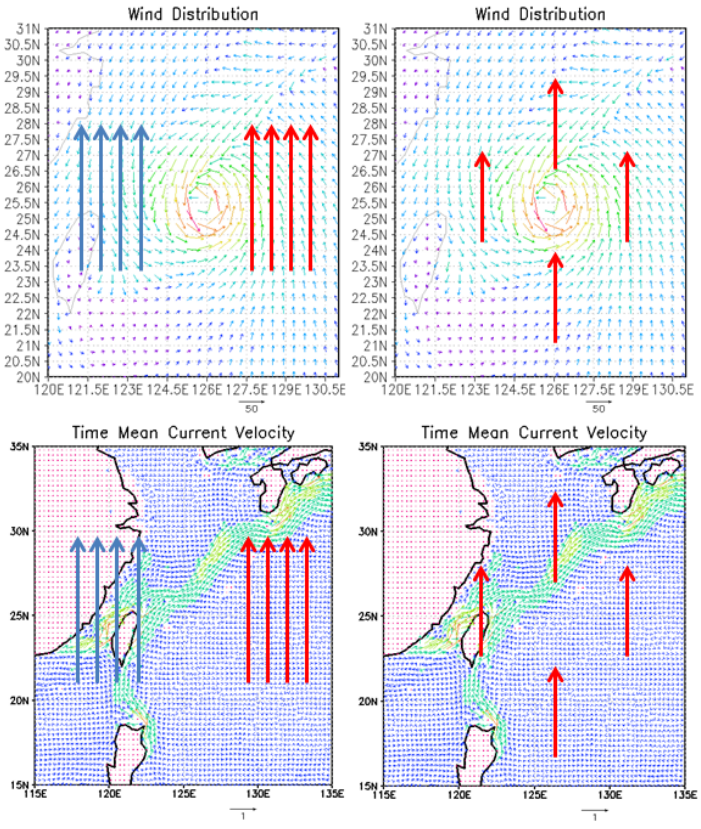

Fig.3.15. Relative locations of ship and typhoon, Kuroshio Current in two cases

As shown in Fig.3.16 and Fig.3.17, the numerical ship tracks of these two cases are given. The horizontal and vertical axis shows the longitude and latitude, respectively. For the Fig.3.16, the color lines are the simulated ship tracks, where the ten lines from left to right represent start locations from L1 to R5, respectively. For the Fig. 3.17, the red, green, blue and purple lines show the tracks from A to D, respectively.

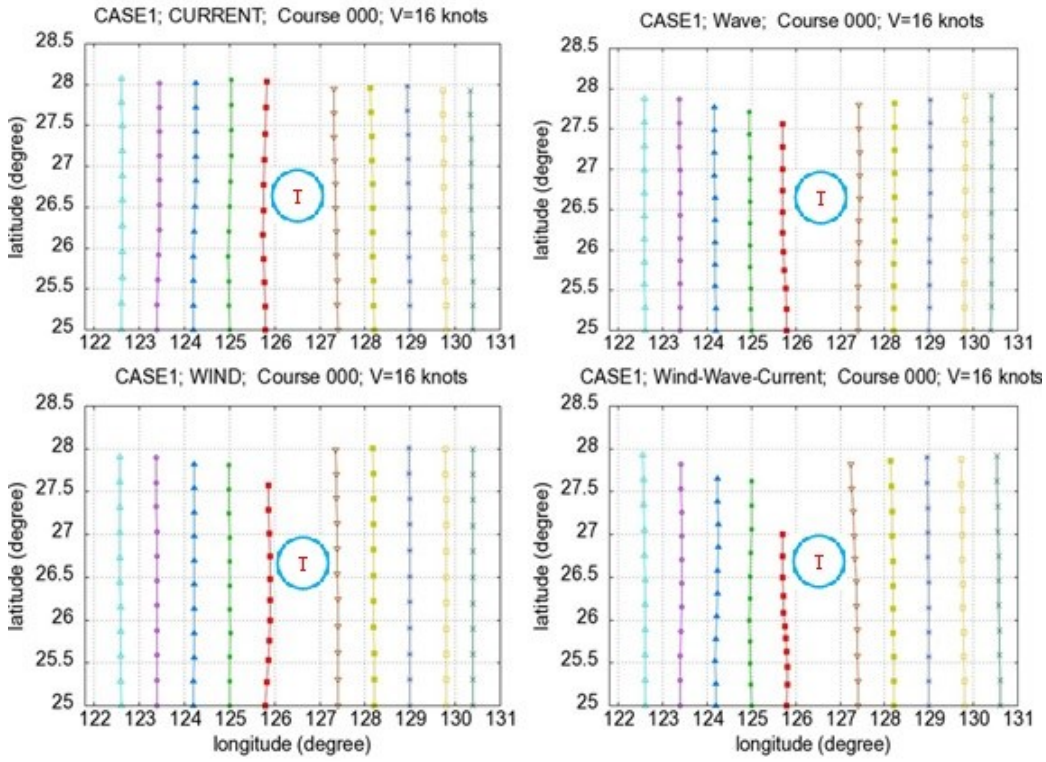

Fig.3.16. Numerical simulation results of ship tracks in Case 1

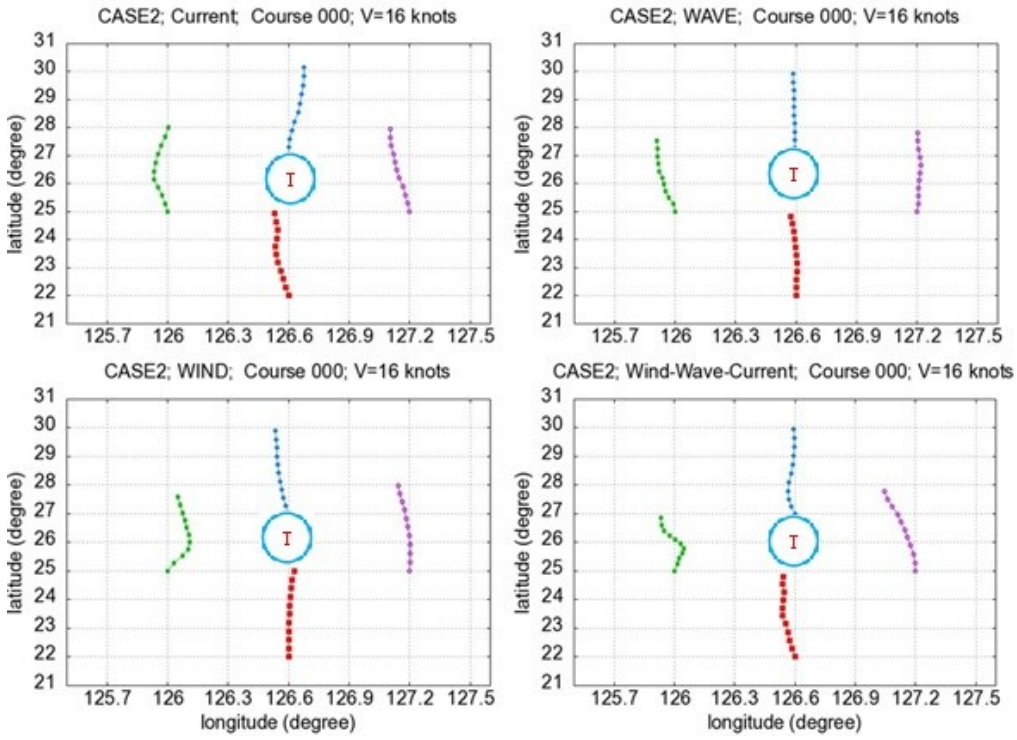

Fig.3.17. Numerical simulation results of ship tracks in Case 2

Effects of the Kuroshio Current can be found from the left-top fig of Fig. 16. The left five tracks (from L1 to L5) show a tendency to sail at a course right than the set course 000 when the ship encounters the Kuroshio Current with a strong northeastern velocity. While affected by a relative weaker current with a western to west-northern direction, the right five tracks (from R1 to R5) tend to drift to the left side of the original set course. Besides, ship can sail a longer distance with a following Kuroshio Current (from L1 to L5), while sailing against the ocean current can has an opposite influence (from R1 to R5).

For the wave factor, the right-top fig of Fig. 16 show that head waves have a strong effect on pushing against ship navigation by generating added resistance, which reduce the ship's sailing distance in the condition of a same sailing time period. And this effect becomes larger when the ship sails closer to the typhoon eye where added resistance increase as the significant height increase (Gerritsma et al., 1961; Gerritsma and Beukelman, 1972; Lloyd, 1989). Besides, a larger drift angle can be found when the angle of encountering waves is 090 and 120, where the side forces and turn moment are stronger.

For the wind impact, a similar result can be concluded as wave influence. The strong head wind can also generate a large added resistance because of the superstructure of the ship model, which decreases sailing distance by consuming more ship energy provided by the propeller, as shown from the left five tracks of the left-down of Fig.3. 16. However, the right five lines of the same figure can illustrate the longer distances when the ship sails with a following wind. Sailing with a stronger following wind in the right quadrant, see Fig.3.14-a, can add to speed of about 2 knots than sailing against wind in the left quadrant.

As shown in the left-top figure of Fig.3.17, the green and blue lines (track B and C) are affected by the northeastern Kuroshio Current while the other two mean that the ship is affected by the western ocean surface current.

For the wave effects, as the green and red lines in the right-top figure of Fig. 3.17 shows, strong side forces coming from the starboard side make is drift to the opposite side (left then the set course), and wave resistance also have a negative influence on sailing distance.

A tendency to drift to its opposite side against the lateral wind force can be clearly found in the left-down figure of Fig. 3.17, an anti-clockwise direction of ship drift in this figure agree well with the typhoon wind distributions.

To give a more clear and direct results quantitatively, the calculated drift angles and track distance and also available from Table.3.5 and Fig.3.18. The drift angle was calculated by the start point and end point. For the Fig. 3.18-a, b; the number from 1to 10 of the horizontal axis represent simulation tracks from L1 to R5, respectively. For the Fig. 3.18-c, d; the number from 1to 4 of the horizontal axis represent simulation tracks from A to D, respectively.

Compared with the effects of current, the influence of wind and waves on ship sailing distance are larger, as given in the Fig. 3.18-b. A speed loss of about 3 knots can be observed in the track L5 of case1 and B of case2, where the head wind and waves make strong resistance. It is also illustrated from the Fig. 3.18-a, that waves tend to have a larger influence on ship's drift angle then wind when the ship sails at the direction following the typhoon track. The green line in the same figure also figures it out that a

following ocean current, see from L1 to L5, has a smaller influence than a lateral one, as from R1 to R5, on the ship's drift angle.

Table.3.5 Simulation results of these two cases

	drift angle (degree)				track distance (nm)			
Case1	wind	wave	current	wind-wave-current	wind	wave	current	wind-wave-current
L1	0.54031	0.18594	0.14521	0.7222	178.203	176.2092	188.3472	179.5158
L2	0.24399	0.34009	0.78416	0.09341	177.3372	175.7316	184.4616	172.4172
L3	0.13128	0.71829	0.79198	0.56477	172.7418	169.5762	184.2954	162.5358
L4	0.40463	0.84937	0.7268	2.76221	171.9048	166.1928	187.0554	160.6764
L5	1.0947	2.05853	0.34273	2.33002	158.238	157.284	186.375	123.078
R1	0.82074	0.47451	1.59482	2.69077	182.4876	171.4224	180.8754	172.6536
R2	0.33246	0.55889	1.46155	1.28336	183.8454	172.9824	181.2672	174.81
R3	0.24551	0.6277	1.0079	0.66431	184.0332	175.3986	182.3886	177.609
R4	0.16544	0.29621	1.37802	1.33362	183.4566	177.7596	179.0694	176.0718
R5	0.14371	0.20509	1.18472	1.16092	183.3138	178.7244	179.3496	178.539
Case2	wind	wave	current	wind-wave-current	wind	wave	current	wind-wave-current
A	0.55656	0.43927	1.26517	1.04929	183.0738	173.4324	179.7858	171.1458
B	0.93211	1.77075	0.10316	1.83551	159.4104	155.4972	184.4268	114.2928
C	1.11938	0.23303	1.15095	0.15582	176.964	178.5576	192.2322	181.4592
D	0.97125	0.02697	1.55823	2.75565	182.3874	172.5396	181.2042	170.7012

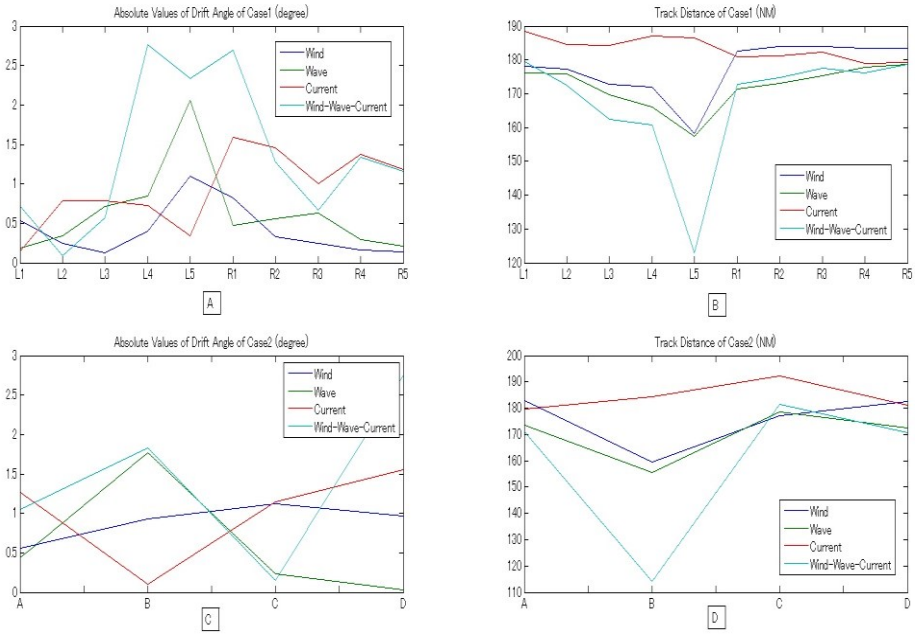

Fig.3.18. Effects of weather and ocean on ship navigation

3.3 Summary

Several simulations were performed in the study for numerical navigation of an oceangoing ship in coastal areas to make the construction of the numerical ship navigation system. The aim was to evaluate the effectiveness of numerical ship navigation system in the simulation of weather, as well as the effects of various factors on ship navigation. The conclusions are as follows:

1. Combining the numerical models WRF, SWAN, and POM, effective and high-resolution data of wind, waves, and currents can be generated.

2. Calculated data can be applied on numerical ship navigation, which can calculate the influence of wind, waves, and currents on an oceangoing vessel based on the MMG ship maneuvering model has been proved possible as a method of studying the ship motion's reaction to the weather and ocean. This method can quantitatively calculate the drift angle as well as the distance at which a ship is affected by the weather and ocean.

3. For the Osaka Bay Area case, by comparing different drift tracks, it can be confirmed that the effects of wind, waves, and currents on the ship navigation during these two typhoons.

4. For the East China Sea Area case, the Kuroshio Current has been found having a significant effect on navigational time as well as fuel costs in the ECSA. Taking the Kuroshio Current effect into consideration may help ships navigate more economically. The reduction of time as well as the fuel cost of navigating along the Kuroshio Current main path has been quantitatively confirmed; conversely, it has also been proved that navigating in the opposite direction will increase the navigational cost significantly.

5. Variable spatial resolutions could be selected to calculate different cases by using numerical weather and ocean models. Fine enough information of meteorological and marine phenomena could be provided to conduct the numerical simulation of ship navigation.

The Numerical Navigation System constructed here has shown its feasibility to study about influences of weather and ocean on ship navigation, which could also be utilized as the basis of developing a weather routing system based on an ocean-going bulker (Sasa Kenji, et al. 2015) taking weather and ocean effects into account. It is possible to achieve an optimum ship routing based on the combination of the present-completer numerical ship navigation system and the optimization algorithm which is to be discussed in the next chapter.

References

Fujiwara, Toshifumi; Ueno, Michio; Nimura, Tadashi. Estimation Of Wind Forces And Moments Acting On Ships. Journal-Society of Naval Architects Of Japan, 1998, 183: 77-90.

Gerritsma et al., 1961. J. Gerritsma, J.J. Van der Bosch, W. Beukelman. Propulsion in regular and irregular waves, International Shipbuilding Progress, 8 (82) (1961), pp. 285–293.

Gerritsma and Beukelman, 1972. J. Gerritsma, W. Beukelman. Analysis of the resistance increase in waves of a fast cargo ship, International Shipbuilding Progress, 19 (217).

Hasegawa,K., 1980. On a performance criterion of autopilot navigation.Journal of the Kansai Society of Naval Architects, Japan 178, 93–104.

Kashiwagi, M., Mizokami, S., and Tasukawa, H., 1999. Application of the Enhanced Unified theory to Seakeeping Calculations of Actual Ships. Proc. of 4th Japan–Korea Joint Workshop on Ship and Marine Hydrodynamics (Fukuoka), p.59-66.

Kijima,Katsuro, etal.,1990. On the manoeuvring performance of a ship with the parameter of loading condition.Journal of the Society of Naval Architects of Japan.168, 141–148.

Kunij KOSE et al, 1981. Concretization of the Mathematical Model of Ship Maneuverability. Proceedings of the 3rd Symposium on Ship Maneuverability, 28-81.

Lloyd, 1989. A.R.J.M. Lloyd. Sea-keeping: Ship Behaviour in Rough Weather, Ellis Horwood.

Ogawa, T., 1981. The basics of a mathematical model of ship maneuverability. Proceedings of the 3rd Symposium on Ship Maneuverability, 9–26.

Sasa Kenji, et al. "Evaluation of ship performance in international maritime transportation using an onboard measurement system-in case of a bulk carrier in international voyages." Ocean Engineering 104 (2015): 294-309.

Yoshimura, Y., et al.,1989. Mathematical model for the manoeuvring ship motion in shallow water (3rd report)—Manoeuvrability of a twin-propeller twin-rudder ship. Journal of the Kansai Society of Naval Architects, Japan 211, 115–126.

Yu-Chia Chang, Ruo-Shan Tseng, Guan-Yu Chen, Peter C Chu and Yung-Ting Shen (2013). Ship Routing Utilizing Strong Ocean Currents. Journal of Navigation, 66, pp 825-835.

CHAPTER 4

OPTIMUM SHIP ROUTING BASED ON NUMERICAL SHIP NAVIGATION SYSTEM

To complete an optimum ship routing system for safer, more economical and environment-protection ship navigation, beside of global scale weather and ocean information as well as the before-built numerical ship navigation system, an optimization algorithm for optimum ship routing is also required to reduce navigational cost of time and fuel as well as achieving other targets such as ship safety assurance, cargo protection, crew comfort and maintenance of fleet schedule by taking influences of ocean states on ship motion into consideration. Instead of trying to avoid all adverse weather and ocean, an algorithm for optimum ship routing should be able to help ships find the best balance to minimize time of transit and fuel consumption without placing the vessel at risk to weather damage or crew injury.

4.1 Introduction to optimization algorithms for optimum ship routing

Several optimization algorithms for ship weather routing have been studied and given by other researchers in the past several decades. Those mostly used optimization algorithms include the isochrone method (James 1957), Dijkstra algorithm (Dijkstra, 1959; Padhy, 2008), Calculus of variations (Bijlsma, 1975), Dynamic Programming (Chen, 1978; Avgouleas, 2008), and the augmented Lagrange multiplier (Tsujimoto, Tanizawa, 2006).

For the algorithm of calculus of variations, the ship routing is solved as a continuous optimization problem in necessary conditions to give a local extreme to an objective function J, a number of routes for various initial settings such as ship's headings and propeller revolutions have to be calculated to get the solution to J. Besides, the accuracy of the solution could be decreased because of those complex numerical differentiations when the environmental conditions become severe. Additionally, it can be difficult to treat ship routing as a stochastic optimization problem, which makes it impractical for real case ship routing.

And dynamic programming can give the functional recursion equation to solve the ship routing problem formulated as a discrete optimization problem based on the Bellmen's principle of optimality. However, the accuracy of this method greatly depends on the fineness of grid system, which needs a lot of calculation time and memory space for an accurate solution.

By treating the ship routing as a discrete optimization problem, the isochrone method proposed by James can get the minimum time route by repeatedly computing an isochrones which is defined as an outer boundary of the attainable region from the departure point after a certain time according to requirements and possible conditions of weather and ocean states. However, the isochrone method proposed by James is more suitable to be used by hand than computers.

To make up the limitations that the isochrone method proposed by James does not give the correct isochrones in a strict sense as well as its lack of suitability for computerization, Hagiwara has tried to make an modified isochrone method (Hagiwara et al. 1999), which is straightforward and computer-friendly, has been utilized in our study because of its higher acceptance by the navigational staff and its good accuracy compared with others. The detailed algorithms of the modified isochrone method can be found in works of Hagiwara (Hagiwara, 1985; 1987; 1989).

4.2 Optimum ship routing by the combination of optimization algorithm and numerical ship navigation system

Taking the objectives of optimum ship routing such as minimum transport time considering speed loss in sea way and minimum fuel cost considering added resistance in waves and total distance into account, it can be confirmed again that high-resolution weather and ocean information as well as ship responses to these weather and ocean states which may cause involuntary speed reduction and ship drifting are of great importance to an accurate optimum ship routing. For which the numerical ship navigation system (as mentioned in Chapter 3) can give a solution with high-resolution global scale weather and ocean generated by atmospheric and oceanic models (as mentioned in Chapter 2).

As the first step to utilize the modified isochrone method, one optimum ship routing problem: the minimum time routing (MTR) is calculated as an example and then

discussed based on the before-calculated weather and ocean information as well as ship responses to those ocean states. Throughout the optimum routing simulations, the advantages of optimum ship routing based on the combination of the modified isochrone method and numerical ship navigation system are fully demonstrated.

In the minimum time routing problem (MTR), the optimum ship routings are performed between Osaka Bay ($34^{\circ}38'N;135^{\circ}26'E$) and Malacca ($2^{\circ}13'N;102^{\circ}09'E$) by using the Equivalent MV (Hagiwara, 1989.). Considering the basic information of the Osaka-Malacca case ('O-M route') such as the great circle distance between two ports as well as the proper range of propeller resolution number, the "certain time" is set to be 6 hours regardless of the set ship speed as 25 knots. And stage number from the departure point to the destination point has been set to 50. Considering the flexibility of the modified isochrone method as well as the high-resolution of 0.1×0.1 degree weather and ocean information generated by models, the important increments for discretizing the routing problem are set as follows:

(1) Time-interval between successive isochrones: $\Delta \mathrm{t} = 6$ hours
(2) Sub-time-interval for calculating ship's speed, drift angle, etc. $\Delta \mathrm{t1} = 1$ hours
(3) Increment of ship's heading for constructing the isochrones: $\Delta \mathrm{C} = 2$ degree
(4) Resolution of the isochrones (i.e. local width of the sub-sector): $\Delta \mathrm{d} = 6\ \mathrm{n.m}$

Then other settings such as the number of ship's headings to be searched is set to 60; the number of sub-sector is set to be 80, which means there are 40 sub-sectors on each side of the great circle route between these two ports. The isochrone is regarded as a final one when the shortest rhumbline distance from that isochrone to the destination becomes less than $1.5 \times V_s \times \Delta t$ (which is 225 n.m.). The topography of navigable area for the 'O-M route' and the detailed settings for the modified isochrone calculations are given as Fig.4.1 and Table.4.1, respectively.

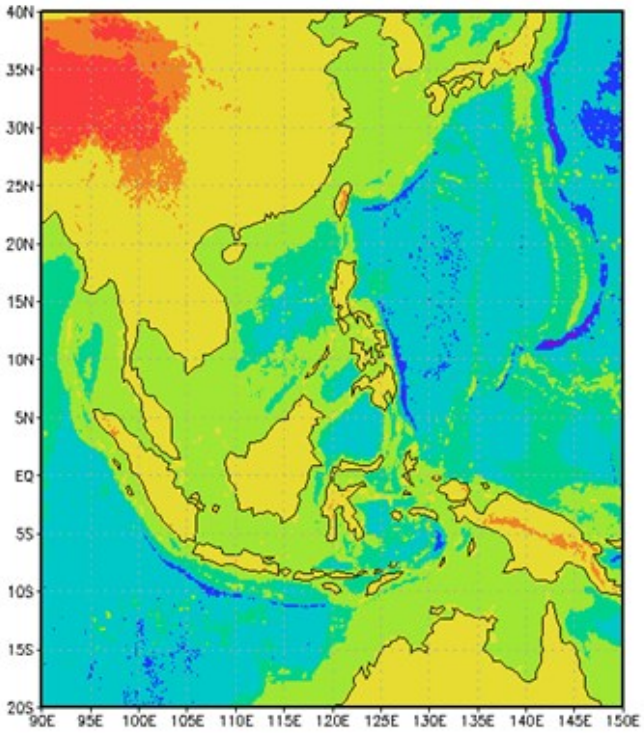

Fig.4.1. Topography of navigable area for the Osaka-Malacca (O-M) route

Table.4.1. Detailed settings for the modified isochrone method calculations

Calculation Area	90E-150E; 20S-40N
Calculation Time	21-31, May, 2011
Spatial resolution of topography, weather & ocean calculation	0.1×0.1 degree
Input time interval of weather & ocean	1 hour
Time-interval between successive isochrones	6 hours
Sub-time-interval for calculating ship's speed, drift angle, etc.	1 hour
Increment of ship's heading for constructing the isochrones	2 degree
Resolution of the isochrones	6 n.m
Number of ship's headings to be searched	60
Number of sub-sector	80
Shortest rhumbline distance between the final isochrones and destination point	$1.5 \times V_s \times \Delta t$
Set ship's speed	25 knots
Minimum water depth for ship's draft clearance	50 m

In the following simulations, the shapes of isochrones, passage time, and fuel consumptions are compared with those of the great circle routes, which are calculated by the same sub-time-interval.

At first, the ship sails from Malacca to Osaka, and as pilot time and estuary traveling are deliberately left out of the investigation as they have only small variations, the route optimization focuses on the open water part of the voyage. For that reason the route optimization starts at the eastern end of the Malacca Strait (105°E, 1°N) and ends in the estuary of Osaka Bay (135°E, 34°N). It spans a distance of roughly 2600 nm. Sailed at 25 knots it would take about 104 h, approximately 4 days. Fig.4.1 shows the minimum time route for the M-O and O-M navigation calculated by the modified isochrone method based on the weather and ocean data generated by the global scale atmospheric and oceanic models.

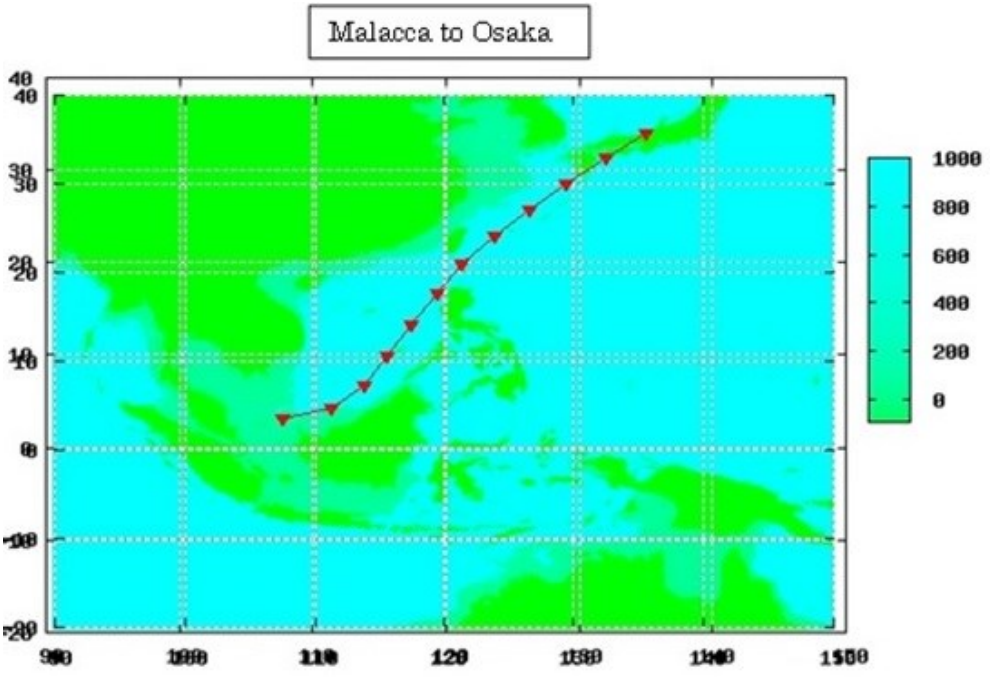

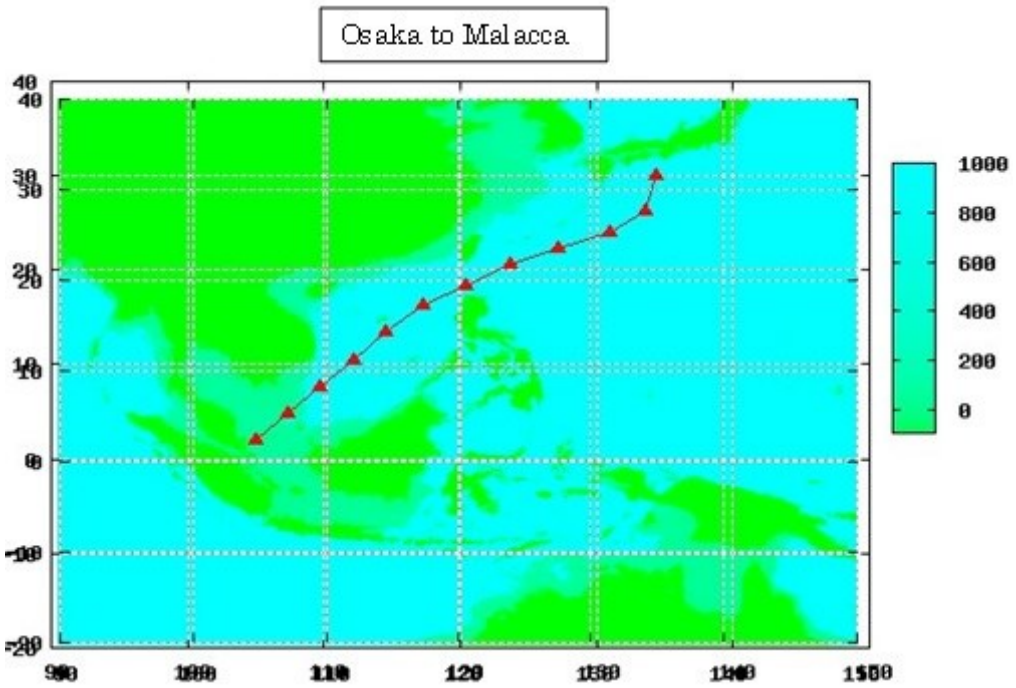

Fig.4.2. Minimum time route (MTR) for the M-O & O-M routes

Table.4.2. Calculation results of the MTR & GC cases

Results of M-O & O-M cases		Navigation time (H)	Navigation distance (N.M)	Fuel consumption (Tons)	Average ship speed (Knots)
M-O Case	MTR	112.71	2726.43	691.01	24.18
	GC	120.53	2559.68	741.88	21.24
	Variation (GC-MTR)	+7.82	-166.75	+50.87	-2.94
O-M Case	MTR	114.23	2752.24	699.26	24.09
	GC	122.17	2557.68	753.29	20.94
	Variation (GC-MTR)	+7.94	-194.56	+54.03	-3.15

4.3 Summary

Throughout the chapter 4, the optimum ship routing system is constructed to solve the minimum time routing problem (MTR) as a trail. Results have shown that this proposed

method can be applied to calculate the necessary route information by using the combination of numerical ship navigation system as well as the modified isochrone method. Although the voyage distances of the MTR become longer than the GC route, passage time and fuel consumption can be considerably saved.

However, owning to the high fuel cost and the high requirements of greenhouse gas emission for ship navigation, shipping company as well as ship owners is nowadays paying more and more attention to another problem, the minimum fuel routing (MFR). After the first trail constructing the optimum ship routing system for minimum time routing (MTR), the minimum fuel routing (MFR) as well as other minimum objectives are supposed to be added into this system in the near future.

References

Avgouleas, Kyriakos. Optimal ship routing. Diss. Massachusetts Institute of Technology, 2008.

Chen, H., 1978. A dynamic problem for minimum cost ship routing under uncertainty. Ph.D. thesis, MIT, Cambridge, MA.

Bijlsma, Sake Johannes. *On minimal-time ship routing*. Diss. TU Delft, Delft University of Technology, 1975.

Böttner CU (2007) Weather routing for ships in degraded conditions. International Symposium on Safety, Security and Environmental Protection. National Technical University of Athens, Athens

Delitala, Alessandro Mario Sergio, et al. 2010. "Weather routing in long-distance Mediterranean routes." Theoretical and applied climatology, 102.1-2, 125-137.

James, R. W., 1957. Application of wave forecasts to marine navigation. U.S. Oceanographic Office, SP-1, July, 1957.

Hagiwara, H., 1985. A study on the minimum fuel consumption route-II: Simulation in the North Pacific Ocean. Journal of Japan Institute of Navigation, 72, 87–96.

H. Hagiwara and J. A. Spaans (1987). Practical Weather Routing of Sail-assisted Motor Vessels. Journal of Navigation, 40, pp 96-119. doi:10.1017/S0373463300000333.

Hagiwara H (1989) Weather routing of (sail-assisted) motor vessels (Ph.D. thesis). Delft University of Technology, Delft

Hoffschildt M, Bidlot JR, Hansen B, Janssen PAEM (1999) Potential benefit of ensemble forecasts for shiprouting. ECMWF Technical Memorandum no. 287.

Motte, Roger. "Weather Routing of Ships." Safety at Sea International 74 (1975).

Notteboom, Theo, and Pierre Cariou. "Fuel surcharge practices of container shipping lines: Is it about cost recovery or revenue-making." Proceedings of the 2009 International Association of Maritime Economists (IAME) Conference. IAME, 2009.

Padhy CP, Sen D, Bhaskaran PK. Application of wave model for weather routing of ships in the North Indian Ocean. Natural Hazards 2008, 44 : 373–85 .

SAETRA, Ø. (2004), Ensemble Shiprouting, ECMWF Technical Memorandum 435, Reading/UK

Szlapczynska, Joanna, and Roman Smierzchalski. Adopted isochrone method improving ship safety in weather routing with evolutionary approach. International Journal of Reliability, Quality and Safety Engineering 14.06 (2007): 635-645.

Tsujimoto M, Tanizawa K (2006) Development of a weather adaptive navigation system considering ship performance in actual seas. In: Proc OMAE 2006 (25th Int Conf on Offshore Mechanics and Arctic Engineering), Hamburg, Germany, 4–9, June 2006.

CHAPTER 5

REVIEWS, CONCLUSIONS AND RECOMMENDATIONS FOR FUTURE DEVELOPMENT PREFERENCES

In this thesis, a numerical ship navigation system was built at first, and then an optimum ship routing system was constructed based on the combination of the numerical ship navigation system and an optimization algorithm, and comprehensive simulations of optimum routing for a model ship sailing on the Osaka-Malacca (O-M) route were executed to verify the effectiveness of those proposed methods.

In Chapter 1, the introduction to optimum ship routing was proposed at first, through which, the previous studies on this topic were introduced; definition of the optimum ship routing was discussed based on various views on the optimum ship routing problem from former researchers. Then the definition, motivation, study progress as well as the future development of the numerical ship navigation system were then described. Finally, objective and outline of this thesis were given.

In Chapter 2, as the first step to construct the numerical ship navigation system, numerical simulations of weather and ocean environments in both coastal sea area and global scale area were executed. Modernized atmospheric and oceanic models in both regional and global scale were briefly introduced and then utilized to make those numerical simulations, and finally simulation results are verified by observation data and the results were also analyzed and discussed.

Next, based on the high-resolution weather and ocean information generated in Chapter 2, the numerical ship navigation system was built by using a container ship model for which the necessary ship model parameters, ship responses to the before-calculated weather and ocean data, and the ship maneuvering model (MMG). To confirm the effectiveness of the constructed numerical ship navigation system, various simulations both in the Osaka Bay area and the East China Sea area were executed. The reasons why these two areas were selected were also illustrated. The proposed method as well as

constructed numerical ship navigation system was found effective when compared the results with results from other studies.

In Chapter 4, to further the former study of numerical ship navigation system, an optimum ship routing system was constructed by combining the optimization algorithm called the modified isochrone method proposed by Hagiwara with the numerical ship navigation system. At first, optimization algorithms for optimum ship routing studied by previous researchers were introduced and discussed, and then several computer simulations for a model ship sailing between Osaka-Malacca routes were executed for various objectives such as minimum time, minimum fuel as well as minimum cost. Then the minimum time route were calculated, and results show that by adding other minimum objective routes into the present system, the newly constructed optimum ship routing system is able to help achieve safer, more economical and environment-friendly international ship navigation by saving cost of time and fuel as well as reduce the greenhouse gas emissions.

To further develop the present-proposed optimum ship routing system, the following points are supposed.

(1) To figure out the detailed ship motion information along the optimum route, ship maneuvering model such as the MMG model mentioned in Chapter 3 could be added into the optimization algorithms such as the modified isochrone method utilized here in Chapter 4.

(2) To make the best voyage plan with minimum time or minimum fuel cost according to the ports distances and the estimated time of Arrival (ETA), optimum ship speed utilization should be considered based on predicated weather and ocean information as well as the detailed ship performances in those ocean states.

(3) To achieve a higher accuracy of optimum ship routing system, a higher-accuracy weather and ocean information is required, which may also be replaced by the real ocean states when there are unacceptable variations between the predicated and on-board observed conditions in the real ship navigation. Therefore, an interface-friendly on-board optimum ship routing system combined with higher spatial resolution weather and ocean information shore-based super computer calculations through low communication cost may be a choice.

PUBLICATIONS

Journal paper:

1: Chen Chen, Shigeaki Shiotani, Kenji Sasa. Numerical ship navigation based on weather and ocean simulation. Ocean Engineering, Volume 69, 1 September 2013, Pages 44–53.

2: Chen, Chen, Shigeaki Shiotani, and Kenji Sasa. Effect of ocean currents on ship navigation in the east China sea. Ocean Engineering 104 (2015): 283-293.

3: Chen Chen, Shigeaki Shiotani, Kenji Sasa. Study on a Numerical Navigation System in the East China Sea. *Applied Ocean Research* 53 (2015): 257-266.

4: Chen Chen, Shigeaki Shiotani, Kenji Sasa. Effects of Weather and Ocean on Ship Traffic in the Eastern Seto Inland Sea. Journal of Japan Society of Civil Engineering, ser. B3 (Ocean Engineering), Vol. 70, No. 2, I_942-I_947, 2014.

5: Sasa Kenji ; Terada Daisuke ; Shiotani Shigeaki ; Wakabayashi Nobukazu ; Ikebuchi Takuro ; Chen Chen ; Takayama Atsuyoshi ; Uchida Makoto. Evaluation of Ship Performance in International Maritime Transportation using an Onboard Observation System—In Case of a Bulk Carrier for International Voyages. Ocean Engineering Journal 104, 294-309. 2015.

International Proceedings:

1: Chen Chen, Shigeaki SHIOTANI and Kenji Sasa: Application of Numerical Ship Navigation in Coastal Area, Oceans 2013, San Diego of California, CD-ROM, pp.1-6, Sep, 2013.

2: Chen Chen, Shigeaki Shiotani, Kenji Sasa. Effect of Weather and Ocean on Ship Navigation in a Coastal Area of Japan. Proceedings of the INTERNATIONAL SYMPOSIUM INFORMATION ON SHIPS, Hamburg, Germany, 04 - 05 September 2014.

3: Chen Chen, Shigeaki Shiotani, Kenji Sasa. High-resolution Numerical Ship Navigation in a High Wind Situation. Proceedings of the14th International Conference on Computer Applications and Information Technology in the Maritime Industries, 11-13 May 2015, Ulrichshusen/Germany.

.

Other co-authored reference papers:

1: Sasa, K., Chen, C., Shiotani, S., Ohsawa, T. and Terada, D., “Numerical Analysis of Failed Forecasts of Waves under Low Pressures from Viewpoint of Ship Operation”, Proceedings of the 33rd International Conference on Ocean, Offshore and Arctic Engineering, OMAE2014, pp.1-8, June, 2014.

3. 塩谷　茂明，柳　馨竹，陳　辰. AIS データによる早期津波伝播予測の可能性に関する研究、沿岸域学会誌 Vol.26　No.3,pp.129-140、平成 25 年 12 月.

2: 笹 健児、陳 辰、塩谷茂明、若林伸和、寺田大介：沿岸から離れた海域における波浪特性と船舶運航への活用に関する基礎的研究、土木学会論文集 B3（海洋開発）特集号、Vol.71、2015 年 11 月.

ACKNOWLEDGEMENTS

Accepted by the Graduate School of Maritime Sciences of Kobe University through the International Priority Graduate Program, I started my MD course around four years ago. With my knowledge background as ship navigation and my interest in optimum ship routing, I chose the theme “weather routing for ship navigation” to focus after discussing with my super adviser, Prof.Shiotani, to whom I owe my deepest gratitude for his acceptance me as a MD course student, for his encouragement to publish our study results, for his outstanding composition of guidance and freedom, and also for his generous support whenever I asked for. Without his kind help and guidance for these years, I can’t get smooth study and satisfying results.

I also want to express my gratitude to Prof.Sasa, who has also provided me great help on both my study and my life here as an international student. His valuable discussions on my papers have been important to my study.

Additionally, sincere thanks are given to other professors as well as researchers such as Prof.Ohsawa in Graduate School of Maritime Sciences of Kobe University, Prof.Shoji in Tokyo University of Marine Science and Technology, Prof.Kano in National Maritime Research Institute, and Prof. Takahasi in JAMSTEC because of their kind and important contribution and inspiration to my study.

Special thanks are also given to office staffs of Graduate School of Maritime Sciences of Kobe University who have helped me by supporting care for my life as an international student.

Also many thanks should be given to other students in our laboratory for their kindness on my study.

Special thanks I owe to my beloved parents, my wife and daughter for their reliable support on both mental and financial aspects. The spatial distance between China and Japan separates us physically; however, it can never affect our concern about each other emotionally.

NOMENCLATURE

p_h	hydrostatic component of the pressure in Eq.(2.1)
p_{hs}	values along the surface in Eq.(2.1)
p_{ht}	values along the top boundaries in Eq.(2.1)
η	vertical coordinate in Eq.(2.1)
V	covariant velocities in Eq.(2.2)
ω	contravariant 'vertical' velocity in Eq.(2.2)
θ	potential temperature in Eq.(2.2)
γ	ratio of the heat capacities for dry air in Eq.(2.3-2.8)
R_d	gas constant for dry air in Eq.(2.10)
p_0	a reference pressure in Eq.(2.10)
F_U	forcing terms arising from model physics in Eq.(2.3)
F_V	turbulent mixing in Eq.(2.4)
F_W	spherical projections in Eq.(2.5)
F_Θ	the earth's rotation in Eq.(2.6)
S	source/sink term in Eq.(2.13)
$H(x, y)$	bottom topography in Eq.(2.15)
$\eta(x, y, t)$	surface elevation in Eq.(2.15)
U , V	components of the horizontal velocity of tidal current in Eq.(2.16)
ω	velocity component of the normal direction to the σ plain in Eq.(2.16)
f	Coriolis coefficient in Eq.(2.16)
g	acceleration of gravity in Eq.(2.16)
K_M	frictional coefficient of the sea bottom in Eq.(2.16)
F_x , F_y	horizontal viscosity diffusion coefficients in Eq.(2.16)

A_M	Smagorinsky Diffusivity in Eq.(2.21)
d	mean water depth in Eq. (2.2.2.1)
U	(depth- and time- averaged) current velocity in Eq. (2.2.2.1)
$F(f_r, \theta)$	frequency-direction spectrum in Eq. (2.2.2.4)
$F(k, \theta)$	different spectra in Eq. (2.2.2.4)
c_g	group velocity in Eq. (2.2.2.6)
E	total variance
D/ Dt	total derivative of wave action density spectrum in Eq. (2.2.2.7)
S	net effect of source and sinks for the spectrum F in Eq. (2.2.2.7)
$\mu,\ \emptyset$	Longitude and latitude in Eq. (2.2.2.8)
R	radius of the earth in Eq. (2.2.2.9), (2.2.2.10), (2.2.2.11)
$U_\emptyset,\ U_\mu$	current components in Eq. (2.2.2.9), (2.2.2.10)
θ	a Cartesian definition in Eq.(2.2.2.11)
S_{in}	wind-wave interaction term in Eq. (2.2.2.12)
S_{nl}	a nonlinear wave-wave interactions term in Eq. (2.2.2.12)
S_{ds}	a dissipation (`whitecapping') term in Eq. (2.2.2.12)
S_{ln}	linear input term in Eq. (2.2.2.12)
S_{bot}	wave-bottom interactions in Eq. (2.2.2.12)
S_{db}	depth-induced breaking in Eq. (2.2.2.12)
S_{tr}	triad wave-wave interactions in Eq. (2.2.2.12)
S_{sc}	triad wave-wave interactions term in Eq. (2.2.2.12)
S_{xx}	additional, user defined source terms in Eq. (2.2.2.12)
m	mass in Eq. (3.1)
$m_x,\ m_y$	added mass in Eq. (3.1)

u , v	components of the velocity in the directions of the x-axis and the y-axis, respectively in Eq. (3.1)
r	angular acceleration in Eq. (3.1)
I_{zz} , J_{zz}	moment of inertia and the added moment of inertia around G, respectively in Eq. (3.1)
N	moment around the z-axis in Eq. (3.1)
θ	potential temperature in Eq. (3.1)
ρ_A	density of the air in Eq. (3.1)
θ_A	relative wind direction in Eq. (3.3)
V_A	relative wind velocity in Eq. (3.3)
A_L , A_T	frontal projected area and lateral projected area, respectively; in Eq. (3.3)
C_{XA} ,etc	Coefficients (Fujiwara, T. 1998) in Eq. (3.3)
ρ	water density in Eq. (3.5)
L	ship length in Eq. (3.5)
d	ship draft in Eq. (3.5)
U	ship's speed in Eq. (3.5)
R	resistance of the hull in Eq. (3.5)
S	wetted surface area in Eq. (3.6)
u	speed component at X direction in Eq. (3.6)
k	ship form factor in Eq. (3.7)
ΔC_f	roughness factor in Eq. (3.7)
C_w	wave drag factor in Eq. (3.7)
R_n	Froude number in Eq.(3.8)
$X'_{\beta r}$, $X'_{uu}etc$	various coefficients in Eq.(3.5)

FIGURE LIST

No.	Title	PP.
1.1	Compositions of the Numerical Ship Navigation System	4
1.2	Flow chart of the supposed optimum ship routing system	6
2.1	WRF-ARW η coordinate	13
2.2	The sigma coordinate system applied in the POM model	17
2.3	Topography of the Osaka Bay	19
2.4	Weather charts of simulated typhoons	21
2.5	WRF Domain for wind calculation in Osaka Bay	21
2.6	Surface wind distributions in Osaka Bay	22
2.7	Comparisons of wind velocity and direction	23
2.8-A	Surface tidal distribution of tidal current in these two typhoon cases	24
2.8-B	Surface tidal distribution of tidal current in these two typhoon cases	24
2.9	Comparison of sea level between observation and POM calculation	25
2.10	Comparison of calculated and observed significant wave height	26
2.11-A	Distributions of significant wave height in two typhoon cases	27
2.11-B	Distributions of significant wave height in two typhoon cases	27
2.12	Geography of the East China Sea Area (ECSA)	28
2.13	Main shipping routes in the ECSA	28
2.14	Ocean current data of the North Pacific (long-time mean; November)	29
2.15	Locations of ship accidents that occurred during tropical typhoons	30
2.16	Typhoon track and key information from the National Institute of Informatics	31
2.17	Comparison of WRF calculation and JMA observation	32
2.18	Wind velocity distributions from WRF model at 21:00, 28th, May, 2011 (UTC)	33
2.19	Distribution of significant wave height at 21:00, 28th, May, 2011 (UTC)	34
2.20	Comparison of Significant Wave Height between SWAN calculation and NOWPHAS observation	35
2.21	Bottom topography of the POM model. The contour interval is 500 m. The maximum depth is artificially fixed at 6000 m.	38

2.22-A	Time mean sea surface height in the hind cast process	41
2.22-B	Time mean sea surface height in the hind cast process	41
2.23	Averaged ocean surface current vector distribution of the calculation area by POM; 0.1*0.1 degree; 1992-2012.	42
2.24	Enlargement of bin-averaged velocity east of Luzon and Taiwan.	42
2.25	Enlargement of bin-averaged velocity in the East China Sea.	43
2.26-A	Comparison of daily mean Sea Surface Height Anomaly (SSHA) data between the model calculation and the JODC observation in the hind cast process; ISHIGAKI	44
2.26-B	Comparison of daily mean Sea Surface Height Anomaly (SSHA) data between the model calculation and the JODC observation in the hind cast process; NAHA	44
2.26-C	Comparison of daily mean Sea Surface Height Anomaly (SSHA) data between the model calculation and the JODC observation in the hind cast process; TANEGASHIMA	45
2.27	Locations of SSH observation stations along the continental slope in the ECSA	45
2.28	Brief program flow chart of the WW3 model	48
2.29	Distribution of tanker number in the world	53
2.30	Daily transit volumes through world maritime oil chokepoints	53
2.31	Calculation results of MSSG-A and MSSG-O for the Osaka-Malacca route	55
2.32	Topography of three nests in WW3 calculation. (A): Largest nest (0E-359.5E,75S-75N); (B): Middle nest (60E-280E, 50S-60N); (C): Inner nest (90E-150E, 20S-40N)	56
2.33	Wave information generated by WW3 model for the largest nest. (Time period: 2011052700-2011052800; Time interval: 6 hours)	60
2.34	Wave information generated by WW3 model for the middle nest. (Time: 2011052800)	61
2.35	Wave information generated by WW3 model for the inner nest. (Time: 2011052800)	61
3.1	Body plan of the ship mode SR108	68
3.2	Responses of the ship model SR108 in ocean waves	69
3.3	Coordinate system of the MMG model	70

3.4	Course settings for numerical navigation in the Osaka Bay Area case	73
3.5	Numerical simulations of ship navigation by SR108 in Osaka Bay of No.1 typhoon	76
3.6	Numerical simulations of ship navigation by SR108 in Osaka Bay of No.2 typhoon	79
3.7	Course settings for numerical navigation in the East China Sea Area case	81
3.8	Numerical ship tracks in the Course 045 group	83
3.9	Numerical ship tracks in the Course 225 group	85
3.10	Numerical ship tracks in the Course 090 group	87
3.11	Numerical ship tracks in the Course 270 group	88
3.12	Effect of the Kuroshio Current on ship's drifting and speed variations in all cases	89
3.13	Meridional and zonal wind speed around the typhoon eye (126.6 E; 26.3 N)	91
3.14	Graph descriptions of the two simulation cases	91
3.15	Relative locations of ship and typhoon, Kuroshio Current in two cases	92
3.16	Numerical simulation results of ship tracks in Case 1	93
3.17	Numerical simulation results of ship tracks in Case 2	94
3.18	Effects of weather and ocean on ship navigation	96
4.1	Topography of navigable area for the Osaka-Malacca (O-M) route	103
4.2	Minimum time route (MTR) for the M-O navigation	105

TABLE LIST

NO	Name	P.P
Table.1.1	Number of ships lost 2006-2010	5
Table.2.1	Calculation settings of WRF calculation in the Osaka Bay case	22
Table.2.2	Parameter settings of WRF calculation in the ECSA case	31
Table.2.3	Parameter settings of Wave calculation in the ECSA case	33
Table.2.4	Values of the vertical sigma coordinates used in the POM	38
Table.2.5	Key settings of POM model calculation	40
Table.3.1	Principal Properties of the SR108	67
Table.3.2	Simulation designs for different cases in the East China Sea Area case	81
Table.3.3	Drift angles, drift distances, and speed variations in all cases	89
Table.3.4	Simulation designs for different cases in the East China Sea Area case	92
Table.3.5	Simulation results of these two cases	96
Table.4.1	Detailed settings for the modified isochrone method calculations	103
Table.4.2	Calculation results of the MTR & GC cases	105